



University of
Massachusetts
Amherst

Additive Manufacturing of Homopolymers and Polymer-Nanoparticle Composites using the Cold Spray Deposition Technique

Item Type	Dissertation (Open Access)
Authors	Sundara Rajan, Kashyap
DOI	10.7275/55291
Rights	Attribution-NonCommercial 4.0 International
Download date	2026-04-22 08:30:57
Item License	http://creativecommons.org/licenses/by-nc/4.0/
Link to Item	https://hdl.handle.net/20.500.14394/55291

ADDITIVE MANUFACTURING OF HOMOPOLYMERS AND POLYMER-
NANOPARTICLE COMPOSITES USING THE COLD SPRAY DEPOSITION
TECHNIQUE

A Dissertation Presented
by
KASHYAP SUNDARA RAJAN

Submitted to the Graduate School of the
University of Massachusetts Amherst
in partial fulfilment of the requirements of the degree of

DOCTOR OF PHILOSOPHY

September 2024

Mechanical Engineering

© Copyright by Kashyap Sundara Rajan 2024

All Rights Reserved

ADDITIVE MANUFACTURING OF HOMOPOLYMERS AND POLYMER-
NANOPARTICLE COMPOSITES USING THE COLD SPRAY DEPOSITION
TECHNIQUE

A Dissertation Presented

by

KASHYAP SUNDARA RAJAN

Approved as to style and content by:

Jonathan P. Rothstein, Chair

Jae-Hwang Lee, Member

Jessica Schiffman, Member

Sundar Krishnamurty, Department Head
Mechanical and Industrial Engineering

ACKNOWLEDGEMENTS

I would like to thank everyone who has been a part of this dissertation. In particular, I would like to thank Professor Rothstein for his patience, support, and guidance. I would also like to thank my committee for all their valuable suggestions and inputs. Many thanks to my parents who have been my guiding light throughout my life. My teachers and professors were also an invaluable part of my life, not just for teaching me, but also for going above and beyond and shaping me into the person I am today. Special thanks to Prof. Steven Beck of the music department for all the studio lessons. I would like to acknowledge the support of my family who have assisted me in many forms and my friends who have helped me in various ways, both personally and professionally so that I could reach this stage in my life. Lastly, I would like to thank God.

ABSTRACT

ADDITIVE MANUFACTURING OF HOMOPOLYMERS AND POLYMER-
NANOPARTICLE COMPOSITES USING THE COLD SPRAY DEPOSITION
TECHNIQUE

SEPTEMBER 2024

KASHYAP SUNDARA RAJAN

B.Tech., AMRITA UNIVERSITY

M.S., UNIVERSITY OF MASSACHUSETTS AMHERST

Ph.D., UNIVERSITY OF MASSACHUSETTS AMHERST

Directed by: Professor Jonathan P. Rothstein

Cold spray is an additive manufacturing technique where solid powder particles bond with a target substrate upon high-velocity impact. It offers advantages over traditional coating methods, preserving materials' properties without harmful by-products.

While extensively researched for metal-on-metal coatings, cold spray's application to polymers is relatively new. This dissertation comprises three studies focusing on cold spray of polymers. The first investigates coating metal substrates with polymeric powders, a topic with limited prior research. It systematically examines parameters such as particle and substrate temperature, substrate surface roughness, and the effect of priming on deposition efficiency and adhesion strength. The results indicate that there exists a deposition window of velocity, impact angle and temperature for good deposition, and the spray parameters need to be maintained within this window.

The second study explores using polymer composites in cold spray. Nano-sized copper and silicon dioxide particles are added to high-density polyethylene (HDPE) to create composites. The research examines how concentration, particle size, and impact energy affect deposition. Results show that copper and SiO₂ behave differently when added to HDPE, and there is not a monotonic increase in the efficiency of the cold spray process with the increase in the filler material. Instead, an optimal particle concentration is found for each composite powder that maximizes the deposition efficiency. This optimal concentration varies with particle size and type.

The third study investigates adding carbon nanotubes (CNTs) to HDPE powders. CNTs are known for their exceptional properties including strength, toughness, and electrical and thermal conductivity. The research demonstrates that both the composite powder processing and the cold spray process itself significantly influence the morphology, distribution, and orientation of CNTs within the HDPE matrix, and consequently, the properties imparted by the CNTs. Notably, the cold spray process is found to positively impact CNT orientation in the final deposit, which can be inferred from the enhanced electrical conductivity of the CNT-HDPE deposit.

These findings offer valuable insights into creating polymer composite coatings using cold spray and establish it as an efficient alternative to conventional coating techniques.

TABLE OF CONTENTS

	Page
ACKNOWLEDGEMENTS	iv
ABSTRACT.....	v
LIST OF TABLES.....	x
LIST OF FIGURES	xi
CHAPTER	
1. INTRODUCTION	1
1.1 Introduction to Polymers.....	1
1.2 Introduction to Polyethylene.....	1
1.3 A Brief Overview of Coating Techniques	6
1.4 The Cold Spray Coating Technique.....	11
1.5 Polymer Cold Spray	16
1.6 Introduction to Composite Materials: Silica Nanoparticles.....	26
1.7 Copper Nanoparticles for Composites	28
1.8 Carbon Nanotubes as Composite Filler Materials	28
1.9 Scope of the Dissertation	33
2. EXPERIMENTAL SETUP AND CONDITIONS	35
2.1 Polymer Powder and Synthesis.....	35

2.2 Silica and Copper Nanocomposite Synthesis	36
2.3 CNT-HDPE Composite Synthesis	39
2.4 Electrical Conductivity Experiments	42
2.5 Metal Substrate Preparation	42
2.6 The Cold Spray Setup	44
2.7 Adhesion Strength Testing.....	47
2.8 Compression Tests	48
3. COLD SPRAY OF HDPE ON METAL SUBSTRATES	51
3.1 Effect of Particle Temperature.....	51
3.2 Effect of Surface Roughness.....	53
3.3 Adhesion Tests.....	57
3.4 Effect of Intermediate Primer Layer	61
3.5 Conclusions.....	63
4. COLD SPRAY OF POLYMER COMPOSITES.....	65
4.1 SiO ₂ – HDPE Composite Powders	65
4.2 Mechanisms for Interaction Between Composite Powders and Substrate..	67
4.3 Cu-HDPE Composite Powders	73
4.4 Conclusions.....	78
5. COLD SPRAY OF CNT-HDPE COMPOSITES	81
5.1 Deposition of CNT-HDPE Composite Powders.....	81

5.2 Conductivity Measurements	84
5.3 Young's Modulus.....	87
5.4 Conclusions.....	89
6. CONCLUSIONS.....	92
7. A NOTE TO THE NEXT STUDENT	99
Bibliography	102

LIST OF TABLES

Table	Page
1. List of sandpaper grit designations and the corresponding average surface roughness values	43

LIST OF FIGURES

Figure	Page
1. Structure of the polyethylene molecule	2
2. Schematic diagram showing linear and branched polyethylene	4
3. Schematic of a typical cold-spray system [60]	12
4. Shapes of powder feed particle and substrate crater formation 50 ns after impact for (a) aluminum particle impacting a copper substrate at 400 m/s and (b) copper particle impacting an aluminum substrate at 500 m/s [61]	14
5. Deposition efficiency as a function of particle impact velocity for like on like deposition [77]	18
6. Deposition window as a function of particle impact velocity and particle temperature for polystyrene particles cold sprayed on LDPE substrates [77]	19
7. (a) A representation of the tensile tests on cold spray specimens and (b) stress-strain curves on cold sprayed and melt cast samples of HDPE [77]	22
8. Chirality indices in a sheet of graphene [139]	30
9. Different type of CNT structures [139]	30
10. A TEM image of the 200 nm silica particles [164]	36
11. A pictorial representation of the 4-step process required to make the micro and nanocomposite powders	37
12. SEM images of the composite powders used in this dissertation. The images include (a) micro-SiO ₂ particles in HDPE, (b) nano-SiO ₂ particles in HDPE and (c) 40 nm Cu particles in HDPE at mass fractions of 9.1 %, 0.99 % and 1.96 % respectively and (d) milled pure HDPE powder	39

13. A pictorial representation of the 6-step process for making the CNT-HDPE composite powders	41
14. Scanning Electron Microscopy image of the surface of CNT-HDPE composite powder. The CNTs are visible as threads that are pressed into the HDPE powder surface	41
15. LDPE film and deposition on metal substrate. The LDPE films are 12.5 μm and are melt-cast onto the metal substrate	44
16. Schematic of the cold spray setup.....	46
17. Picture of the cold spray setup	47
18. A schematic of the adhesion test setup	48
19. A schematic of the compression tests for the CNT-HDPE samples	49
20. Deposition Efficiency, DE, of HDPE on untreated, room temperature aluminum substrates as a function of particle temperature.....	52
21. Optical profilometer maps and corresponding heat maps of aluminum substrate surfaces that are (a)-(b) untreated, (c)-(d) treated with 50 grit sandpaper in a unidirectional fashion and (e)-(f) treated with 50 grit sandpaper in a random fashion	54
22. Deposition efficiency for surfaces with treated by unidirectional scratching (●) and random scratching (▲) as a function of (a) sandpaper grit designation and (b) RMS surface roughness. The deposition efficiency of an untreated surface is represented by a dashed line (--) in (a) and is plotted with the unidirectional data in (b). All deposits were produced with a particle temperature of $T_p = 80^\circ\text{C}$, a surface temperature of $T_s = 20^\circ\text{C}$ and a particle impact velocity of $U_p = 240 \text{ m/s}$	55
23. Scanning Electron Microscopy (left) and Optical microscopy (right) images of the cold spray deposition of HDPE on a 50-grit randomly scratched aluminum substrate. The optical	

microscope focuses on the cross-section, while the SEM focuses on the deposition from above, both highlighting the conformal mapping of the particle onto the substrate, the lack of gaps or voids, and the lack of distinguishing individual HDPE particles 57

24. Tensile stress as a function of time from the adhesion tests of a series of cold spray deposits of HDPE particles on a smooth aluminum substrate (■), an aluminum substrate scratched with 50 grit sandpaper in a unidirectional pattern (●) and an aluminum substrate scratched with a 50-grit sandpaper in a random pattern (▲). The maximum stress is the adhesive stress to completely detach the deposit from the substrate. All deposits were produced with a particle temperature of $T_p = 80^\circ\text{C}$, a surface temperature of $T_s = 20^\circ\text{C}$ and a particle impact velocity of $U_p = 240 \text{ m/s}$ 58

25. Adhesion stress of the cold sprayed HDPE deposit on aluminum for different surface patterns of surface roughness. All deposits were produced with a particle temperature of $T_p = 80^\circ\text{C}$, a surface temperature of $T_s = 20^\circ\text{C}$ and a particle impact velocity of $U_p = 240 \text{ m/s}$ 60

26. Cold spray deposition efficiency, DE, of HDPE particles on an aluminum substrate with an LDPE coating of various thickness. All data are for a particle temperature of $T_p = 80^\circ\text{C}$, a surface temperature of $T_s = 80^\circ\text{C}$ and a particle impact velocity of $U_p = 240 \text{ m/s}$. For reference, a linear trendline is placed through the data. Note that the deposition efficiency for an infinitely thick LDPE surface under these same conditions is $\text{DE} = 8.4\%$ [77] 63

27. Deposition efficiency plotted as a function of the mass fraction of SiO_2 particles in the composite HDPE powders. The data include results for both micro- SiO_2 (-●-) and nano- SiO_2 (-▲-) particles incorporated into the SiO_2 -HDPE composite powder. 66

28. Impact kinetic energy of the composite particles plotted as a function of the mass fraction of SiO ₂ (-•-) and Copper (-■-)	70
29. Estimated surface coverage of the HDPE composite particles plotted as a function of the mass fraction of nano-SiO ₂ (-▲-), micro-SiO ₂ (-•-) and Copper (-■-) composite powders	72
30. Hypothetical rendering showing the impacting particle interaction with the substrate and how the orientation of the particle can affect deposition for an 8 μm SiO ₂ particle added to HDPE (a) Poor deposition and (b) Good deposition. Image is not drawn to scale	73
31. Cold spray deposition efficiency of Copper-HDPE composite powders on an HDPE substrate plotted as a function of the mass fraction of copper in the composite powders	75
32. SEM image of a cut through the interface between a HDPE substrate (top) and a cold spray deposition (bottom) of a Cu-HDPE composite powder with $m_f = 1.96\%$	76
33. Back scatter from SEM showing copper nanoparticles on the top surface of a Cu-HDPE composite at $m_f = 4.76\%$	77
34. Energy dispersive spectroscopy plot of the Cu-HDPE deposit at a mass fraction of $m_f = 4.76\%$ which clearly indicates a copper peak at 0.95 keV	78
35. Deposition efficiency of the cold spray process plotted as a function of the mass fraction of CNT filler in the HDPE matrix	82
36. (a)-(b) SEM images at different magnifications of the underside of the CNT-PE composite deposition at a mass fraction $m_f = 3.86\%$	84
37. Conductivity tests performed on the cold sprayed CNT-HDPE (-■-), cold sprayed Cu-HDPE (-•-) and melt-cast CNT-HDPE (-▲-) samples	87
38. Young's modulus of the melt cast (-▲-) and cold sprayed (-■-) PE-CNT composites	88

CHAPTER 1

INTRODUCTION

1.1 Introduction to Polymers

In this dissertation I will be developing an additive manufacturing technique that can deposit polymer powders on different substrates in order to form coatings and three-dimensional structures. The word polymer is derived from two Greek words: “Polus” and “Meros”, meaning “many parts” and is used to describe all materials that are made up of many repeating units, either a single atom or a small group of chemically combined atoms. Polymers are an important component of life itself, and are present in various forms and shapes throughout history. In the last century, they have been the subject of an increasing amount of research, and have been recognized and understood as a coherent group. Over the years, it has become possible to produce polymers for a variety of applications through chemical reactions [1]. Synthetic polymers were first derived as substitutes for natural polymers like rubber and silk, but with the second World War, a vast range of new and specifically designed polymeric compounds were developed, like plastics, rubbers and fibers, all of which are used in modern consumer products. In the past 50 years, this rapid development has meant that there is a lot of research is focused on these synthetic polymers, and specifically their applications and use cases [1].

1.2 Introduction to Polyethylene

One of the simplest and most common examples of a polymer, and one that is used extensively throughout this dissertation, is polyethylene (PE), which is made up of the

repeat unit $\text{-H}_2\text{C-CH}_2\text{-}$ as shown in Figure 1. This polymer is made by joining molecules of ethene, which is $\text{CH}_2 = \text{CH}_2$. Each molecule of ethene is the monomer, and many molecules of ethene combined form the polymer. When ethene molecules are combined, the double bond between the two carbon atoms is replaced by single bonds to other molecules of ethene, which forms the polymer comprising of repeat units of $\text{-H}_2\text{C-CH}_2\text{-}$. [2]. A representation is provided in figure 1. Polyethylene has a broad spectrum of physical properties which can be tuned precisely, which makes it highly suited for a lot of applications. Toughness, hardness, and clarity are a few of the properties of polyethylene that can be varied based on the application. The key lies in the structure of the polyethylene molecule, which can be controlled by manipulating the process of polymerization [2].

Polymers like polyethylene are typically very long chains made up of 10^3 to 10^6 monomers with an average molecular weight of 10^4 to 10^7 g/mol.. Concentration, molecular weight, molecular weight distribution and branching of the backbone all contribute to the unique behaviour of the polymers [3].

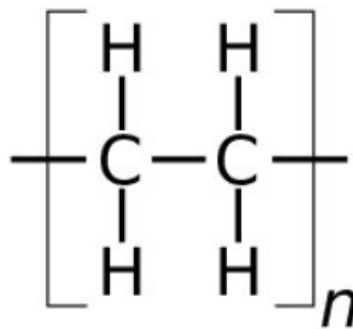


Figure 1: Structure of the polyethylene

Polymers can also come in branched varieties. The linear polyethylene in figure 2, where the carbon backbone is a one long chain is known as high density polyethylene (HDPE). In certain cases, branching of the polymer backbone can occur based on the synthesizing conditions imposed by the manufacturer. The branching of the polyethylene leads to a different class of materials known as low density polyethylene (LDPE). The behaviour, properties and use cases of the polyethylene is highly influenced by the experimental conditions of the polymerization process. HDPE and LDPE structures are shown in figure 2. HDPE in particular is used extensively in industrial applications owing to its low permeability, corrosion resistance, stiffness, relatively high tensile strength, low permeability, and high abrasion resistance [4]. A few common applications include pipes, food storage containers, trash can bags, grocery bags, crates, and toys [2].

It is also important to understand the process of polymerization that makes the polyethylene because different grades of polyethylene will be explored in detail throughout this text. Conventional high-pressure polyethylene has been made in the United States since World War II, principally by the Bakelite Division of Union Carbide and Carbon Chemicals Corporation and by E. I. du Pont de Nemours and Company under license from Imperial Chemical Industries [2]. Imperial Chemical Industries controlled the basic patent in the United States, which has now expired. This patent broadly covered polymers consisting essentially of $-C_2H_4-$ groups, melting in the range 100-120°C., characterized by a semicrystalline structure (figure 3), and having a molecular weight above 6000 [2,5].

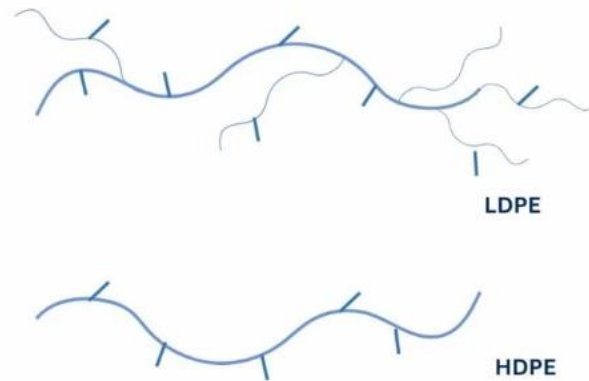


Figure 2: Schematic diagram showing linear and branched polyethylene

The mechanical properties of polyethylene are also vital to its use in many cases. Mechanical properties are a response at a molecular levels, that is the movement and rearrangement of component molecules and a distortion of the initial structure when subjected to an external forces such as compression, tension, shear, flexion, torque etc. A brief discussion will be made of the tension tests involving polyethylene in subsequent parts of this chapter, but the important thing to note is that the typical mode of polyethylene deformation is one of yielding and necking followed by strain hardening [4]. Localized yielding is especially noticeable in samples with higher degrees of crystallinity, in which necks form that may have a cross-sectional area of less than one-tenth of that of the original specimen. When stretched perpendicular to its principal orientation direction in a tension tests, the polyethylene sample yields in discrete regions and thins down preferentially to form one or more necks. As elongation continues, the necks grow and merge, encompassing the complete sample. The final stage, strain hardening, occurs when the necked region draws homogeneously prior to break [4].

When a polyethylene sample is subjected to external stress there is an initial deformation prior to yield that is homogeneous and is largely recoverable when the stress is removed. This initial linear region of elasticity at small strains can vary from 1% to 2% for highly crystalline samples up to 50% or more in high co-unit copolymers and ionomers. This modulus is known as the Young's modulus or the elastic modulus. The elastic modulus of a sample is a measure of its rigidity which means that the higher the modulus is, the stiffer the sample is going to be. Yielding occurs when the sample ceases to deform homogeneously and starts to deform heterogeneously . In samples with degrees of crystallinity greater than approximately 40%, the yield point corresponds to the first maximum in the force versus elongation curve [4]. The sharpness of the yield peak exhibited during force versus elongation measurements reflects the distinctness of the neck observed visually. Highly crystalline samples, which exhibit distinct yield peaks, initially deform in a localized region to create a neck. The neck is highly oriented, having a much smaller cross-sectional area than the undeformed regions that coexist in series with it. Samples with very low levels of crystallinity exhibit neither localized necking nor a distinct yield peak [4].

It is also worth talking about the electrical conductivity of polyethylene, because the study of conductivity becomes important later in this dissertation. Polyethylene is widely known as an electrical insulator[4], that is, it does not easily permit the transport of electricity. This is primarily due to the negligible polar component of the carbon-carbon and carbon-hydrogen bonds in the structure of polyethylene. There are no free electrons in the structure which makes polyethylene an electrical insulator, and the lack of an ability to

polarize makes it inert to electrical fields. So, polyethylene is generally known as an insulating material [4]. The principal electrical characteristics of polyethylene can be defined in terms of its resistivity, permittivity, dissipation factor, dielectric strength, and arc resistance. The first three characteristics are important at low electrical stress, while the latter two are more important at high electrical stresses. Resistivity is an important parameter to characterize when talking about electrical conductivity, particularly in the case of polyethylene. It is a measure of the resistance of the material to electrical flow. Bulk resistivity is a material property and it is largely a factor of the intrinsic nature of the material and any additives if present. It depends on the thickness and is inversely proportional to the cross sectional area.

1.3 A Brief Overview of Coating Techniques

A significant portion of this dissertation is dedicated to studying coatings, specifically spray coatings using polymers. However, it is important to look at and evaluate different coating techniques to understand where spray coatings fit into the overall research field of coatings and what techniques currently exist to create coatings of polymeric materials. There are a wide variety of applications for which coatings can be used, for both functional and aesthetic reasons. The primary reason is to enhance the longevity of solid materials, and this is primarily seen in the automotive and aviation industry. But there are a wide range of supplementary reasons such as increasing the hardness of the base material, changing the surface feel and texture, electrical and thermal insulation, changing the wettability and hydrophobicity, anti-corrosion behaviour, biocompatibility and so on [6,7]. Coatings are also widely used in the electronics industry to make high precision

components. Choosing the right material to form a coating is of utmost importance, and hence careful thought must be given to the not just the process of coating, but the material selection as well. Different materials such as polymers, metals, composites, ceramics and alloys can be used as coatings [8,9].

Let us take a brief look at different coating techniques. A variety of coating techniques exist, each with their unique abilities and processing challenges [10]. One such class of techniques is known as vapour deposition, which can be split into two categories – Physical Vapour Deposition (PVD) and Chemical Vapour Deposition (CVD). PVD is known for its ability to give corrosion and wear resistance and mechanical properties to the surface of the material that is being coated. There is a lot of control over the process, and all the properties of the coating can be adjusted on demand. The process works by transferring the source material into a vapour under vacuum, and then condensing on the surface of the substrate to create a film [11,12]. The thermal energy required for successful evaporation can come from different sources like electron beams or heating wires. This thermal energy heats the atoms of the source material, which get vaporized and travel through the vacuum to deposit on the substrate. However, this technique works best for metals. PVD of polymers is possible, but challenging since the degradation of polymers is quite likely during the process [13,14]. Chemical Vapour Deposition is the other type of vapour deposition technique. In this process, the substrate gets exposed to a set of volatile material precursors, where a chemical reaction creates a deposition on the surface of the material [15]. The by-products of this reaction are usually removed by a vacuum pump, but in some cases can remain in the chamber. CVD is an extremely versatile technique and

is compatible with a wide range of materials including polymers[16–18], however, the challenge comes in with the temperature of the process which can approach 900°C, which is difficult for temperature sensitive materials.

Sol-gel is a coating technique that is widely used for biomedical applications [19–21]. It is done in many forms like dip coating, spraying, and spinning. It is also particularly effective at enhancing previously existing coatings, because it is a liquid permeating process, which means that it can easily seal porous coatings. The solution, or Sol, is made by dissolving appropriate precursors in a solvent. This is then heated at a predefined temperature to facilitate the phase change in order to make a gel phase, hence the name sol-gel. The substrates are then dipped into the gel at different speeds and held for different lengths of time depending on the application. Sol-gel is quite versatile really, and boasts a high adhesion of the coating layer, enormous flexibility in the coating process, an ability to coat complex geometries, and comparatively lower cost than other coating techniques[22,23]. It is, however, not without issues – the thickness of the coated layer can sometimes be non-uniform depending on the process, and it is also a relatively slow process. therefore, also quite effective in making hybrid materials where organic materials are bonded to inorganic materials through the introduction of functional groups, and therefore is quite well used for polymer coatings including Poly(dimethylsiloxane) (PDMS), Poly Ether Ketone (PEK) and polycarbonate [24–27].

A few other techniques also exist for coatings, especially in the context of polymer coatings, such as powder coatings, dip coatings, spin coatings and spray coatings. Spin coating is one of the most well-known techniques for creating a coating of a polymer film

[28]. The basic principle of spin coating is as follows: a polymer in a solvent is dispensed on top of a wafer, which requires to be coated. The wafer is spun at a high speed, and the centrifugal force causes the solution to spread from the center to the outside. The solvent is chosen for its volatility, which means that it can be evaporated away quickly, leaving behind the polymer as a film [28]. Spray and dip coatings of polymers are also very effective. Powder coatings involve the application of a polymer powder on the target substrate, and heat or chemical treatment to bind the polymer to the substrate [29]. Spray coating involves a polymer in a solvent that is sprayed onto a substrate, and the solvent can be evaporated away, and dip coating involves dipping the substrate in a solution that consists of a solvent and a polymer [30]. Both techniques either involve the use of a volatile solvent, which results in fumes, or the need for chemical or heat treatment, which requires significant effect. Solvent free spray coatings exist, and will be covered in the context of thermal spray coatings. Therefore, naturally, there arises a question of creating coatings of polymers on different substrates without harmful vapours or fumes, or the need for special treatments

Thermal spray is an additive manufacturing/coating process that is used to propel materials (in powder form) through a jet of air or a chosen carrier gas, onto a target substrate. The impact converts the kinetic energies of the particles to heat, which causes localized softening and deformation of the particles, which flow over the substrate to create a coating[31–33]. Thermal spray can be used to create coatings of a variety of materials including metals, polymers, ceramics, composites and so on. Thermal sprays also have a significant advantage over other coating processes because they are comparatively simplistic processes and also allow for coatings and repairs on-the-go in the field. They are

also known for the thickness of the sprayed deposit, which is considerably higher than what is offered by electroplating, CVD or PVD processes, relative speed of the coating process and their versatility and compatibility with a variety of materials including metals, alloys, plastics, ceramics, and composites [34]. Thermal spray processes are used for a variety of applications ranging from functional (protection of the substrate from wear and corrosion) to aesthetic [35,36]. A variety of thermal spray techniques exist, such as high velocity air fuel (HVOF), high velocity oxyfuel (HVOF), flame, wire and plasma arc spraying, and cold spray [37,38].

It is worthwhile to briefly look at the different thermal spray techniques before moving to cold spray which forms the bulk of this dissertation. HVOF is a spray coating process where a fuel mixture (acetylene, propane, hydrogen or natural gas) undergoes a continuous combustion in a special designated chamber to provide a stream of hot gas at high pressure. The combustion chamber releases the products into a nozzle to create a spray at a speed approaching 1000 m/s [39–41]. After combustion, the coating materials are injected into this hot stream of air, which is passed through a nozzle and directed at a substrate. The hot coating materials are pushed against the surface of the substrate to form the coating. HVOF primarily works with metals like tungsten, chromium, aluminium, and zirconium [41] and some polymeric materials like nylon [42] if they are able to withstand the pressures and temperatures of the process without degrading. HVOF is primarily used for creating corrosion resistant coatings [43–45].

Plasma spray coating is the next type of spray coating. A plasma gun provides a high temperature DC/induction plasma capable of melting metals, ceramics, and polymers. Due to the high speed of plasma at the tip of the nozzle, the molten material is instantly deposited on the substrate. Plasma coating has a high strength of adhesion and wear resistance. The versatility of this technique means that different types of materials like powders, slurries and suspensions can all be sprayed [46]. Primarily used for nickel-chromium alloys [47,48], plasma coating is also used for polymers like PEEK and nylon for various applications including nonstick coatings, moldings, and moisture protection. Vacuum plasma coating in particular is used for surface modification of plastics, rubbers, metals, and fibers [49–51].

1.4 The Cold Spray Coating Technique

Cold spray, a type of thermal spray is the focus of this dissertation. It was developed at the Institute for Theoretical and Applied Mechanics at the Russian Academy of science. It is a thermal spray process where the powder materials that form the final coating remain in the solid state throughout the spray process. This ensures that problems such as oxidation, phase change, and property degradation that are generally associated with elevated temperatures and melting can be effectively avoided during the spray process [52–54]. Cold spray can be used to create coatings for aerospace, antibacterial and various protective coatings [55,56]. The main advantages of cold spray are the fact that there are no volatile organic solvents used in the process, which makes it viable as an environment-friendly process. It can also be used to coat large substrates under a variety of environmental conditions. Other benefits include the relatively low time frame of the

process and the relatively low-cost factor which has drawn considerable attention to research in this area [57–59].

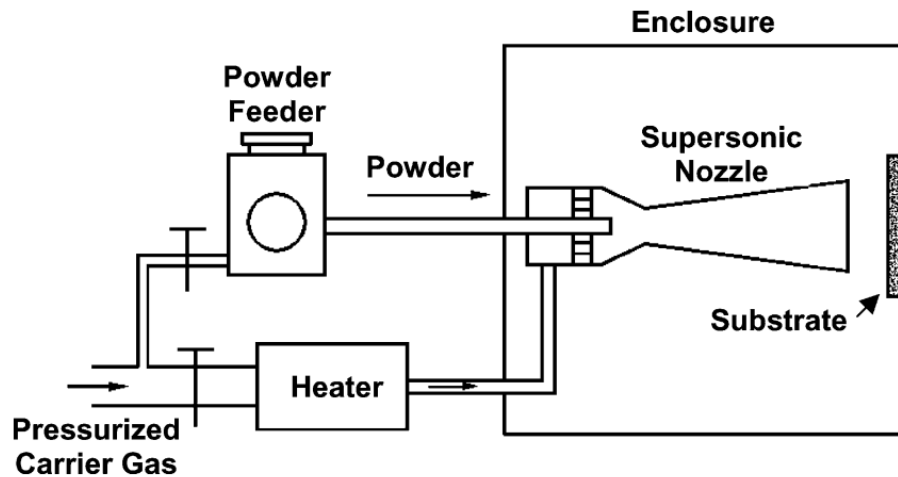


Figure 3: Schematic of a typical cold-spray system [60]

A typical cold spray system is depicted in figure 3. The setup consists of a hopper/powder feeder, a heater, a pressurized gas source and a nozzle. The nozzle is directed at the substrate or the target to be coated. The high-pressure gas is passed through the heater and accelerated toward the nozzle, eventually impinging on the substrate. The powder feeder contains particles in powder form that will eventually become the coating. This powder feeder is agitated as per requirements. The powder particles are dropped into the stream of pressurized gas, accelerated through the nozzle, and impact the substrate at high kinetic energies, which is rapidly decreased to zero. This causes the particle-substrate interface to soften, which leads to good bonding. Further discussion on bonding mechanisms is provided in subsequent paragraphs.

Early research studies in cold spray focused on depositing metal particles onto metal substrates [60–62]. Both computational and experimental studies showed that as the metal particle impacts the surface, the velocity of the particle very quickly decreased to zero [63]. As such, the large kinetic energy of the particle is transformed and this is seen in the large plastic deformation evident in a localized zone surrounding the particle-substrate interface. Consequently, a jet materializes at the interface, and carries material from both the substrate and the impacting particle. It has been theorized that this jet carries away the oxide layers and contaminants that are commonly present on the surface of metals. Hence, clean metal surfaces are brought into intimate conformal contact with one another, which results in excellent bonding. Sample images of metal particles impacting metal substrates are shown in figure 4.

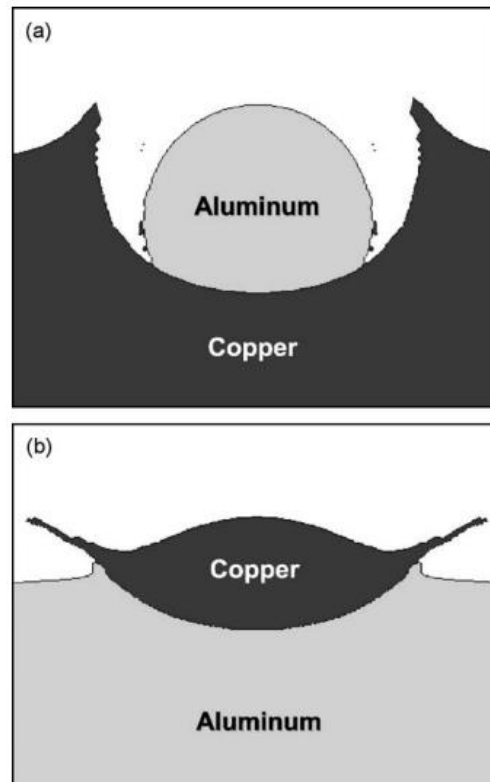


Figure 4: Shapes of powder feed particle and substrate crater formation 50 ns after impact for (a) aluminum particle impacting a copper substrate at 400 m/s and (b) copper particle impacting an aluminum substrate at 500 m/s [61]

The formation of a material jet at the interface is generally considered a precursor to good bonding, however, the actual bonding mechanism has been theorized in many forms including mechanical interlocking, adhesion, and interfacial flow/adiabatic shear instability [60,61,64,65]. Interfacial instability is the most promising bonding mechanism. The kinetic energy of the particle during impact is fully converted to heat, which results in localized plastic deformation of both the particle and the substrate. Due to the high speeds of the impact, the heat does not have sufficient time to diffuse far from the zone of the

impact, which coupled with the high shear rate (on the order of 10^9 s^{-1}) results in localized temperature rise and the formation of surface features on the surface of the substrate and the particle through perturbations. This manifests in the form of interfacial roll ups, that is, the surface of the substrate can have features like ripples or small microscale vortices as a result of the energies dissipated during the impact of the particle on the substrate. This in turn increases the surface area available for contact, and causes increased adhesion and mechanical interlocking at microscale [61]. Topochemical reactions and mechanical interlocking are considered bonding mechanisms for ductile materials. Metallurgical bonding along with mechanical interlocking drives bonding in metals, but polymeric materials, which are the focus of this dissertation do not possess the advantage of metallic bonding. However, multiple impacts of polymer particles can cause a peening effect which is beneficial to bonding [66,67]. Due to the large volume of particles impacting during the cold spray process, it is difficult to inspect the interaction between a single impacting particle and the substrate. There have been numerical studies that have looked at impacts of single particles on substrates [61,68,69] which clearly document the effect of particle velocity, temperature, physical properties, and the material type on the whole cold spray process, however, the studies are limited in capacity by the restrictions set due to the nature of the numerical simulations. More recently, single particle impact experiments have proven extremely beneficial in studying cold spray, in particular, understanding the interaction between a single particle and the substrate [58,70].

1.5 Polymer Cold Spray

Over the last few decades, cold spray research has focused on depositing metal particles onto metal substrates, but there is increasing interest in creating coatings of polymer powders onto various substrates [53,55,59,64,71]. The soft nature of polymers, lower thermal conductivity and differing intermolecular structure make polymers react differently than metals upon high-speed impacts onto a solid substrate [57,72]. Successful cold spray deposition of polymer powders is the result of extremely high strain rates experienced in both the impacting particles and substrate during deposition [73]. These high strain rates can lead to local thermal softening and large plastic deformation of both the particle and the substrate. At these strain rates, the heat dissipated upon impact does not have sufficient time to diffuse into the substrate or the core of the particle. This localized heating has been shown to lead to an adiabatic shear instability where the plastic strain releases heat in the particle and substrate leading to thermal softening of the solids, which in turn leads to further deformation, heat release and softening [74]. When both the particle and the substrate are polymeric, the high shear and mismatch in viscosity between the particle and the substrate can lead to a flow instability that can induce mechanical mixing, interlocking and entanglement between the polymer present in the impacting particle and the polymer of the substrate [61,75]. In addition, the peening effect caused by unsuccessful impacts of subsequent polymeric particles or hard inert particles added to the powder can enhance the plastic deformation, reduce surface roughness, and eliminate the pores between the deposited particles, making deposition more likely and the final deposition smoother and less porous [66,76].

The material properties of the polymer particles also introduce boundaries on the external, physical parameters of the cold spray process. Generally, supersonic velocities are required to deposit metal particles onto metal substrates. In polymers, however, deposition can be achieved using subsonic velocities at an order of magnitude lower than those required for metal particle cold sprays, which is extremely beneficial, as disruptive phenomena such as shocks can be eliminated [61,77]. The temperatures of the polymer particles and substrates should also be kept relatively low as compared to metal substrates, to avoid melting and degradation of the polymer. Early literature in this field showed the polymer-on-polymer deposition had a process efficiency (defined as the ratio of the mass of deposition to the overall mass of the powder used) of 0.5% [57,78]. In comparison, metal particles can be deposited onto metal substrates with an efficiency of close to 100% [55,79,80]. Further research showed that deposition efficiency can however be improved to up to 10% by choosing the right polymer powder (high density polyethylene or HDPE for short) and the right polymeric substrate (low density polyethylene or LDPE for short) [72]. Deposition efficiency, however, is not fixed, and varies significantly based on process parameters. An example of variation in deposition efficiency is shown below in figure 5, where it varies as a function of the velocity with which the cold sprayed particle impacts the surface of the substrate for various like on like depositions, that is, the particles and the substrates are made of the same material.

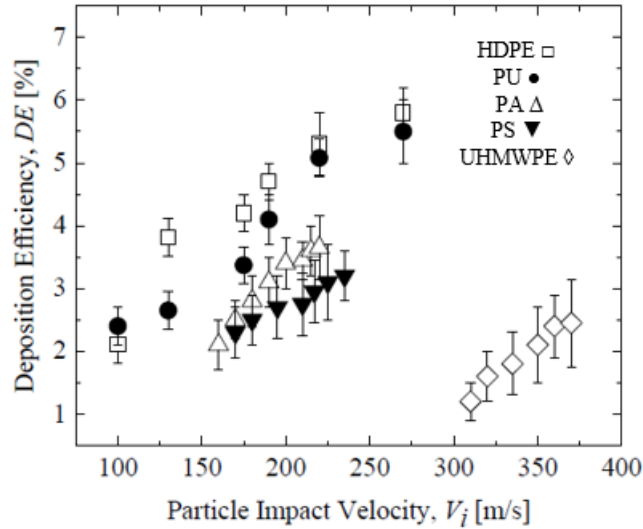


Figure 5: Deposition efficiency as a function of particle impact velocity for like on like deposition [77]

Emerging literature has also extensively documented the parameters such as particle velocity, temperature, angle of impact, particle size and type for creating depositions of other polymers such as ultra-high molecular weight polyethylene (UHMWPE), polyacrylamide (PA), polystyrene (PS) and polyurethane (PU) [58,66,72,77]. It is important to note that there exist specific ranges of parameters for successful polymer cold spray deposition. Going above a certain temperature can cause the polymers to become tacky or degrade, affecting the flow of the powder out of the hopper. There is a critical minimum velocity for successful deposition, however, there also exists a maximum value above which the air stream can impact stresses onto the existing deposition and cause them to be removed from the substrate. This range of parameters is known as the deposition window and a sample deposition window is shown in figure 6. Similarly, the distance between the nozzle tip and the substrate, also known as the standoff distance, and the angle of the substrate relative to the nozzle/air stream can also drastically impact deposition.

Adding inert peening particles to the polymer powder was also found to positively influence deposition because of the beneficial compressive stresses induced in the particle [66,77].

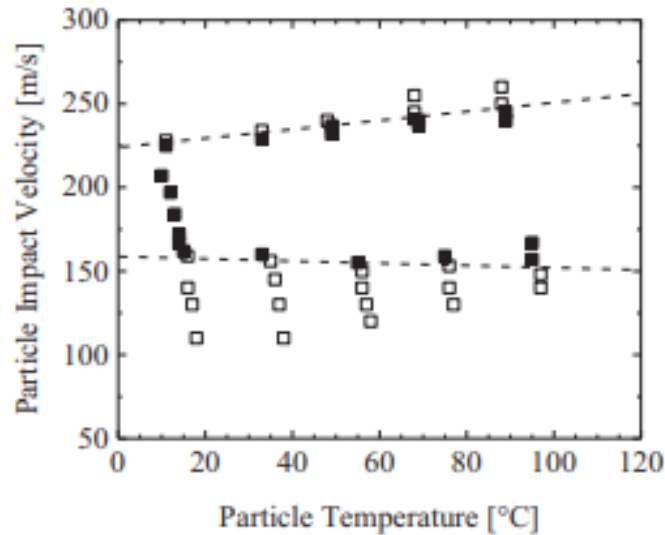


Figure 6: Deposition window as a function of particle impact velocity and particle temperature for polystyrene particles cold sprayed on LDPE substrates [77]

Previous research from our lab focused exclusively on polymeric cold spray. The first research study focused on building an in-house cold spray system that was able to reliably spray polymer powders [81]. This system is also used in the experiments that form this dissertation. High Density Polyethylene (HDPE) was sprayed onto a variety of substrates such as Low-Density Polyethylene (LDPE), PolyVinyl Chloride (PVC) and PolyOxyMethylene (POM) and HDPE. It was observed that increasing the temperature of the particles decreased the critical velocity of deposition (critical velocity is the minimum velocity required for successful deposition). The critical velocity was in the range of 100-500 m/s. The particle temperature was capped at 70°C above which the particles became

tacky and didn't flow well. Similarly, different nozzles were used in the study, including a converging-diverging nozzle which was removed in subsequent studies because of the risk of shock waves that could potentially damage a good deposition. Optimizing the spray parameters (keeping the particles at 50°C, velocity at 162 m/s, and standoff distance between the nozzle and substrate at 15 mm), researchers were able to obtain a deposition efficiency of ~8%, for depositing HDPE particles on LDPE substrates.

The next study focused on depositing Polyacrylamide (PA) and Polystyrene (PS) particles on LDPE, PA, and PS and comparing them to single particle impact experiments [58]. It was noted that the cold spray critical velocity of 160 m/s (PS on LDPE) and 150 m/s (PA on LDPE) was different from the single particle impact critical velocity of 120-140 m/s (PS on LDPE) and 170-180 m/s (PA on LDPE). Deposition efficiency was similarly capped at 5% for the cold spray process whereas 100% was seen in single particle tests. Like-on-like deposition was seen in cold spray but not in the single particle tests, which was attributed to enhanced plastic deformation of the particle and the substrate, and the effect of successive particle collisions. Plastic deformation in particles from single impact tests were comparable to the plastic deformation seen in simulations [82]

Next, an extensive parametric study was conducted looking at the deposition of HDPE, PA, PS, Polyurethane (PU) and Ultra High Molecular Weight Polyethylene (UHMWPE)[77]. It was seen that PU particles had a minimum velocity for successful deposition on LDPE and PU substrates, whereas on PVC and POM substrates, it had a

window of velocities within which successful deposition occurred. PA particles, similarly, had a minimum velocity for deposition on LDPE, and a deposition velocity window for PA, PVC, and POM. Polystyrene had a deposition window on all substrates (LDPE, PS, PVC, and POM). Highest deposition efficiencies were seen under optimized conditions for HDPE impacting LDPE (~8%) and HDPE impacting HDPE (~5.6%) at a spray velocity of 270 m/s, particle temperature of 80°C and substrate temperature of 100°C. It was also noted through SEM studies that the porosity of the deposit decreased once the spray conditions were optimized. Cold spray of polymers is particularly interesting and warrants a lot of study because mechanical properties including hardness, elastic modulus and tensile strength were found to be nearly the same for cold sprayed and their corresponding melt-cast samples. HDPE powders were melt-cast into blocks, and correspondingly, HDPE powders were cold-sprayed onto HDPE substrates. The samples were attached to a dog bone and tested in tension. All the samples showed cohesive failure within the cold spray deposit, and no detachment of the deposit from the substrate, indicating a strong bond between the particles and the substrate. A schematic of the tensile tests performed on cold sprayed and melt-cast samples, and the corresponding stress strain curves are shown in figure 7. Similar results were observed for cold-sprayed and melt cast samples of other samples as well [77].

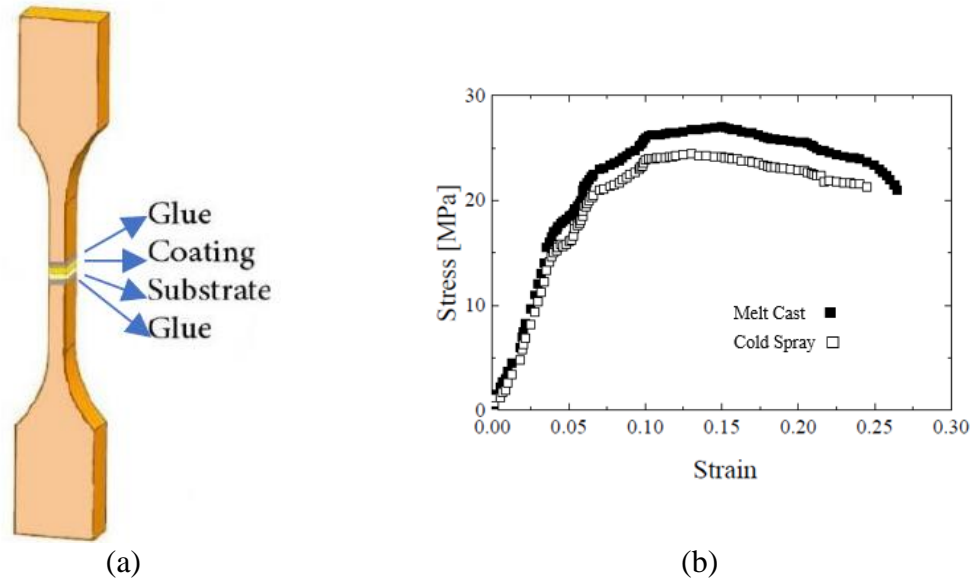


Figure 7: (a) A representation of the tensile tests on cold spray specimens and (b) stress-strain curves on cold sprayed and melt cast samples of HDPE [77]

Finally inert glass particles were added to the cold spray particles to investigate the effect of peening on deposition. This significantly improved the deposition efficiency with the highest efficiency reaching ~11% for HDPE particles impacting LDPE substrates. It was observed that a weight percentage of 10-20% was the ideal amount of glass particles to be added to the cold spray powder. When a subsonic nozzle was used, the glass particles didn't deposit along with the polymer particles whereas there was some deposition of the glass particles when a supersonic nozzle was used [66].

More research is emerging in the field of polymer cold spray. Researchers have sprayed PolyEther Ketone Ketone (PEKK) onto different grades of PEKK substrates, with a process efficiency approaching 75%. It is to be noted that the spray temperatures (150-200°C) and pressure upstream of the nozzle (6-10 bar) is considerably higher than what has

been previously tested for polymer cold spray. The degree of crystallinity of the polymer also played a significant role in deposition, with low crystallinity being correlated with high deposition efficiencies and lower porosity [83]. Numerical studies looked at impacts of polymer particles onto polymer substrates. While the substrate deformed more as a result of increasing particle diameter, the simulations showed that there was a specific particle diameter (40 nm) for which the critical velocity required for successful deposition was minimum. Continuing with the simulations, it was seen that when spraying (Polyethylene Ether Ketone) PEEK and Acrylo Butadiene Styrene (ABS) particles onto PEEK substrates, plastic deformation governed the bonding between the particles and the substrates whereas when copper particles were sprayed onto PEEK substrates, mechanical anchoring was the primary bonding mechanism. Thermal gradients within the particle during cold spray were also studied. Particles with thermal gradients had higher strain localization at the zone of higher temperature. The conclusion that particles with a warm, soft outer layer outperformed a particle with a cold hard layer in terms of adhesion was drawn. However, it was noted that these simulations were performed under idealized conditions and under a specific set of assumptions that cannot be translated to real-life cold spray conditions [68,69,84,85].

Single particle micro-ballistic experiments also provide valuable insights into the cold spray process. The experiment is termed LIPIT (Laser Induced Particle Impact Test) where an ablation laser pulse (5-8 ns pulse duration) is created using a Neodymium doped Yttrium Aluminum Garnet laser to accelerate a single particle placed near the focal point of the laser ablation on a PDMS substrate. A femtosecond laser source is combined with

three electro-optic modulators to provide imaging up to 40 million frames per second. A photonic crystal fiber is used to convert the laser pulses to white light, thereby ‘imaging’ the particle and its trajectory. It was noted, from experiments comparing the single impact tests and the cold spray process, that both methods yielded similar critical velocities for Polyacrylamide and Polystyrene particles. However, there is a 100% deposition efficiency in the LIPIT experiments as compared to 5% for cold spray, which was attributed to differences in LIPIT and cold spray such as the effect of subsequent particle impacts and airflow being eliminated in LIPIT. The peening effect of subsequent particles not being present in LIPIT also was the reason that like-on-like deposition was not observed in LIPIT but was seen in cold spray, because the peening effect causes enhanced plastic deformation in both the primary particle and the substrate. Plastic deformation of the particles on impact using LIPIT was found to be comparable to plastic deformation values obtained through CFD simulations of cold spray [58].

Pre-heating the powder particles was shown to benefit the deposition process and mechanical strength in low-pressure cold spray systems. In high-pressure systems, however, the pre-heating had the opposite effect, attributed to the plastic deformation happening away from the particle-substrate interface. The authors note that pre-heating in high-pressure systems may cause clogging in the nozzle, which is detrimental to the flow [86,87]. Lastly, the effects of molecular weight on deposition were also studied. Low molecular weight PS was sprayed onto PS substrates, and it was seen that because of the low molecular weight, there was less resistance to plastic deformation and fracture, correspondingly higher failure, and fragmentation upon impact. The fragmented pieces act

as precursors to subsequent impacting particles to aid deposition. Higher molecular weight PS is more ductile and resistant to deformation, and therefore undergoes more plastic deformation, but still has insufficient thermal softening that is necessary for good deposition [88,89].

Cold spraying composite materials is especially useful because the relatively low temperatures used in cold spray ensure that the original properties of the materials and the microstructures can be safely preserved without detrimental effects like oxidation or phase transition [90]. Metal-ceramic composites, when cold sprayed, showed increased deposition efficiency with increasing the concentration of ceramic particles, however, there seemed to be an optimum volume fraction of ceramic particles for it to have a positive impact on deposition. Similarly, an optimum concentration of ceramic particles was necessary to have sufficient metal particle-metal substrate contact necessary for good adhesion [91]. Spraying metal particles and metal composite powders on polymer substrates is different from spraying polymers onto polymer substrates. The primary bonding mechanism for metal on polymer cold spray seems to be the softening of the substrate and the mechanical interlocking of the metal particle in the polymer substrate. There exists a critical window of parameters for successful deposition for parameters like particle velocity and temperature, above which the particles tend to erode the substrate. Specifically, in cases of depositing mixed metal powders on carbon fiber reinforced epoxy, it was found that having a low-pressure cold spray system resulted in good deposition [92]. The bonding mechanism in metal-composite cold spray is not fully understood, but can be inferred to be significantly different than metal-on-metal cold spray bonding. The current idea is that mechanical bonding is what exists between cold sprayed composites and the

substrates. Since this is weak and has low bonding strength, it is worth exploring this field of study to see if bonding strength can be improved. Researchers suggest multiple step processes for cold spray such as cold spray and ultrasonic rolling, cold spray and laser remelting or post spray treatments of the substrates to ensure good adhesion between the particles and the substrate [93,94].

1.6 Introduction to Composite Materials: Silica Nanoparticles

Finally, this literature review must focus on understanding composite materials because of the variety of benefits they offer and their versatility in engineering applications. Composite materials can be used to enhance the physical and chemical properties of the base material. A composite material comprises of a base matrix, and the filler material, usually nanoparticles, and together they form the composite. In the particular case of this dissertation, HDPE is going to form the base matrix, and the filler materials will be Silicon Dioxide (SiO_2), otherwise known as silica, copper nanoparticles, and carbon nanotubes. Each of these materials are chosen for their unique properties and characteristics, and their propensity to form composite materials, which are explained in the following paragraphs. Silicon dioxide (SiO_2) nanocomposites have been shown to be part of high performance functional coatings of organic/inorganic hybrid materials. Combining SiO_2 with a polymer matrix is a reliable way of obtaining increased tensile strength and impact resistance. Silica nanocomposites can also be used as carriers for other functionalities to the composite coatings and act as a resistance to the wear and degradation of the overall coating [95]. Though the degree to which SiO_2 benefits the base polymer matrix highly depends on the mode of formulation of the composite material, all techniques of composite material

making have been shown to improve the mechanical properties and thermal stability of the overall coating, and SiO₂ nanocomposites have properties that are superior to the pure polymer matrix [96,97].

SiO₂ nanoparticles have benefits that far exceed the mechanical benefits and their ability to form nanocomposites [98,99]. The surface of the nanoparticle can be functionalized in many ways during synthesis to achieve the desired characteristics [100]. It was shown that silica nanoparticles can be functionalized to load and release ibuprofen as a drug [101]. They can also be functionalized to encapsulate quantum dots and magnetic nanoparticles [102]. Emerging research also shows that other polymers can be selectively grown on the surface of the silica during synthesis for the detection of neurotransmitters [103]. Silica nanoparticles are promising carriers for drug delivery [104,105], and the entrapment of drugs in silica has been shown to increase drug delivery, absorption, dissolution and decrease the toxicity of the drugs, because of their potential to have good biocompatibility [106,107]. Silica nanoparticles also have excellent applications in agriculture [108,109]. Seeds treated with silica show greater resistance to fungi attacks, and have higher nutritional content and germination rate [110,111]. Silica when combined with polymers also increases the toughness and showed increased resistance to friction and wear [112,113] and silica-polyethylene glycol composites are also agents for enhanced oil recovery, and can act as stabilizers for foams and emulsions [114,115].

1.7 Copper Nanoparticles for Composites

In a similar manner, copper nanoparticles have their own unique benefits, ranging from the physical to the biological [116,117]. Particularly, copper, in the nanoparticle form has been shown to inhibit bacterial growth [118,119], and serve as drug delivery agonists in the realm of cancer therapeutics [120]. Copper nanoparticles, when part of a composite, have also been shown to have reliable antifungal and bacteriostatic properties, thus making them very useful. Copper nanoparticles are also extremely effective in protective coatings. It was seen that copper nanoparticles as part of a wound dressing increased the healing rate, because of copper's ability to inhibit the formation of proteins [121]. Dispersing the copper into the polymer matrix is a proven way of ensuring that copper can still exhibit its properties while not leeching into the surroundings. This makes copper nanocomposites useful in a variety of scenarios [122–124]. This is primarily due to the interactions between the polymer and the copper particles which increases the antibacterial capacity of the composite over time [125], the capability for long term ion release [122], and the increase in surface area with the dispersion of copper nanoparticles [126]. Copper nanocomposites can serve to reinforce other materials, or can be combined with other materials to be reinforced themselves [127]. Compounding carbon nanotubes with copper through electrodeposition has shown to increase the strength of the composite material by three times over that of pure copper [128].

1.8 Carbon Nanotubes as Composite Filler Materials

Carbon nanotubes are perhaps some of the most versatile materials available today. They are also excellent choices as filler materials in composite material production because

of their sheer versatility, and the potential benefits they offer such as increased strength, toughness, thermal and electrical conductivity [129,130]. Carbon nanotubes are formed by rolling sheets of graphene into tubes, and they exist in multiple forms: single walled, double walled and multi walled. The direction in which the sheet is rolled greatly influences the physical and chemical properties of the tubes [131]. Arc discharge and laser ablation are the first methods used to synthesize carbon nanotubes [132–134] and work by the condensation of carbon at elevated temperatures in the gaseous phase, which is obtained by the evaporation of solid carbon. However, in the past few decades, techniques like high pressure catalytic decomposition and various types of CVD have also emerged as promising techniques [135–138].

The direction in which the graphene sheet is rolled dictates both the shape and the properties of the nanotube. In general, there are 3 types of nanotubes based on the chirality indices: armchair, chiral, and zigzag, as represented in figures 8 and 9 [139,140]. The chirality vector is denoted by a pair of indices n and m which are the number of unit vectors along the two directions in the lattice structure of graphene. If $m = 0$, the nanotube is called ‘zigzag’ if $m = n$ it is called ‘armchair’ and every other combination of the indices is termed a chiral orientation [141]. A good example of the structure influencing the properties of the CNT is the electrical transport. Not all CNTs are capable of electrical transport. Armchair CNTs with $|n - m| = 3i$ are metallic conductors. Zigzag CNTs with $|n-m| = 3i \pm 1$ are semiconductors and chiral CNTs are metallic conductors only if $2n + m = 3i$, else they are semiconductors, where i represents an integer [142].

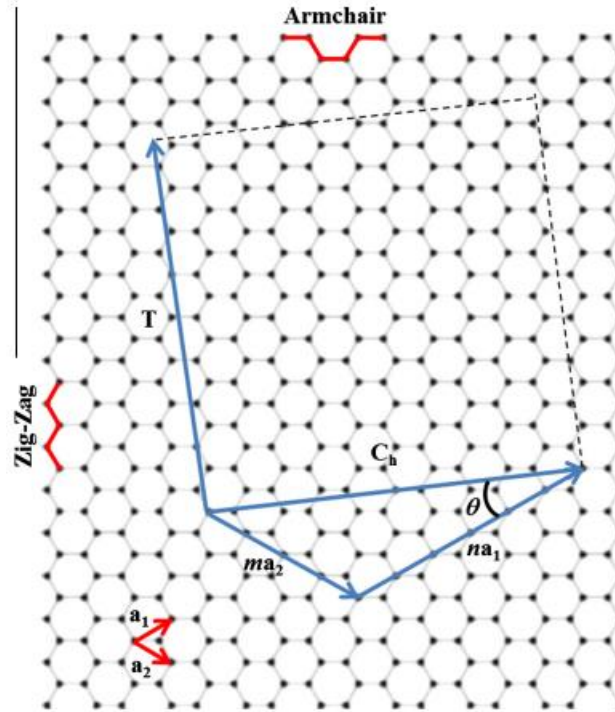


Figure 8: Chirality indices in a sheet of graphene [139]

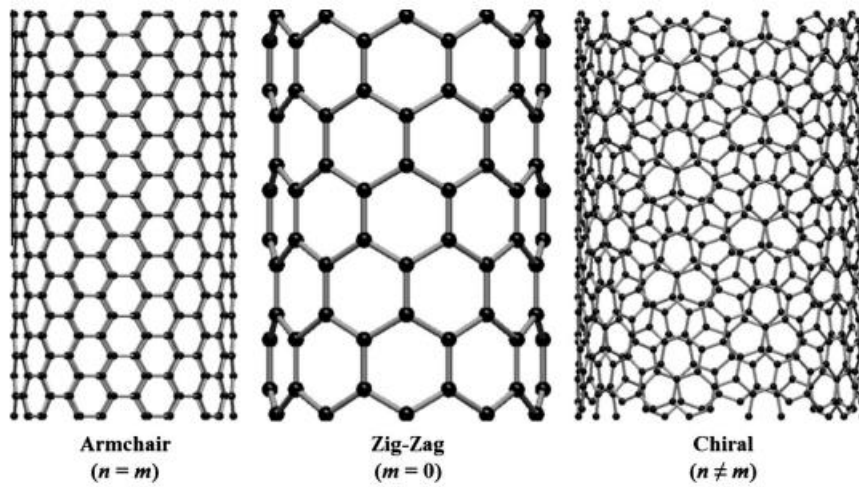


Figure 9: Different type of CNT structures [139]

Carbon nanotubes can be combined with polymers like polyethylene to form PE-CNT composites that have a variety of benefits [143]. However, it is not always the case that adding carbon nanotubes to polymers can have a linear increase in the properties. Similar to other filler materials for composites, carbon nanotubes offer their benefits, albeit preferentially, and the potential for increased properties like strength and conductivity heavily depends on the mode of processing of the composite. [144,145]. For example, the mechanical benefits that CNTs offer, like their increased strength and toughness, especially along the length of the tube, is highly dependent on both the type of nanotubes used and the process in which they are combined with the polymer to form composites. Shaffer and Windle's characterization of CNT-polymer composites [146], one of the first on the subject showed that the stiffness of the composite material was quite low, and it was theorized that the low value was more dependent on poor stress transfer than the nanotube themselves. Also, a fact that was interesting and relevant was that the nanotubes were more active in their role of reinforcing the polymer above the glass transition temperature of the latter. Further research on CNT-polymer composites made by solution-mixing and drop casting showed that 1 wt% CNTs can increase the Young's modulus by a factor of 1.6-1.8, thereby having a significant impact on the properties of the material [147,148]. Similarly, other researchers have noticed increases of 36% and 42% in the stiffness of the composite upon 1wt% addition of multiwalled CNTs [148–150]. Increases of ~90% and higher in the modulus of the composite material are possible at higher loadings of CNTs, approaching 10 wt% [151–153]. The highest numbers observed were Young's moduli of about 80GPa and tensile strengths of 1.8GPa, which further reinforces both the utility of CNTs, and their applications in a wide variety of situations [154,155]. It is also quite vital to observe and

study the failure of composite specimens to understand how CNTs reinforce the polymer matrix. In a landmark study on failure of CNT-polymer composites using TEM to initiate a crack in the specimen, it was observed that cracks often originated in regions of low CNT concentration, and propagated along the CNT-polymer interface or in regions of low CNT density. Along the failure line, it was also seen that CNTs either broke or pulled out of the matrix, suggesting the need for more homogeneity and purity in the CNTs, and a chemical bond between the CNT and the polymer via functionalization of the CNTs to improve the mechanical properties of the composite [149].

CNTs are also known for their electrical conductivity, and correspondingly, the electrical conductivity of CNT-polymer specimens is well documented in the literature. It has been noticed, especially that the conductivity of the polyethylene-CNT composite matrix has a sudden increase by several orders of magnitude beyond a critical concentration of CNTs in the PE matrix. This has been termed the percolation threshold and has been observed by many researchers [156–159]. Longer CNTs generally show a lower percolation threshold in polymer matrices as compared to their shorter counterparts [160,161]. Carbon nanotubes are used especially for being incorporated into bulk polymers that have extremely low conductivity themselves, in order to improve the transport of electricity through the polymer matrix. This is particularly useful in cases where there should not be an electrostatic buildup in a component that interferes with regular working, for example, in radar systems, where an electrostatic charge buildup can interfere with the communication frequencies. Hence it is important to not just understand the percolation

and electrical conductivity, but to choose the type and dimensions of the CNT carefully for the desired application.

1.9 Scope of the Dissertation

As summarized above, there has been significant research in the field of cold spray specifically with polymer powders. Metal-on-metal cold spray has been extensively investigated and the process has been thoroughly optimized to ensure the highest levels of deposition efficiency. Polymer-on-polymer cold spray is not as efficient as metal-on-metal, however studies in this area are gaining traction. There is also some research into depositing metals or metal-polymer composites onto polymeric substrates using cold spray [64,67]. However, the literature in polymer-on-metal cold spray is scarce, owing to the difficulty in the technique itself and the mismatch in the material properties of the polymers and metals. HDPE particles were deposited onto metal substrates using cold spray in research by Alhulaifi et al [162]. There was a minimum critical velocity above which deposition occurred and the efficiency of the process was not mentioned. At higher velocities, however, as was mentioned earlier, it was noticed that the jet of air tended to dislodge the particles from the metal surface. Cold spray was also used to deposit UHMWPE particles onto aluminum substrates, but alumina powder was mixed with the polymer particles to promote inter-particle bonding. Finally, Sulen et al deposited Fluoroethylene Propylene (FEP) on aluminum substrates. The process had an efficiency of about 0.1% and showed very poor adhesion, where the deposited particles were easily stripped from the surface of the substrate [163].

To that extent, this dissertation focuses on polymer cold spray. The first set of experiments focuses on depositing polymer particles on metal substrates using the cold spray technique. HDPE particles are sprayed onto aluminum substrates. A few parameters are looked at for their ability to influence deposition such as particle temperature, substrate temperature, substrate roughness and topology, and the presence of an intermediate primer polymer layer on the substrate to boost deposition [76]. The strength of adhesion of the polymer deposition to the substrate is also characterized and analyzed using adhesion tests, and inferences are drawn to understand the extent to which these parameters influence deposition. This dissertation also focuses on various types of polymer composite powders (polymer-SiO₂, polymer-Cu and polymer-CNT nanocomposites) and the feasibility of the cold spray process in creating coatings of these powders on polymer substrates. Absent from the literature are studies focusing on cold spray of polymers on metal substrates and the use of cold spray to create polymer composite coatings. Hence, the aim of this dissertation is to address the gap in literature.

CHAPTER 2

EXPERIMENTAL SETUP AND CONDITIONS

2.1 Polymer Powder and Synthesis

High Density Polyethylene particles (BYK Ceraflour 916) particles are used as the feed material for all experiments. They had an average particle size of $48\mu\text{m}$ and a density of $\rho = 990\text{kg/m}^3$, a melting point of $T_m = 128^\circ\text{C}$ and a glass transition temperature of $T_g = -90^\circ\text{C}$. Silicon dioxide (SiO_2) and copper (Cu) particles were added to HDPE to create composite powders. SiO_2 particles came in two types: $8\mu\text{m}$ spherical particles (Degussa SIPERNAT 22LS) and fumed silica nanoparticles created by sintering 12nm diameter base particles together to form catenoid shaped particles roughly 200nm in length (Degussa AEROSIL200) [164]. A TEM image of the 12nm silica particles from Albers et al [164] is provided in figure 10 below. Both SiO_2 particles have a density of $\rho = 2650\text{kg/m}^3$. Moving forward, in order to differentiate the composites powders made from the two different SiO_2 particles, the composite powders will be designated micro- SiO_2 and nano- SiO_2 . The copper particles (US Research Nanomaterials Inc) are spherical with a diameter of 40 nm and a density of $\rho = 8000\text{kg/m}^3$. The four step process to making the composite powder is described below:

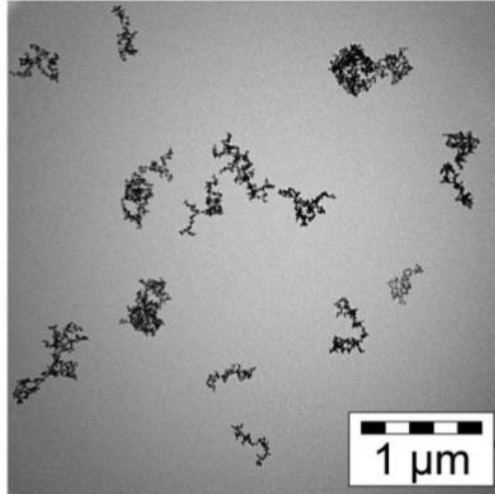


Figure 10: A TEM image of the 200 nm silica particles [164]

2.2 Silica and Copper Nanocomposite Synthesis

The nanocomposite powders are synthesized by mixing the appropriate filler material (silica or copper) with HDPE in a predetermined mass ratio and then put in an oven before ball milling into the composite powder. The 4 step process is outlined below:

Step 1: The SiO_2 and Cu particles are added to HDPE in predetermined mass ratios ranging from 0.5g to 10g of added particles per 100g of HDPE. The mixture is then stirred manually at room temperature to coat the HDPE powder with SiO_2 and Cu particles.

Step 2: The mixture is placed in a 110°C oven for a total of 60min to make the HDPE powder tacky with a manual stirring every 15 min to improve SiO_2 and Cu particle adhesion to the HDPE powder.

Step 3: Next, the mixture is put into a ball mill (Leegol Electric) and milled overnight to produce the final composite powders.

Step 4: Finally, the powder was sieved through a Winco MS3A-8S double fine mesh to remove any large clumps of powder and verified under microscopes to confirm the formation of composite powders. This process is represented in figure 11.

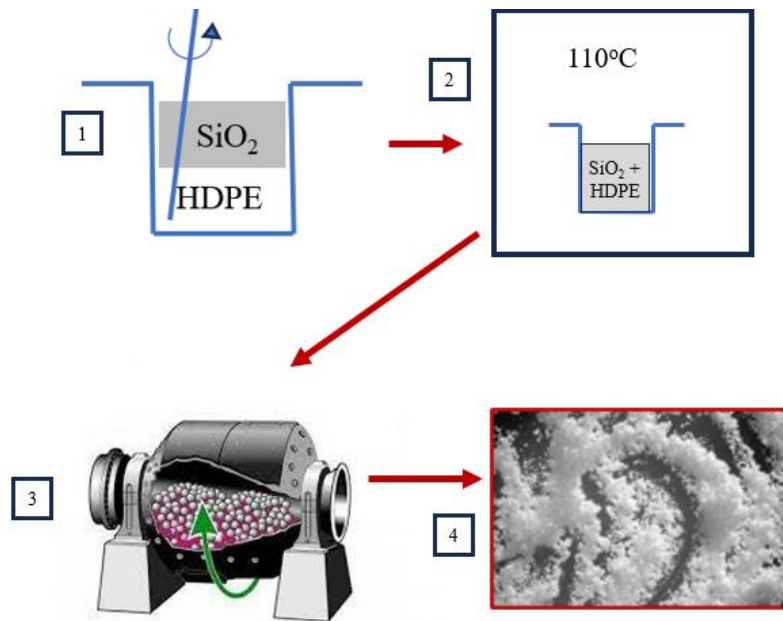


Figure 11: A pictorial representation of the 4-step process required to make the micro and nanocomposite powders

The results are represented using mass fractions of SiO₂ or Cu per 100g of HDPE powder, and the fractions are calculated based on the mass ratios previously mentioned. Special care was taken to ensure that the mass of the HDPE and the SiO₂ or Copper particles was conserved during the heating and milling processes, that is, all the SiO₂ or Copper made it to the surface of the HDPE during the aforementioned processes [165].

Scanning electron microscopy (SEM) images of each of the composite powders were taken using a (Magellan 400 Scanning Electron Microscope) set at 1kV. The images are presented in Fig. 12. The SiO₂ particles can be seen in Fig. 12(a) and 14(b) on the interface of the HDPE particles. In Fig. 12(d), an SEM image of pure HDPE powder is presented to serve as a reference. In 12(a), the relatively large 8μm particles appear as discrete spherical particles randomly distributed over the surface of the HDPE. The smaller SiO₂ particles in Fig. 12(b) are also visible because, as discussed previously, the 12nm base SiO₂ particles have been sintered together to form larger particles roughly 200nm in size. The location of the SiO₂ particles on the surface of the HDPE is stochastic in nature with some aggregation of the nanoparticles evident in Fig. 12(b). Using ImageJ to calculate the fraction of surface area covered by the SiO₂ particles in these and other SEM images results in a surface coverage of roughly 6% for the micro-SiO₂ and 20% for the nano-SiO₂ composites with mass fractions of 9.1% and 0.99% respectively. These values are consistent with our calculations of expected surface coverage presented in chapter 4 assuming all the SiO₂ particles are located on the surface of the particles. Note that due to their smaller size, even at a much-reduced mass fraction compared to the 8μm particles (0.0099 versus 0.091), a much higher surface coverage of the HDPE base particle can be observed when using the nano-SiO₂ particles. Finally, in Fig. 12(c), the copper particles are not visible directly because they are below the resolution of the image. The presence of the copper particles will be definitively demonstrated in the results section through SEM imaging and EDS of the cold spray depositions.

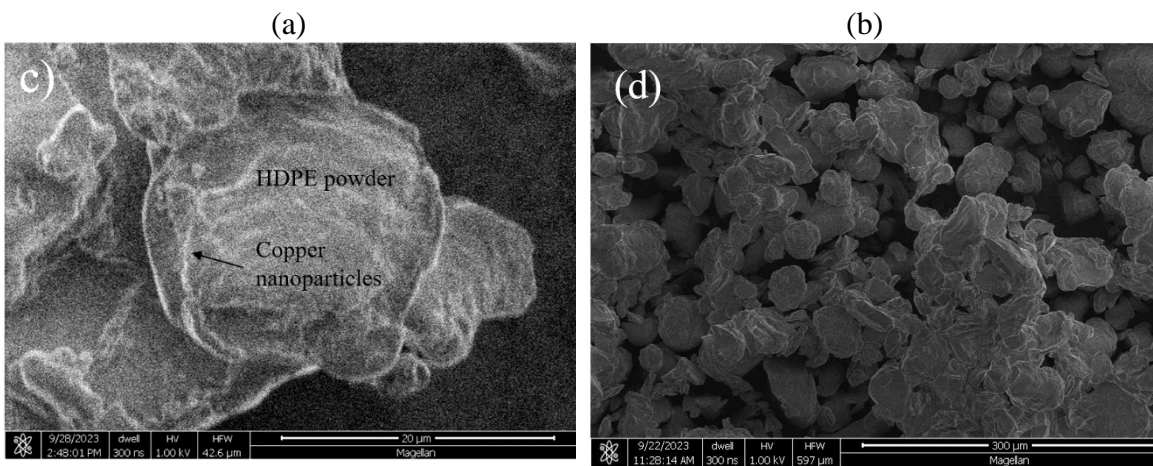
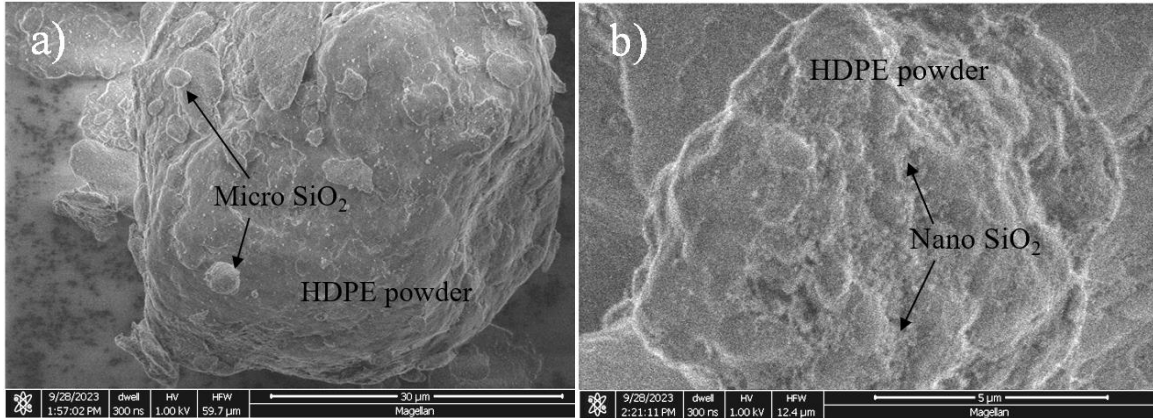


Figure 12: SEM images of the composite powders used in this dissertation. The images include (a) micro-SiO₂ particles in HDPE, (b) nano-SiO₂ particles in HDPE and (c) 40 nm Cu particles in HDPE at mass fractions of 9.1 %, 0.99 % and 1.96 % respectively and (d) milled pure HDPE powder

2.3 CNT-HDPE Composite Synthesis

For the CNT-HDPE composite, research grade multiwalled carbon nanotubes (CNT) of 95% purity (XFNANO advanced materials) were purchased online from Amazon. The tubes have an outer diameter of 10-20 nm and inner diameter of 5-10nm, and are of average length 0.5 – 2μm. The density is $\rho = 2100\text{kg/m}^3$ and the electrical

conductivity is quoted as $EC > 100 \text{ S/cm}$. The 6-step process required to make the CNT-HDPE composites is described below:

Step 1: The CNTs are initially put in Toluene to form a 1:20 solution by mass (1 part of CNT to 20 parts of Toluene). Appropriately, HDPE is measured to form composite powders ranging from 0% CNT to 3.85% CNTs in HDPE by mass. The HDPE is mixed with CNT-toluene slurry by hand.

Step 2: The mixture is pressed into a sheet in a vacuum hot press that operates at 90°C and 35mm Hg of vacuum for 15 minutes.

Step 3: The sheet is then removed from the press and is cut into 4 pieces that are stacked on top of each other.

Step 4: The stack is pressed in the hot press under the same process conditions for the same duration. The cut, stack and press process are repeated twice for a total of 4 presses. The solution is carefully measured to ensure the toluene is removed as much as possible.

Step 5: The final sheet is ground into a coarse powder using an electric coffee grinder (Cuisinart electric coffee grinder – DCG-20BKNTG) and then milled into a fine powder using a ball mill (Leegol Electric) overnight.

Step 6: Finally, the resulting powder was sieved through a Winco MS3A-8S double fine mesh to remove any clumps and is verified to validate the presence of CNTs using microscopy. The process is represented in figure 13. Scanning Electron Microscopy of the powders at 3.85% loading concentration taken using a Volumscope 2 SEM is shown in figure 14.

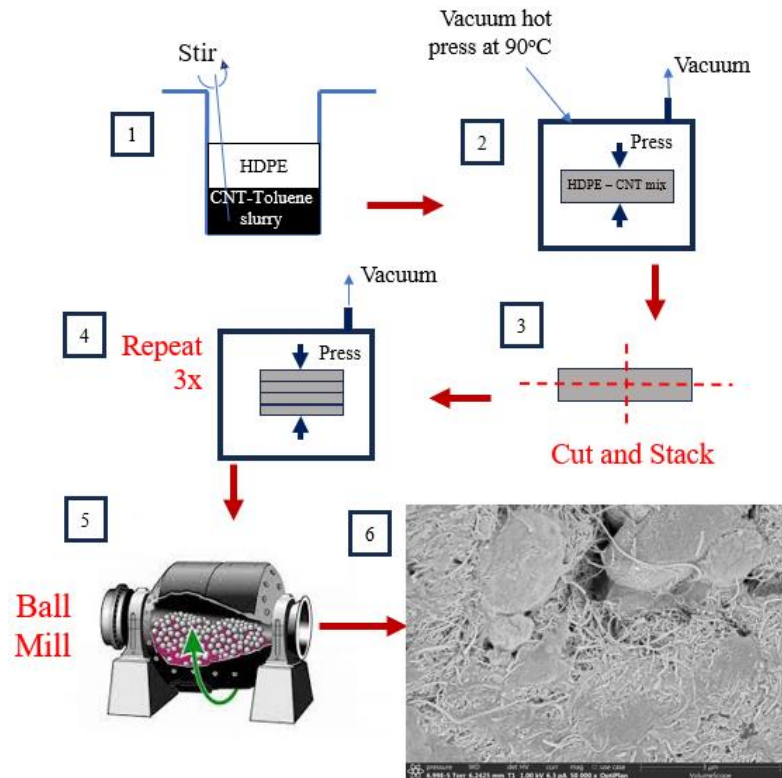


Figure 13: A pictorial representation of the 6-step process for making the CNT-HDPE composite powders



Figure 14: Scanning Electron Microscopy image of the surface of CNT-HDPE composite powder. The CNTs are visible as threads that are pressed into the HDPE powder surface

2.4 Electrical Conductivity Experiments

Melt-cast samples are prepared for the conductivity experiments. For the conductivity experiments, a mold of 5 cm long, 3 mm wide and 3 mm deep is fabricated using 3D printing (Bambu lab X1 carbon). The mold is made using thermoplastic polyurethane (TPU) which is a rubbery material that allows for good de-molding of the melt cast sample. Wires were attached to both the cold sprayed and melt cast samples at intervals of 5 mm distance using MG 8331D conductive epoxy. The wires were attached to a Keithley Sourcemeter S4200 two point probe to ensure that the distance between the two points of the measurement points on the sample is always 5 mm. A voltage of 10-30 V was passed through the sample in intervals of 0.25V for a total of 41 measurements. The current was measured by the probe and plotted against the input voltage to measure the resistance of the sample. The conductivity of the sample was then calculated using the resistance, the cross sectional area and the distance between the probe points.

2.5 Metal Substrate Preparation

For the metal substrates, Aluminum 6061 sheets were purchased at the local hardware store. They were cut into sheets of 2.5cm x 7.5 cm. The sheets were roughened using sandpapers of varying grit designations (50, 240, 360 and 800) for 30 seconds using steady pressure in either a unidirectional back-and-forth manner or a random pattern. A Zygo Nexview 3D Optical Profilometer was used to estimate the surface roughness and the resulting topography of the substrates after scratching. The surface roughness values are catalogued in the table below. In general, as the grit designation increased, the surface

roughness decreased because higher grit sandpapers tended to be finer. The roughness values are tabulated in Table 1.

Sandpaper grit designation	Randomly scratched surface roughness [μm]	Unidirectionally scratched surface roughness [μm]
No treatment	0.35	
50	0.92	1.98
240	0.63	0.92
360	0.47	1.02
800	0.34	0.36

Table 1: List of sandpaper grit designations and the corresponding average surface roughness values

For the final part of the study, a primer polymer layer was applied to smooth, untreated aluminum substrates. LDPE was used for this purpose. 12.5 μm LDPE sheets with $T_m = 110^\circ\text{C}$ and glass transition temperature $T_g = -110^\circ\text{C}$ were melt cast in 1, 2, 3 and 4 layers onto the substrates to understand the effect of the thickness of the primer layer on deposition. The LDPE sheets were placed onto the substrates, then the LDPE+metal substrate was pressed between Teflon pieces. A 100g weight was placed on top and everything was placed in a 150°C heated oven for 30 minutes to get a smooth, uniform, well-adhered LDPE film on the substrate (Figure 15).

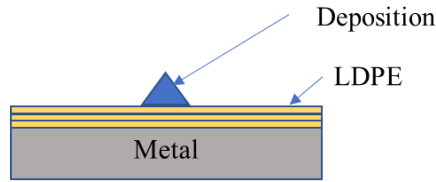


Figure 15: LDPE film and deposition on metal substrate. The LDPE films are 12.5 μm and are melt-cast onto the metal substrate

2.6 The Cold Spray Setup

The cold spray setup was a custom-built laboratory-scale cold spray setup, detailed in Bush et al [72]. The system has a consumer grade single-stage air compressor capable of accelerating the particles up to Mach 2. The nozzle has a 9.5 mm diameter and a throat diameter of 1.6 mm. A 1.85 kW consumer-grade single-stage air compressor is used to generate the air stream. The compressed air travels through filters and a pressure regulator before entering a heated pressure vessel, which has the powder feeder. The hot compressed air/powder mixture exits the vessel and travels through the nozzle. This is a linear system design, where the air and the powder are heated and mixed together and there is no parallel routing of the cold-powder and carrier gas to be mixed at the mouth of the nozzle.

The nozzle was made by drilling a 1.6mm pilot hole through a 6061-aluminum rod. Tapered end mills are then used to cut the converging and diverging portions according to calculations. The aluminum pressure vessel is further heated with three 500W omega MB1 band heaters. The temperature of the pressure is monitored using an internal bore thermocouple (Omega BT) and controlled using a PID temperature controller (Omega CN2110). The inner diameter of the pressure vessel is 38 mm and the total length is 27

mm. Conditions at the inlet of the nozzle are monitored using a thermocouple for temperature and an Omega PX309-300GV pressure transducer. Powder was fed by using a vibratory powder dispenser in the pressure vessel. A pneumatic vibrator (Cleveland Vibrators VM25) was mounted on a connecting rod above the pressure vessel. The rod ran through a slip-fit bushing into the vessel, where it transmitted the vibrations to an attached aluminum cylindrical vessel capped with a coarse wire mesh which contained the powder. A spring was mounted on the vibrating assembly to prevent pressurized air from pushing the connecting rod out of the pressure vessel.

A 2D stage was fabricated and controlled by an Arduino operated by an opensource software package (Repetier-Host). A PCB heater was placed on top of the stage to enable substrate heating up to 120°C. The stage can be controlled with an accuracy of a tenth of a millimeter and can be used to draw custom patterns or can take STL files as input to make pre-defined patterns. Further details of the setup can be found in Bush et al [72]. The flow is kept subsonic and hence the nozzle is a converging nozzle. The polymer powders were fed from a preheated hopper with a flow rate between 30 and 50 g/min. The substrate was placed 10 mm from the exit of the nozzle. A 1D inviscid compressible flow model of the gas and particle dynamics created by Champagne [80] was used to calculate the velocity and the temperature of the polymer particles. A temperature controlled 2D stage was used to move the substrate in controlled patterns and speeds to create deposition patterns consisting of 1D lines and 2D circular deposits. The 1D deposits are approximately 5 cm in length and were drawn at a speed of 40 mm/s. The cross section of the deposit is a triangle with a base length of roughly 2.48 mm and height of 1.2 mm. The 2D circular

deposits used to measure adhesion strength had an area of 35 mm² and 1.1 mm thickness. The cold spray setup schematic is shown in figure 16 and a picture of the setup is shown in figure 17.

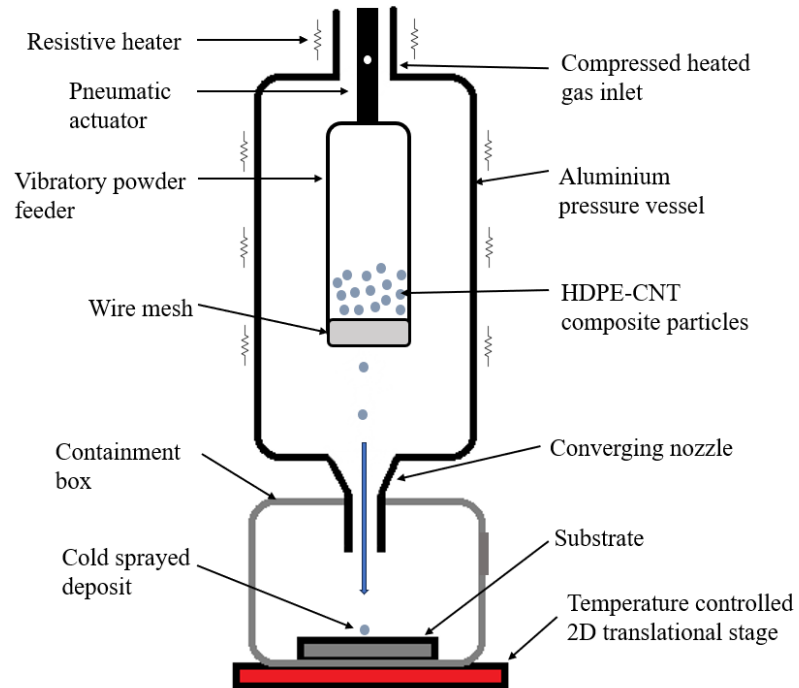


Figure 16: Schematic of the cold spray setup

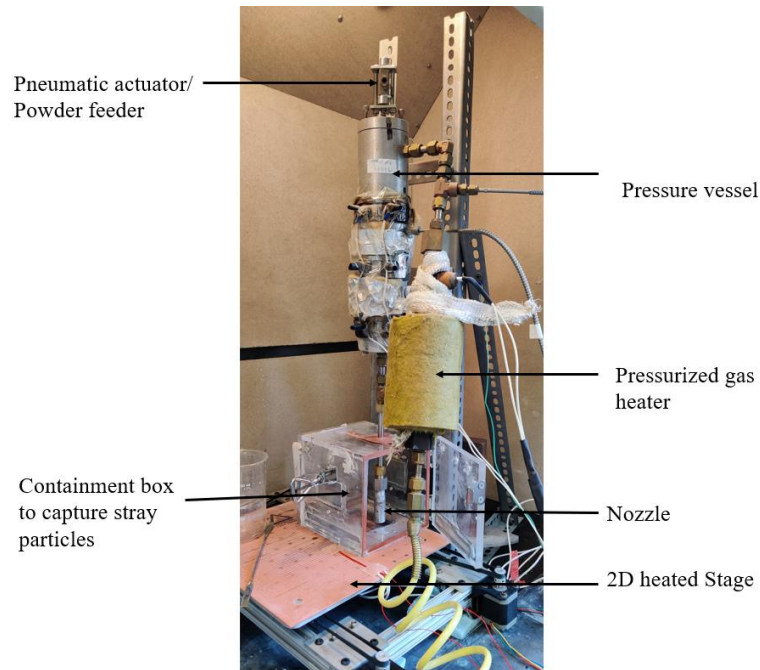


Figure 17: Picture of the cold spray setup

2.7 Adhesion Strength Testing

For the adhesion tests, a circular deposit with aforementioned dimensions was created. A linear stage was used to apply a constant extensional velocity while a force transducer (Mark-10, Model M4-5) was used to simultaneously measure the tensile stress in the sample. Super glue was used to attach mounting plates to both the bottom of the substrate and the top of the deposit so that the sample could be firmly mounted to both the linear stage and the force transducer. Special care was taken to ensure that the mounting plate was only glued to the HDPE deposit and not the surrounding metal. During gluing, a compressive force of 4 N was applied for 10 minutes to ensure proper adhesion. The linear stage was then programmed to move a distance of 1 cm at a uniform velocity of 0.01 cm/s while the force transducer sampled the data at 10 samples per second. To ensure accurate calculation of the stress from the force versus time data, the area and the thickness of each

deposition tested were individually measured using optical techniques. From these measurements, the variation of deposition size was found to be less than 10% of the average values listed above. A schematic of the setup is shown in figure 18.

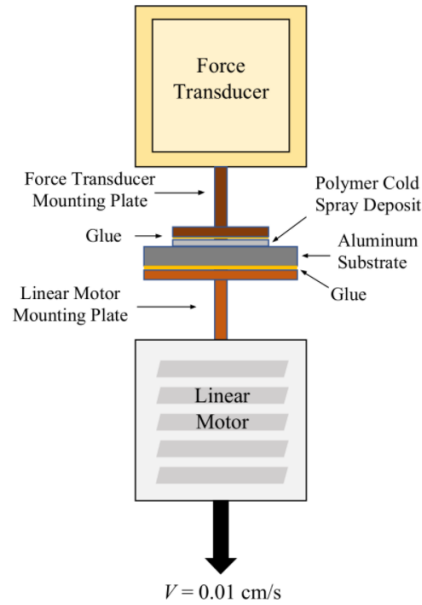


Figure 18: A schematic of the adhesion test setup

2.8 Compression Tests

Compression tests are performed on both the melt cast and the cold sprayed CNT-HDPE composite samples. The melt cast samples have a cross section of a square with an area of 4mm x 4mm and a thickness of 1.5mm. The cold sprayed samples have a cross section of a square with an area of 4mmx4mm with a thickness of 0.75mm. The melt cast samples are made by placing the powder into a TPU mold of the same dimensions as the sample into an oven at 135°C for 30 minutes. The TPU mold is fabricated using 3D printing similar to the mold described in section 2.2. The cold sprayed samples are made by programming the cold spray nozzle to move in the shape of a square using a 3D printing

G-code fed to the Repetier host system. The samples are placed in an Instron machine (BlueHill Universal) between 2 plates. One of the plates is attached to a 5kN force transducer. The Instron machine is programmed to move manually at a speed of $V = 0.033\text{mm/s}$. An initial compressive force of 10 N is applied to the sample before the start of the experiment. The experiment is manually stopped when the force output of the transducer reaches 1000N, at which point the sample has undergone fracture. A setup is shown in figure 19.

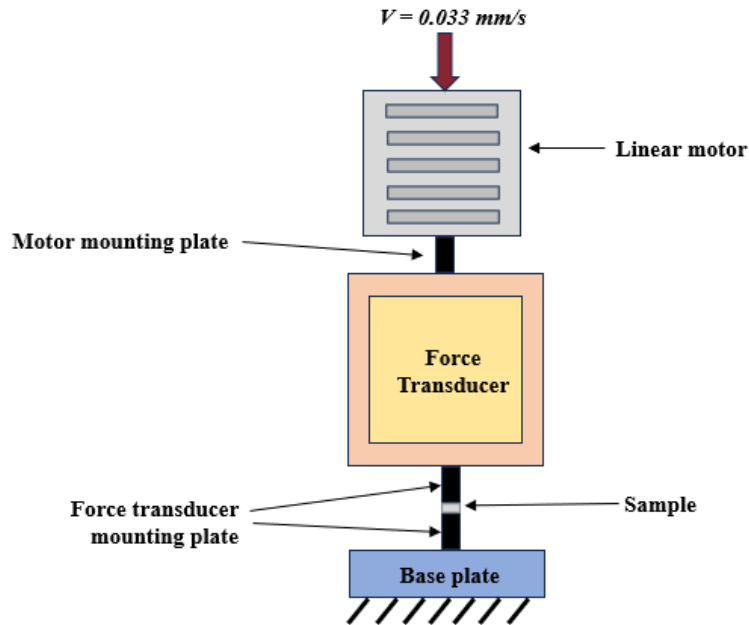


Figure 19: A schematic of the compression tests for the CNT-HDPE samples

A one-dimensional (1D) inviscid model of gas and particle dynamics is used to prototype the system serves as the base for numerical optimization routines [79]. The model uses 1D compressible gas dynamics theory to calculate the velocity, pressure and temperature variations through the nozzle. In a converging-diverging nozzle, the gas is accelerated to choke point (Mach 1) at the throat of the nozzle, and then past sonic flow in

the diverging section of the nozzle, by converting the enthalpy of the gas to kinetic energy. Hence, with the increase in velocity, the pressure and temperature decrease in a known way, that can easily be calculated from theory. The particle velocity is determined by assuming the particles do not disturb the flow field and then calculating the drag force using a simple drag law. For ease of calculations, the lumped capacitance model in the theoretical 1D predictions of nozzle performance is used. This assumption of constant temperature within the particle is valid for metal particles because the Biot number is quite small owing to the large thermal conductivity of the metal particle. However, this assumption breaks down for HDPE and other polymers as their thermal conductivity is much smaller. For the velocities of impact during the cold spray deposition, the resulting Biot number was calculated to be slightly larger than lumped capacitance cutoff of $Bi = 0.1$. This is something to keep in mind if the aim of a study is to understand single particle impact dynamics, especially through numerical methods. For simulations of cold spray experiments, however, the lumped capacitance model serves as a reasonable assumption. The velocity and temperature evolution for mean particle size was calculated as a function of position along the converging-diverging nozzle to determine the impact temperature and velocity of each polymer powder. Further details of the model can be found in Bush et al [72].

CHAPTER 3

COLD SPRAY OF HDPE ON METAL SUBSTRATES

In the following experiments, HDPE particles are sprayed onto metal substrates. The objective is to study the influence of parameters such as temperature of the particles and substrates, surface roughness and the presence of an intermediate primer polymer layer on deposition. The first metric used to quantify the process is the deposition efficiency (DE), defined as the ratio of the mass of powder deposited on the substrate to the mass of the powder from the hopper used in the experiment.

$$DE = \frac{\Delta m_{\text{substrate}}}{\Delta m_{\text{hopper}}} \cdot 100\% \quad (1)$$

3.1 Effect of Particle Temperature

For the first set of experiments, the effect of particle temperature on deposition efficiency was studied. The particle temperature was kept at 40°C, 60°C and 80°C and the substrate was smooth, untreated aluminum maintained at room temperature. Using the 1D inviscid gas flow model described earlier, the particle velocity was estimated to be 240 m/s [80], and this value is constant throughout all the experiments described here. The temperatures mentioned above denote the temperature of the particles in the hopper however, there are temperature fluctuations in the particle in flight, and temperature fluctuations over the volume of the particle, which are well documented in literature.

All experiments are repeated for a minimum of 5 times and a maximum of 10 times to ensure repeatability and the error bars on the data points represent the 95% confidence interval. The data is presented in Figure 20.

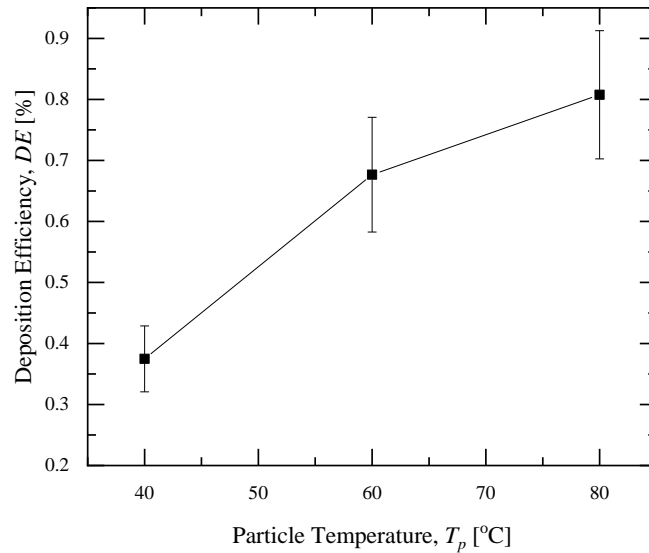


Figure 20: Deposition Efficiency, DE , of HDPE on untreated, room temperature aluminum substrates as a function of particle temperature

It can be clearly seen from the graph that increasing the particle temperature positively benefits deposition, with the deposition efficiency increasing from 0.36% at 40°C particle temperature to 0.81% at 80°C particle temperature. Other researchers have also observed similar trends in their studies – increasing particle temperature leads to better deposition. This is because higher temperatures cause particles to soften [58,72,77,82], hence upon impact, the particles are able to deform better, and conform to the topology of the substrate, which results in stronger adhesion. A high temperature of 80°C was used because, above it, particles became tacky in the hopper, resulting in an inconsistent flow rate. For all experiments henceforth in this chapter, particles will be maintained at 80°C.

3.2 Effect of Surface Roughness

The next parameter that was looked at was the surface roughness. Sandpapers of 50, 240, 360 and 800 grit designations were used to roughen the substrates. The substrates were sanded in a unidirectional back-and-forth pattern and in a random pattern. Examples of surface topology (characterized using a Zygo Nexview Optical Profiler) are shown in figure 21. The surface roughness values have been tabulated in Table 1. The untreated aluminum substrates still have some surface roughness from the manufacturing process, and this can be clearly seen in the profilometer images. It is also interesting to note that treating the surfaces with 800-grit sandpaper, yielded a surface roughness of $0.34\mu\text{m}$ (for randomly scratched surfaces) and $0.36\mu\text{m}$ (for unidirectionally scratched surfaces) which is comparable to the roughness of $0.35\mu\text{m}$ (for untreated surfaces). Treating the surface with 50-grit sandpaper randomly increased the surface roughness to $0.92\mu\text{m}$ whereas treating the surface with 50-grit sandpaper unidirectionally increased the surface roughness to $1.98\mu\text{m}$. Surface roughness decreases with the increase in sandpaper grit designation.

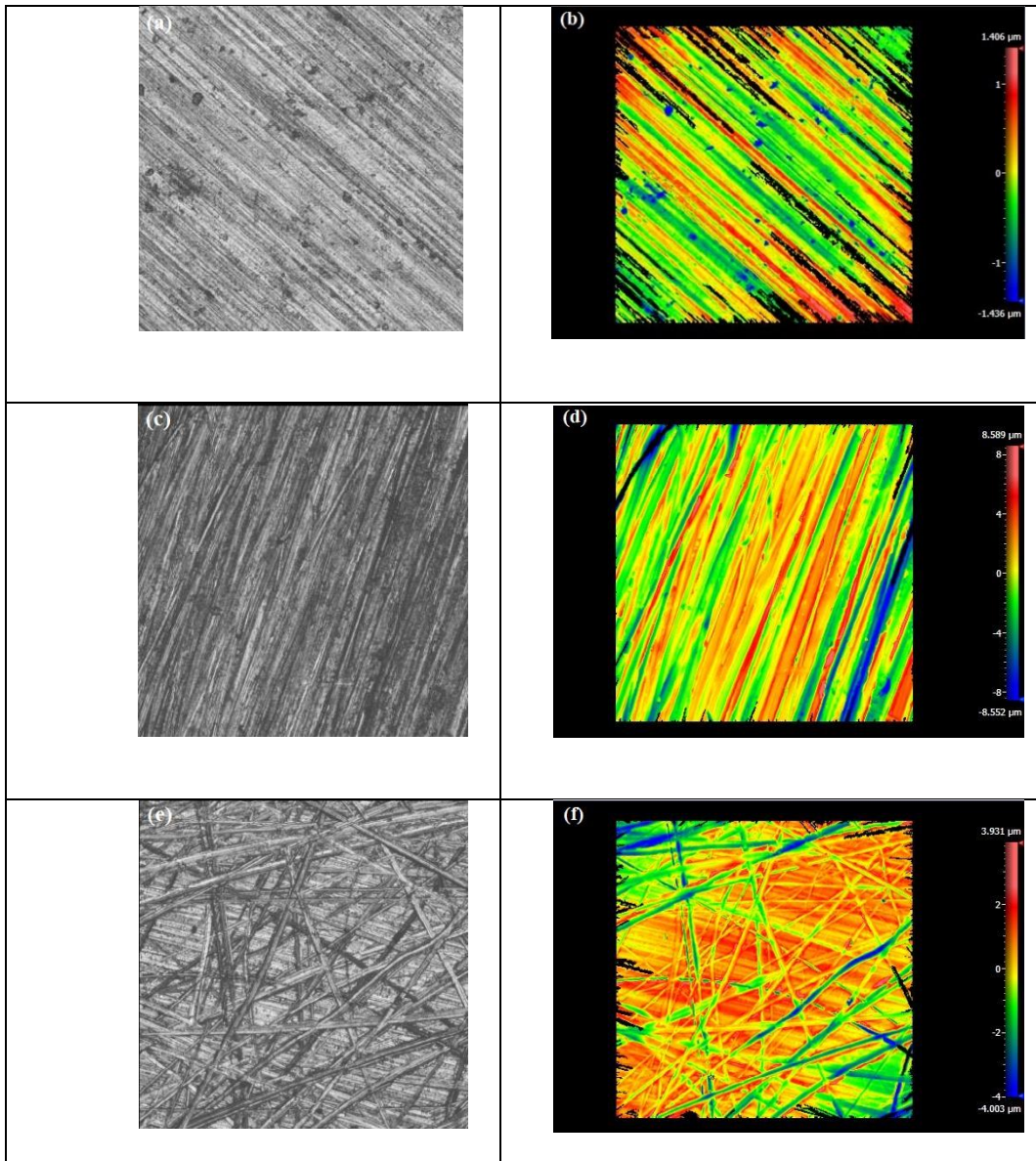


Figure 21: Optical profilometer maps and corresponding heat maps of aluminum substrate surfaces that are (a)-(b) untreated, (c)-(d) treated with 50 grit sandpaper in a unidirectional fashion and (e)-(f) treated with 50 grit sandpaper in a random fashion

Experiments were performed to investigate the effect of surface roughness on deposition efficiency. The particles were kept at 80°C while the substrate was maintained at room temperature. It is evident that surface roughness positively benefits the deposition. Particles sprayed onto 50-grit randomly scratched surfaces have a deposition efficiency of 1.6%, as compared to the 0.81% for untreated surfaces. The pattern of scratching also has an impact, with unidirectionally sanded substrates having lower deposition efficiencies as compared to their randomly scratched counterparts. For example, the 50-grit unidirectionally scratched substrates have a deposition efficiency of 1.3% as compared to the 1.6% for randomly scratched substrates (figure 22).

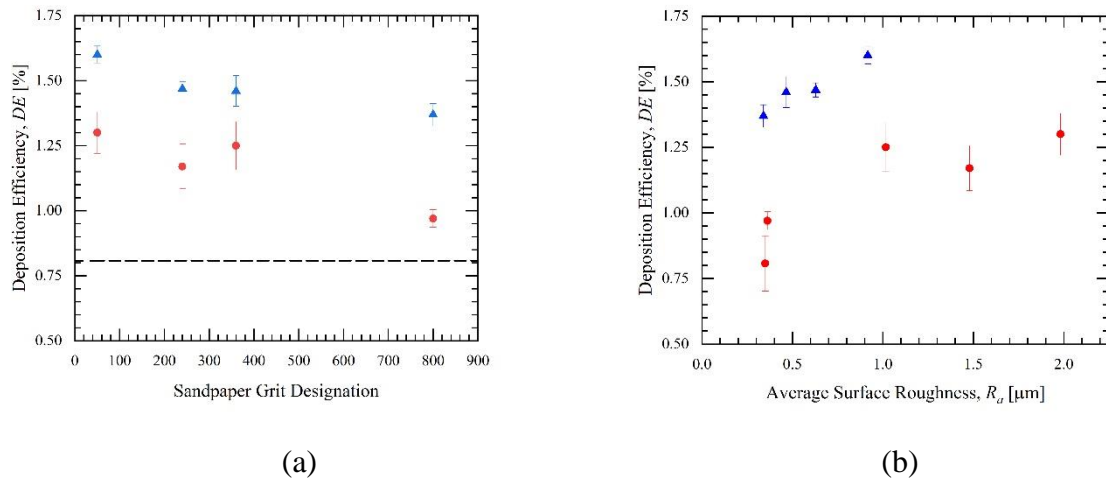


Figure 22: Deposition efficiency for surfaces with treated by unidirectional scratching (●) and random scratching (▲) as a function of (a) sandpaper grit designation and (b) RMS surface roughness. The deposition efficiency of an untreated surface is represented by a dashed line (--) in (a) and is plotted with the unidirectional data in (b). All deposits were produced with a particle temperature of $T_p = 80^\circ\text{C}$, a surface temperature of $T_s = 20^\circ\text{C}$ and a particle impact velocity of $U_p = 240$ m/s

This is because even at the same surface roughness, randomly scratched surfaces would have higher surface area as compared to the unidirectionally scratched surfaces. This is

because of the extremely uneven surface topology imparted to randomly scratched surfaces, compared to unidirectionally scratched surfaces. The random direction of the sanding motion imparts these 3D irregularities to the surface of the substrate, which is beneficial to the particles upon impact because they experience higher localized, concentrated stress upon impact, which makes them flow better, and conformally map to the surface of the substrate. In case of cold spray deposition, the interfacial tension and the work of adhesion are the primary drivers of bonding between the polymer and the substrate. The work of adhesion is defined as

$$W_{PS} = A(\gamma_P + \gamma_S - \gamma_{PS}) \quad (2)$$

Here, A is the actual surface area, γ_P is the surface tension of the particle, γ_S is the surface tension of the substrate, and γ_{PS} , is the interfacial tension between the particle and the substrate. The work of adhesion is heavily dependent on the surface energies of the material of the particle and the substrate and the area of contact between them. Hence, roughening the substrate is an efficient way to increase that area of contact, thereby effectively improving the bonding mechanism between the particle and the substrate. The conformal mapping of the particle to the substrate can be seen in electron microscopy and optical images in figure 23.

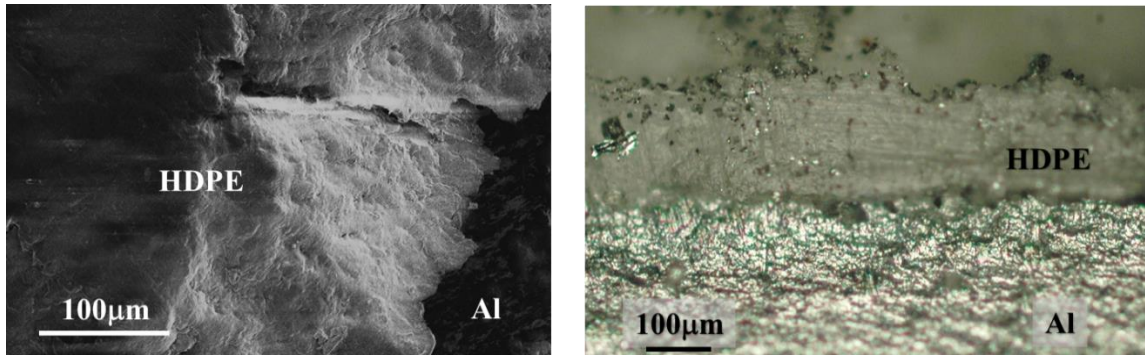


Figure 23: Scanning Electron Microscopy (left) and Optical microscopy (right) images of the cold spray deposition of HDPE on a 50-grit randomly scratched aluminum substrate. The optical microscope focuses on the cross-section, while the SEM focuses on the deposition from above, both highlighting the conformal mapping of the particle onto the substrate, the lack of gaps or voids, and the lack of distinguishing individual HDPE particles

3.3 Adhesion Tests

It also naturally follows, that if the deposition efficiency increases with increase in surface area, then the strength of the bond between the particle and the substrate should correspondingly increase if the surface is roughened. Hence the adhesion strength between the polymer and the metal substrate is quantified to verify this hypothesis. The details of the adhesion test are presented in the experiments section and shown in figure 20. The setup is a pull test; the polymeric deposit is attached to the top mounting plate and the substrate is attached to the bottom mounting plate. The plates are connected to a linear motor and a force sensor respectively. The motor moves the top plate at a velocity of 0.1 mm/s through a distance of 1 cm, while the force sensor measures the force required for the deposit to be fully separated from the surface. To find the stress required for de-bonding, the maximum force recorded in each experiment is divided by the projected area of the deposit (measured optically). A series of sample curves are shown in figure 24. The curves represent the

debonding force between HDPE and an untreated substrate, a surface scratched unidirectionally with 50-grit sandpaper and a surface randomly scratched with 50 grit sandpaper. The initial part of each curve (before de-bonding) is linear which indicates that during the experiments, the HDPE particle is still in the linear deformation region. All the three curves have the same slope, which means that the surface topology of the substrates does not have an impact on the properties of HDPE, and the only difference is the modulus of the force required to separate the deposit from the substrate.

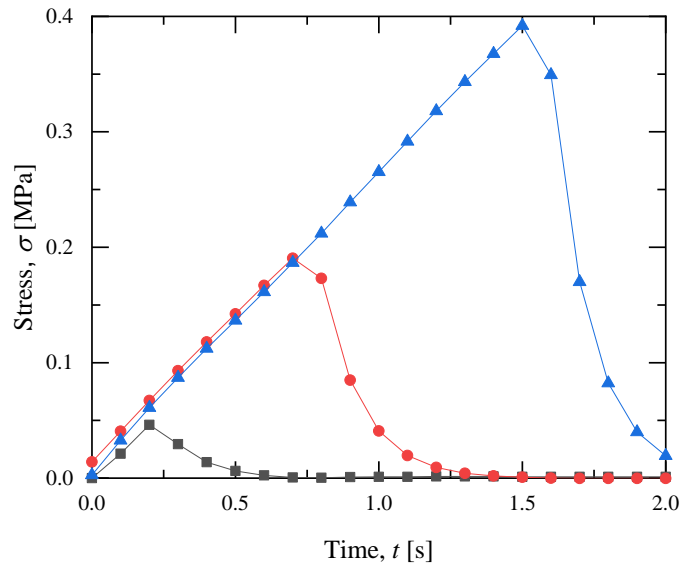


Figure 24: Tensile stress as a function of time from the adhesion tests of a series of cold spray deposits of HDPE particles on a smooth aluminum substrate (■), an aluminum substrate scratched with 50 grit sandpaper in a unidirectional pattern (●) and an aluminum substrate scratched with a 50-grit sandpaper in a random pattern (▲). The maximum stress is the adhesive stress to completely detach the deposit from the substrate. All deposits were produced with a particle temperature of $T_p = 80^\circ\text{C}$, a surface temperature of $T_s = 20^\circ\text{C}$ and a particle impact velocity of $U_p = 240$ m/s

The values of stress required for complete debonding of the deposit from the substrate are plotted in figure 25. It is seen that as the surface roughness increases, more

stress is required to remove the deposit from the surface. All experiments were performed with 80°C HDPE particles cold sprayed onto room-temperature aluminum substrates. The substrates were either smooth, scratched unidirectionally with 50-grit sandpaper or scratched randomly with 50-grit sandpaper. 25kPa was the stress required to separate the deposits from smooth substrates. Unidirectionally scratched surfaces required 180 kPa whereas randomly scratched surfaces required 293 kPa of stress to separate the deposit and the substrate. Compared to the smooth substrates, the force required to remove a deposit from a randomly scratched surface was nearly a 12-fold increase, even though the deposition efficiency correspondingly increased only by a factor of 2.

There are a few factors that play into this increase in adhesion strength. First, even though the projected surface area remains the same, sanding the surface of the substrate increases the actual surface area. Increased surface area means that the impacting polymer particle has a better chance to conformally map to the surface and have good adhesion. Secondly, sanding the surface creates randomized topology with many sharp peaks, which act as points of stress concentration for impacting polymer particles, thereby allowing them to undergo more plastic deformation as compared to particles impacting a smooth substrate. Hence, the particles can flow well and adhere to the surface. Further stresses imparted to the particles, either from a subsequent impact from another particle, or the aerodynamic stresses from the impacting jet can be well utilized in combination with the randomized topology to beneficially deform the particles plastically to ensure good adhesion to the substrates which is seen in figure 25 [66].

Furthermore, from the perspective of the adhesion test, crack propagation is the deciding factor in deciding the strength of the bond. In all the experiments, it was seen that a crack formed at the interface between the deposit and the substrate, and eventually made its way through the entire interaction area between the substrate and the deposit. With the presence of roughness in the topology, the crack has a harder time propagating through the interface. On a smooth substrate, the crack can propagate through quite easily. However, on a scratched surface, the path taken by the crack to propagate is much longer, thereby effectively an indicator of good adhesion between the deposit and the substrate. This is more pronounced in a randomly scratched surface because the path is extremely random. In comparison, in a unidirectionally scratched substrate, the crack can still propagate linearly along the direction of the scratches. All these factors combined give a strong reason for improved adhesion on scratched surfaces.

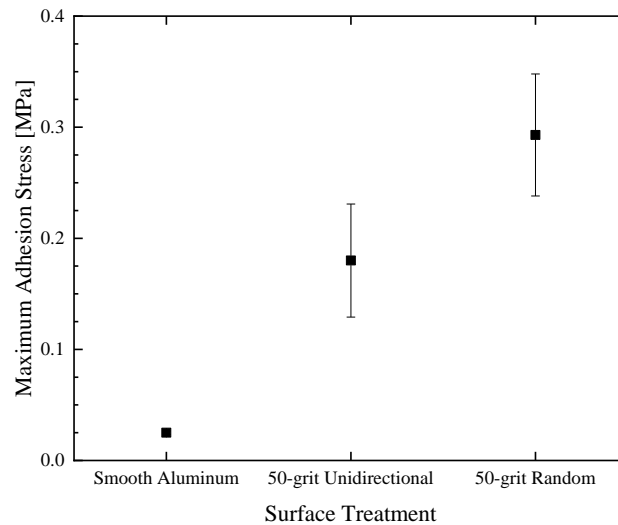


Figure 25: Adhesion stress of the cold sprayed HDPE deposit on aluminum for different surface patterns of surface roughness. All deposits were produced with a particle temperature of $T_p = 80^\circ\text{C}$, a surface temperature of $T_s = 20^\circ\text{C}$ and a particle impact velocity of $U_p = 240 \text{ m/s}$

3.4 Effect of Intermediate Primer Layer

In the final set of experiments, the presence of an intermediate primer polymer layer on the substrate is investigated for its ability to influence deposition. In the previous experiments, it was shown that the primary driving mechanism for bonding between the deposit and the substrate is the work of adhesion, which means that all the kinetic energy of the impacting particle has to be converted to heat and cause plastic deformation for it to adhere to the substrate. However, as discussed earlier [60,61,75], if both the substrate and the impacting particle are polymers, the high shear and mismatch in viscosity between the materials can cause mechanical mixing and interlocking through the phenomenon known as adiabatic shear instability. Previous experiments have shown that HDPE particles on LDPE substrates have a deposition efficiency approaching 10%. Using this reasoning, LDPE thin films were melt-cast on smooth untreated aluminum substrates under the hypothesis that the presence of LDPE will improve deposition. 12.5 μm thick layers of LDPE were melt cast in 1,2,3 and 4 layers onto aluminum substrates. The particle and substrate temperature were both maintained at 80°C and the particle velocity was 240 m/s. An uncoated substrate was chosen as the reference case. Heating a smooth substrate to 80°C and then cold spraying HDPE had a deposition efficiency of 1.75%, and the adhesion strength correspondingly was 92 kPa. This can be attributed to the increased mobility of the HDPE particle due to the high temperature of the substrate. Interestingly, sanding the substrate and heating it still yielded a deposition efficiency of around 1.7%, which is comparable to either heating the substrate or sanding it. Hence it was noted that the two effects did not compound.

From figure 26, it was seen that adding just 1 layer of LDPE to the substrate increased the deposition efficiency from 1.75% to 2.15%, which was in line with the hypothesis, proving that the LDPE layer provided favorable conditions for the HDPE particle to experience adiabatic shear instability and have increased mixing and interlocking. However, the presence of the non-deformable rigid aluminum layer below was still felt, which restricts the ability of the particle and the layer to move and deform. Increasing the number of layers of LDPE showed an increase in deposition efficiency, and it was observed that having 4 layers of LDPE on the substrate corresponded to a deposition efficiency of 3.4%, thereby nearly doubling the efficiency of 1.75% for a smooth substrate. There was a linear correlation between the number of LDPE layers and the deposition efficiency. This correlation could be extrapolated to find the number of LDPE layers that would correspond to deposition onto an infinitely thick LDPE substrate (deposition efficiency of 8.4%). It was seen that 16 layers of LDPE (192 μ m, or 4 particle diameters) would correspond to deposition onto an infinite LDPE substrate.

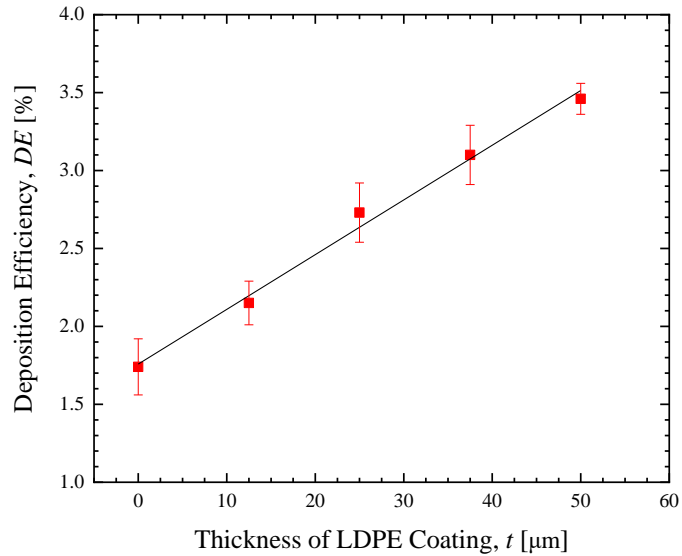


Figure 26: Cold spray deposition efficiency, DE , of HDPE particles on an aluminum substrate with an LDPE coating of various thickness. All data are for a particle temperature of $T_p = 80^\circ\text{C}$, a surface temperature of $T_s = 80^\circ\text{C}$ and a particle impact velocity of $U_p = 240$ m/s. For reference, a linear trendline is placed through the data. Note that the deposition efficiency for an infinitely thick LDPE surface under these same conditions is $DE = 8.4\%$ [77]

3.5 Conclusions

In this chapter, the cold spray deposition of high-density polymeric coatings on aluminum substrates was explored with the goal of improving deposition efficiency and adhesion strength. On smooth, unmodified aluminum substrates at room temperature, increasing the temperature of the HDPE particles in the hopper from $T_p = 40^\circ\text{C}$ to $T_p = 80^\circ\text{C}$ was found to double the deposition efficiency from $DE = 0.38$ to 0.81% . Keeping the particle temperature at $T_p = 80^\circ\text{C}$ and increasing the substrate temperature from room temperature to $T_s = 80$ C again resulted in a doubling of the deposition efficiency to $DE = 1.75\%$. These experiments demonstrate that the temperature and therefore the mobility of the polymer, primarily in the region of polymer-substrate impact where most of the plastic deformation and energy dissipation is occurring, is critically important to improving deposition efficiency. The effect of surface topography was studied by sanding the

aluminum surfaces with different grit sandpapers and patterns to produce surfaces with varying surface roughness. Increasing the surface roughness was found to monotonically increase both the deposition efficiency and the adhesion strength. On this roughened surface, a deposition efficiency of $DE = 1.6\%$ was measured for a $T_p = 80^\circ\text{C}$ particle and a room temperature substrate. This is a 100% improvement over deposition efficiency on a smooth aluminum surface. This same surface showed nearly 1200% improvement on strength of adhesion compared to a smooth aluminum substrate. In general, random scratching patterns were found to produce better deposition efficiency and adhesion strengths than unidirectional sanding.

Finally, the effect of the presence of an intermediate polymer layer was studied. A linear relation was observed between the thickness of the added LDPE layer and the deposition efficiency. A single layer of LDPE $12\mu\text{m}$ thick improved deposition efficiency by 0.5% and an LDPE coating one particle diameter thick was found to improve deposition efficiency to $DE = 3.35\%$. Extrapolating the data to the deposition efficiency of a thick LDPE substrate, it was concluded that an LDPE coating 16 layers or roughly three diameters thick was sufficient to ignore the presence of the metal substrate and approximate the coating as infinitely thick.

CHAPTER 4

COLD SPRAY OF POLYMER COMPOSITES

In this chapter, cold spray is used to create coatings of HDPE composite powders on HDPE substrates. SiO₂ and copper are added as filler materials to HDPE in the process described in chapter 2. The deposition efficiency is evaluated using the same metric described in chapter 3. A few mechanisms are described for their possible role in understanding the trends in the deposition efficiency.

4.1 SiO₂ – HDPE Composite Powders

In Fig. 29, the deposition efficiency of composite powders created using both the micro-SiO₂ and nano-SiO₂ particles are presented for mass fractions, m_f , of the SiO₂ particles incorporated into the HDPE base powder between $0.99\% < m_f < 9.1\%$. In all the experiments shown in Fig. 4, the hopper and substrate temperature were held at 80 °C and the particle impact velocity was calculated to be $V_p = 290\text{m/s}$ for the pure HDPE powder. All the experiments data in Fig. 16 are an average of a minimum of five independent cold spray deposition experiments so that the data could be expressed with proper statistical uncertainty. The error bars superimposed over the *DE* data in figure 27 represent the 95% confidence interval of the average deposition efficiencies. These results represent the first set of data showing that cold spray deposition of polymer composite powders is feasible.

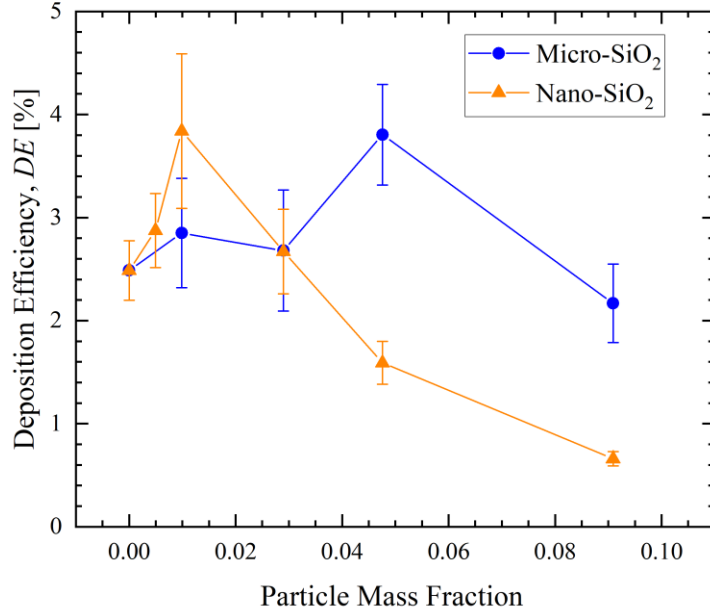


Figure 27: Deposition efficiency plotted as a function of the mass fraction of SiO₂ particles in the composite HDPE powders. The data include results for both micro-SiO₂ (-●-) and nano-SiO₂ (-▲-) particles incorporated into the SiO₂-HDPE composite powder.

The data in figure 27 for both the micro-SiO₂ and nano-SiO₂ HDPE composite powders shows a clear trend. In both cases, the deposition efficiency increases with increasing SiO₂ mass fraction before reaching a maximum and decreasing with the addition of more SiO₂ particles. Thus, both the micro-SiO₂ and nano-SiO₂ HDPE composites powders show a clear optimal mass fraction with respect to deposition efficiency. A similar trend in deposition efficiency was observed by He and Hassani [91] for the cold spray deposition of metal-ceramic composite powders. In figure 29, the deposition efficiency for pure HDPE or the mass fraction of zero case, $m_f = 0$, is included for reference. For consistency, the pure HDPE was put through the same final ball-milling step as the composite powders. For pure HDPE, the deposition efficiency was measured to be $DE =$

2.4% and serves as a baseline to evaluate the other powder compositions. For both composite powders the deposition efficiency was found to initially increase well beyond the pure HDPE case with the addition of SiO₂ particles. For the micro-SiO₂-HDPE composite powders, the deposition efficiency was found to rise to a maximum of $DE = 3.8\%$. This represents a roughly 60% improvement over the pure HDPE case. The nano-SiO₂-HDPE composite powders saw a similar improvement up to $DE = 3.9\%$. The difference between the results for these two composite powders was that the nano-SiO₂-HDPE composite powders reached the peak deposition efficiency at a mass fraction of $m_f = 0.99\%$, while the micro-SiO₂-HDPE composite powders reached the peak deposition efficiency at a much larger mass fraction of $m_f = 4.8\%$. The deposition efficiency for both cases was found to decrease with increasing mass fraction of SiO₂ particles beyond this point. For both cases, the deposition efficiency at the largest mass fractions tested, $m_f = 9.1\%$, was found to fall well below the baseline of the pure HDPE case. For the micro-SiO₂-HDPE composite powders, the deposition efficiency fell to $DE = 2.2\%$, while for the nano-SiO₂-HDPE composite powders the deposition efficiency plummeted to below one percent, reaching $DE = 0.7\%$. The data clearly indicate that increasing the concentration of added SiO₂ particles to HDPE to create composites is beneficial only within a certain range of concentrations. Adding too much is detrimental. The question now, is why.

4.2 Mechanisms for Interaction Between Composite Powders and Substrate

As was discussed in the introduction, increasing the velocity and/or the kinetic energy of the impacting particles generally has a positive effect on deposition efficiency. This has been well documented in both numerical and experimental studies of cold spray

deposition of both metal and polymer particles [61,77]. Additionally, hard inorganic particles with higher densities added to the main polymer particle can function as peening particles. When the inorganic particle strikes a polymer particle that has already been partially embedded in the substrate, it can flatten the embedded particle, improving the contact between the polymer particle and the substrate and thereby leading to better deposition efficiency [66]. The effect of adding the SiO₂ to the HDPE is twofold. First, it increases the density of the powders which we will show in the following paragraph increases the kinetic energy of the powder upon impact of the substrate. Second, based on the way the composites were produced, the SiO₂ particles are expected to be positioned primarily at or near the surface of the composite powders making those particles that don't adhere perhaps act like the glass peening particles used in the literature. Although the peening effect cannot be quantified, the change in kinetic energy can. Here we define the kinetic energy as $KE = \frac{1}{2}m_p V_p^2$, where the mass of the particle is the sum of the mass of the HDPE and SiO₂ in each particle. The impact velocity, V_p , is evaluated using the 1D inviscid compressible flow code provided by Champagne et al. [65,82]. The calculation requires some knowledge of the diameter and shape of the particle. Here we assume the composite particles remain spherical and that the volume of the base HDPE particles is increased by the volume of SiO₂ added to form the composite. The result of these calculations shows that the kinetic energy of the composite powders increases roughly linearly with increasing mass fraction of SiO₂ as shown in Fig. 28. This is because the composite particles are more dense and more massive than the pure HDPE. It thus takes longer for the particles to accelerate in the nozzle meaning that the difference between the particle velocity and the air velocity is larger for longer resulting in an increase in the

aerodynamic drag forces with increasing particle density. As a result, more kinetic energy is transferred to the denser particles as they pass through the nozzle. For the SiO₂-HDPE composite powders, the impact kinetic energy of each particle increases from 2.34μJ for a pure HDPE particle to about 2.53μJ for a SiO₂-HDPE composite particle with a mass fraction of $m_f = 9.1\%$. This represents an 8% increase in the kinetic energy of the particles upon impact. These results only depend on particle density and not size, so they are equally valid for both the micron-SiO₂ and nanoSiO₂ particles. Although it is likely that increasing kinetic energy is a contributing factor for the improvement in deposition efficiency, it is likely other effects, like the peening effect described above also play a substantial role. The peening effect may explain why the nano-SiO₂ particles cause the deposition efficiency to increase more quickly than the larger micro-SiO₂ particle; surface coverage increases more quickly for smaller particles. Similarly, the presence of the SiO₂ particles on the surface of the composite powders may also explain the downturn in deposition efficiency at higher concentrations.

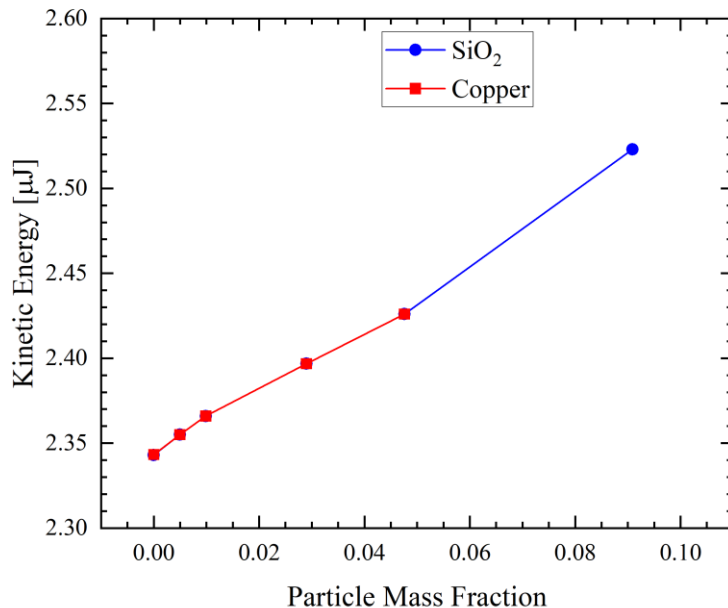


Figure 28: Impact kinetic energy of the composite particles plotted as a function of the mass fraction of SiO₂ (-●-) and Copper (-■-)

Creating composite powders by adding SiO₂ particles to HDPE in a mechanical fashion such as ball milling, where the SiO₂ particles are mechanically driven into the surface of the HDPE particle by repeated physical impacts with the ball bearings results in a composite particle where the majority of added the SiO₂ particles are at or near the surface of the particle and not necessarily in the bulk. This is shown in the SEM images in figure 12 and schematically in the insets of figure 29. As seen in figure 29, the surface coverage is very sensitive to the size of the SiO₂ particles in the composite. That is because at the same mass fraction, as the SiO₂ particles get smaller, the number of particles on the interface increases as does the surface area that they cover. The fraction of surface area covered by the SiO₂ particles is calculated and plotted in figure 29 assuming all the added SiO₂ particles populate the interface of the HDPE base particles. Here, for simplicity, the

nanoparticle SiO₂ particles were assumed to be spherical with a diameter of 200 nm even though the actual shape of the particle is more catenoid and less spherical. Either way, the trends would be similar. For the nano-SiO₂ particles, the surface coverage of HDPE particle saturates very quickly with nanoparticles. By a mass fraction of 4.8%, the interface is fully populated with SiO₂ particles, and the HDPE has been completely encapsulated by SiO₂ particles. At low concentrations and partial surface coverage, the presence of these SiO₂ particles may help the composite powders act as peening particles that improve deposition efficiency. However, as the particle becomes fully encapsulated, the presence of the SiO₂ particles may be detrimental to initial deposition of particles as it would limit the interaction and mixing between the HDPE in the particle and the HDPE substrate which is critical for adhesion and bonding. If little to no HDPE in the composite particle is presented to substrate upon impact, deposition will likely be hindered. This observation also helps explain the difference between the two different sized SiO₂ particles. For the micro-SiO₂, less surface coverage is expected for the same mass fraction as shown in figure 29. As a result, the reduction in deposition efficiency is delayed until higher mass fractions.

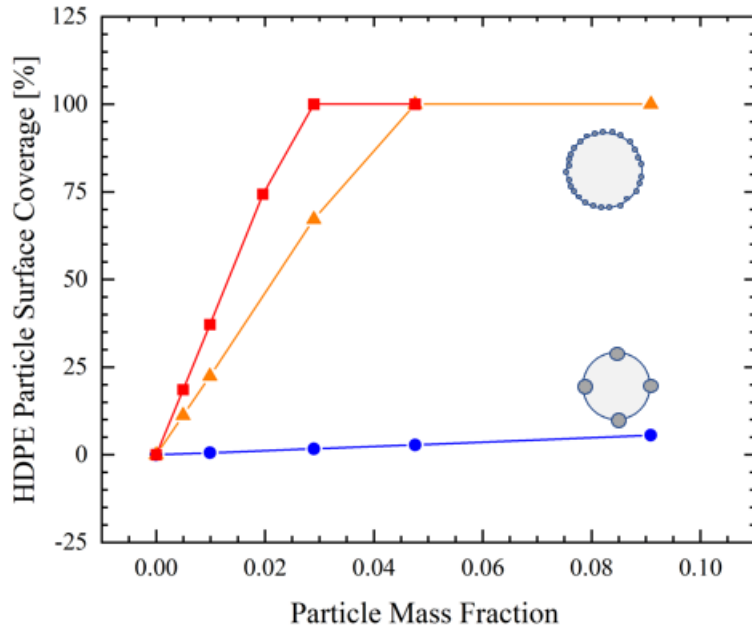


Figure 29: Estimated surface coverage of the HDPE composite particles plotted as a function of the mass fraction of nano-SiO₂ (-▲-), micro-SiO₂ (-●-) and Copper (-■-) composite powders

Specifically, for the micro-SiO₂ composites where complete surface encapsulation is not expected, figure 30 shows one additional mechanism for how surface coverage can affect deposition efficiency. Because the microparticle SiO₂ particle do not completely encapsulate the surface of the HDPE particle, but are relatively large compared to the base HDPE particle size, the orientation of the composite particle upon deposition can have a significant effect on deposition efficiency. If the particle impacts the surface in an oriented for which the interaction is between the SiO₂ particle and the substrate (as shown in 30(a)), a negative effect on deposition efficiency is expected because the HDPE of the particle to interact with the HDPE of the substrate. On the other hand, in Fig. 30(b) a more favorable particle orientation is shown where the HDPE of the particle can interact with the substrate and lead to good deposition. This possible mechanics is yet another reason why the

interaction between the composite powders and the substrate is so complex and in need of further study.

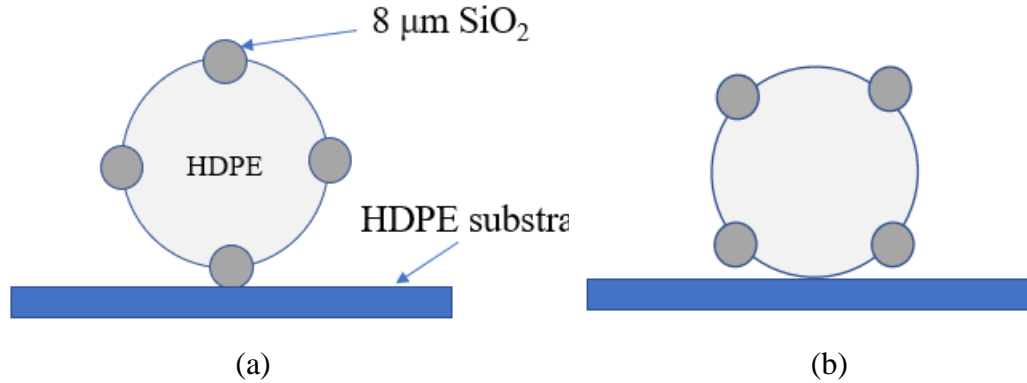


Figure 30: Hypothetical rendering showing the impacting particle interaction with the substrate and how the orientation of the particle can affect deposition for an 8 μm SiO₂ particle added to HDPE (a) Poor deposition and (b) Good deposition. Image is not drawn to scale

4.3 Cu-HDPE Composite Powders

To investigate the effect of additive particle density, copper nanoparticles were used to form Cu-HDPE composites at mass fractions up to $m_f = 4.8\%$. Cold spray deposition was performed using the same operating conditions as the SiO₂ composite powders. Specifically, the hopper and substrate temperature were fixed at 80 °C and the particles were accelerated to $V_p = 290$ m/s. The resulting deposition efficiency is plotted in figure 31 as a function of mass fraction of copper nanoparticles in the composite powders. The trends observed for the Cu-HDPE composite powders are different from what was observed for the SiO₂-HDPE composites. Unlike, the SiO₂-HDPE powders, the deposition efficiency of the Cu-HDPE powders initially decreases, reaching a minimum deposition efficiency of $DE = 1.3\%$ for a mass fraction of $m_f = 9.1\%$, before recovering and increasing

to a maximum of $DE = 2.7\%$ for a mass fraction of $m_f = 2.9\%$. Like the SiO₂-HDPE powders, the deposition efficiency of the Cu-HDPE powders was found to decrease at larger mass fractions. The maximum value of the deposition efficiency observed in figure 31 is statistically the same as the deposition efficiency measured for the pure HDPE powders. Thus, although deposition of Cu-HDPE composite powders is possible, a much tighter window of good deposition is possible when compared to SiO₂-HDPE composites. Operating between a mass fraction of $1.96\% < m_f < 3.8\%$ appears necessary if one wishes to maintain the deposition efficiency of the pure HDPE powders. The cause of the downturn at small mass fractions is not entirely clear. Due to their small size, at a mass fraction of just $m_f = 2.5\%$ the surface of the base HDPE particle will be fully saturated with copper nanoparticles and at $m_f = 0.5\%$ the coverage is nearly 25%. Given that, the density of the particle and the kinetic energy at impact will only increase very slightly at these mass fractions, it is possible that the negative effects of the copper particles saturating the interface of the composite powders outweigh the positive effects of increased impact kinetic energy at these low mass fractions.

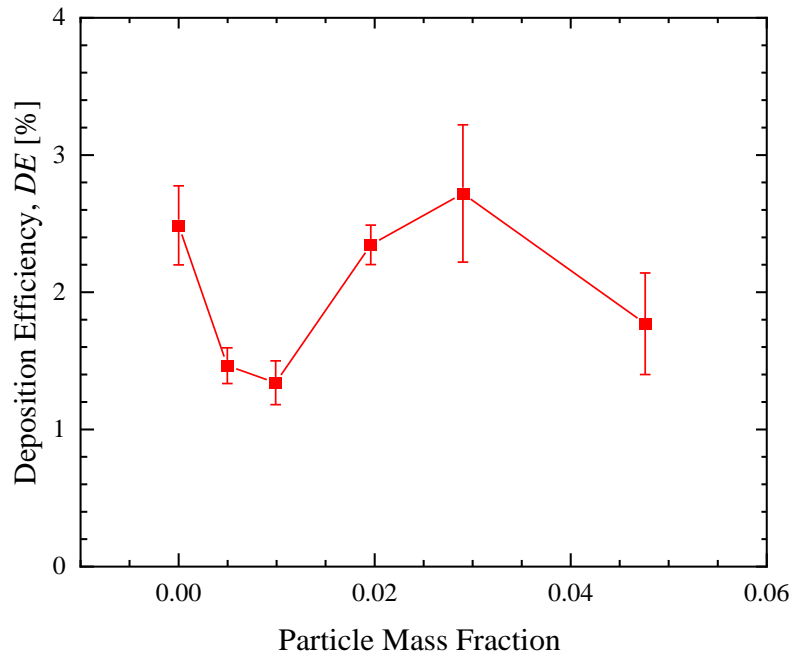


Figure 31: Cold spray deposition efficiency of Copper-HDPE composite powders on an HDPE substrate plotted as a function of the mass fraction of copper in the composite powders

In figure 32, an SEM image of the interface between the HDPE substrate and a cold spray deposition of a Cu-HDPE composite powder with a mass fraction of $m_f = 1.96\%$ is shown. Here the substrate is on top, and the cold spray deposition is below. Note, the smooth uniform deposition and the conformal coating of the substrate. From this image it was observed that the deposition was continuous and uniform with no apparent porosity at the scale with the SEM image. One benefit of using copper nanoparticles in the composite powder is that their high electrical conductivity enhances the contrast in the image, making surface features like the striations observed in figure 12(c) more readily visible. One hypothesis is that these striations are particle rich grain boundaries between deposited Cu-HDPE powder particles. During deposition, the Cu-HDPE composite powders are greatly

deformed and flattened either on their initial impact or by multiple impacts that follow. If we assume that the vertical spacing between striations represents the final thickness of the deposited particles, t , then the deformation ratio of the particle would be more than $DR = D_p/t > 100 : 1$. Given how large this calculated deformation ratio is, it is perhaps likely that these striations also include some wrinkling and buckling of the composite particle interface.

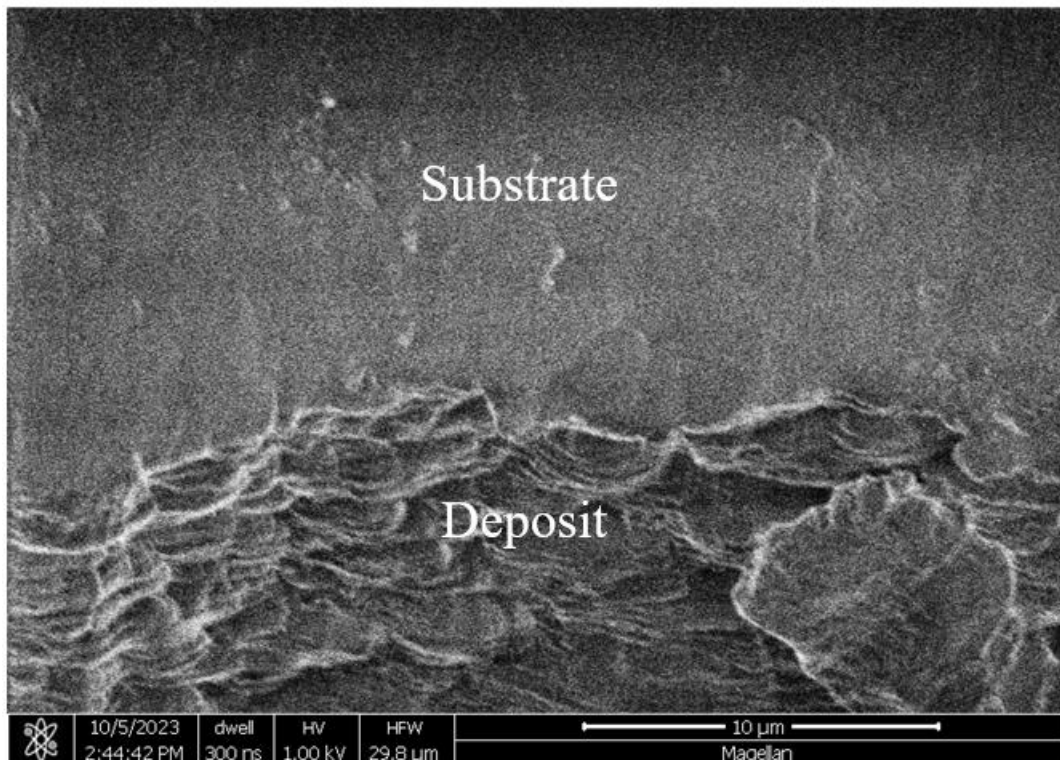


Figure 32: SEM image of a cut through the interface between a HDPE substrate (top) and a cold spray deposition (bottom) of a Cu-HDPE composite powder with $m_f = 1.96\%$

In order to directly visualize the copper nanoparticles in the deposition, the SEM was operated in back scatter mode. The results from the top surface of the deposition as shown in figure 33. Here, the copper particles are clearly visible as bright spots in the image. Although some individual copper particles are clearly visible, many of the copper

particles have clearly aggregated during the manufacturing process. Although clearly seen here, these same particles are not clearly visible in secondary electron images like those in figure 32 suggesting that the copper particles are close to or just below the surface of the HDPE. At this mass fraction of $m_f = 4.76\%$, a volume fraction of just $V_f = 0.59\%$ is expected in the image due to the high density of the copper nanoparticles. Image processing allowed us to roughly calculate the volume fraction of particles present in the image above. If we assume that all the observed particles reside on the surface layer of the deposit, then the surface fraction of polymers is approximately equivalent to the volume fraction. Using this approach, a volume fraction of roughly 0.67 % was calculated from this and other back scatter SEM images of the bottom surface of the deposition which is consistent with the mass fraction added during manufacturing of the composites. Finally, the presence of the copper nanoparticles was further verified by energy-dispersive spectroscopy (EDS) which showed a clear copper peak at 0.95 keV (figure 34).

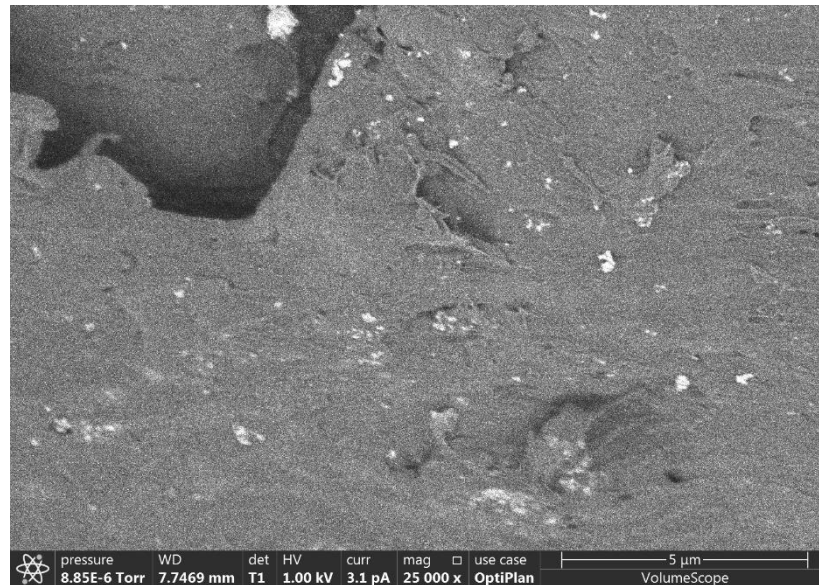


Figure 33: Back scatter from SEM showing copper nanoparticles on the top surface of a Cu-HDPE composite at $m_f = 4.76\%$

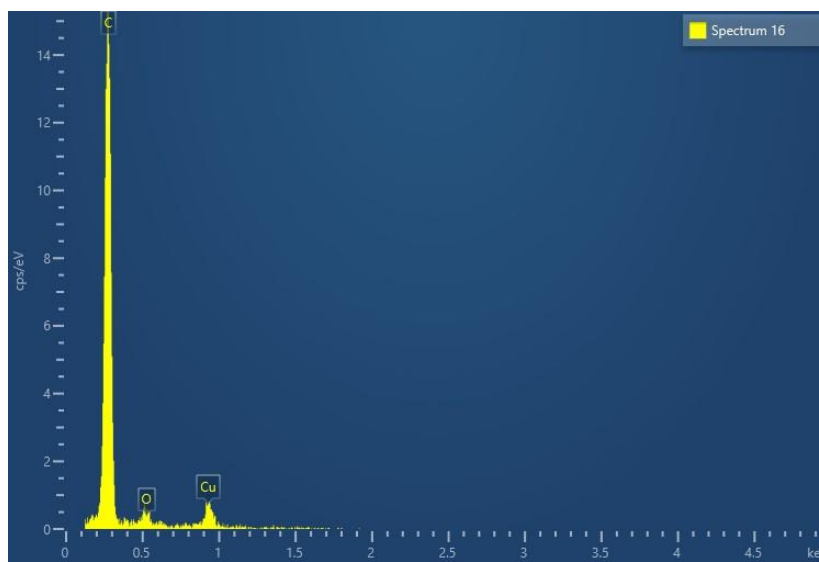


Figure 34: Energy dispersive spectroscopy plot of the Cu-HDPE deposit at a mass fraction of $m_f = 4.76\%$ which clearly indicates a copper peak at 0.95 keV

4.4 Conclusions

This chapter documents the first use of the cold spray additive manufacturing technique to create polymer composite coatings on a polymeric substrate. Specifically, SiO₂-HDPE and Cu-HDPE composites were applied through cold spray to create smooth, uniform coatings on an HDPE substrate. In order to form the composite powders, micro and nanoparticles of SiO₂ were milled together with HDPE powder. The resulting composite powder was cold sprayed onto HDPE substrates, and the amount of powder that forms the deposit was measured against the total amount of powder used in the experiment to calculate the efficiency of the process. The effect of the mass fraction of the added SiO₂ on the efficiency and quality of the cold spray deposition was investigated. In both the micro and nano SiO₂ composites, the addition of SiO₂ to HDPE initially increased the deposition efficiency at low mass fraction, however, an optimal mass fraction of a few percent was found that maximized the deposition efficiency above the efficiency of pure HDPE powder. For the micro-SiO₂ composites, in the highest deposition efficiency was 3.8%, compared

to the 2.4 % efficiency for the pure HDPE powders. A similar number for maximum efficiency, 3.9%, was observed for the nano-SiO₂ composites. Beyond the optimal mass fraction, the further addition of SiO₂ to the HDPE was found to be detrimental to the deposition efficiency. As a result, at the highest particle loadings tested, a decrease in the deposition efficiency well below the efficiency of the pure HDPE powder was observed.

Several physical mechanisms were proposed to explain the observed trends in deposition efficiency. Increasing the mass fraction of SiO₂ increased the density of the composite particle resulting in an increase in the kinetic energy of the powders upon impact of the substrate. It has been shown in the literature that increasing impact kinetic energy positively affects the cold spray deposition efficiency. However, the presence of the SiO₂ particles on the interface of the HDPE powder can also have a negative effect on the deposition efficiency. Surface coverage of SiO₂ hinders the interaction and mixing between the HDPE of the particle and the HDPE of the substrate. This interaction is vital for the particle adhesion, as has been documented in the literature. This is especially true for the nano-SiO₂ powders, which, due to the small size of the SiO₂ particles, quickly saturate the surface of the HDPE particle and thereby drive the optimal mass fraction to lower values compared to the micro-SiO₂ particles. Furthermore, SiO₂ is a hard material, which coupled with the kinetic energy of the composite particle can also lead to substrate erosion. More research is still needed to fully understand the complex dynamics of composite particle impact and adhesion necessary for high efficiency, good quality cold spray deposition. Additionally, further work to develop composite polymer powders with bulk loading of micro and nanoparticles rather than surface loading might help extend the deposition window to higher mass fractions of added particles.

In addition to SiO₂ particles, copper nanoparticles were also added in order to study the effect of particle density. Deposition efficiencies of copper-HDPE nanocomposites were in general no better than those of pure HDPE. In fact, unlike SiO₂-HDPE composites, at low mass fractions of copper < 0.99% the deposition efficiency was found to decrease compared to pure HDPE before recovering at higher mass fractions. These observations led to the discovery of a narrow window of good deposition between mass fractions between 1.5% and 4% for Cu-HDPE powders where deposition efficiencies at least as good as pure HDPE were achievable. SEM imaging of the Cu-HDPE composite powders revealed high particle loadings on the surface of the HDPE powder even at the lowest mass fractions tested. Due to the conductivity of the copper in the Cu-HDPE composite powders, the presence of copper was definitively shown through EDS while the location of the copper nanoparticles is easily identified in SEM images of the coatings after cold spray deposition through backscatter SEM. These measurements suggest a path for future studies to focus on the changes to the solid state properties like electrical and thermal conductivity of the cold sprayed composite deposits with changing SiO₂ and Cu concentration and processing conditions.

CHAPTER 5

COLD SPRAY OF CNT-HDPE COMPOSITES POWDERS

5.1 Deposition of CNT-HDPE Composite Powders

A series of cold spray deposition experiments were performed with PE-CNT composite powders as the feedstock material. The objective is to understand the parameters and process efficiency of spraying polymer nanofiber composite materials, and understand the effect of the spray process on the orientation and distribution of the CNT nanofibers in bulk of the HDPE matrix of the deposit. The first set of experiments focuses on understanding the process efficiency of the cold spray method with the PE-CNT powders. In all the experiments, the hopper and the substrate temperature were 80°C and the impact velocity was 296m/s. The deposition efficiency of the sprayed composite powders is shown in figure 35, with the efficiency on the y-axis and the CNT mass fraction on the x-axis. The zero mass fraction of CNT represents a spray of pure HDPE powder on HDPE substrates with no CNT added. The deposition efficiency is defined as the change in the mass of the HDPE substrate over the mass of the composite powder used. All experiments in figure 35 were performed a minimum of 5 times, representing 5 individual cold spray experiments in order to represent the data with proper statistical significance. The error bars represent the 95% confidence intervals of the average deposition efficiency.

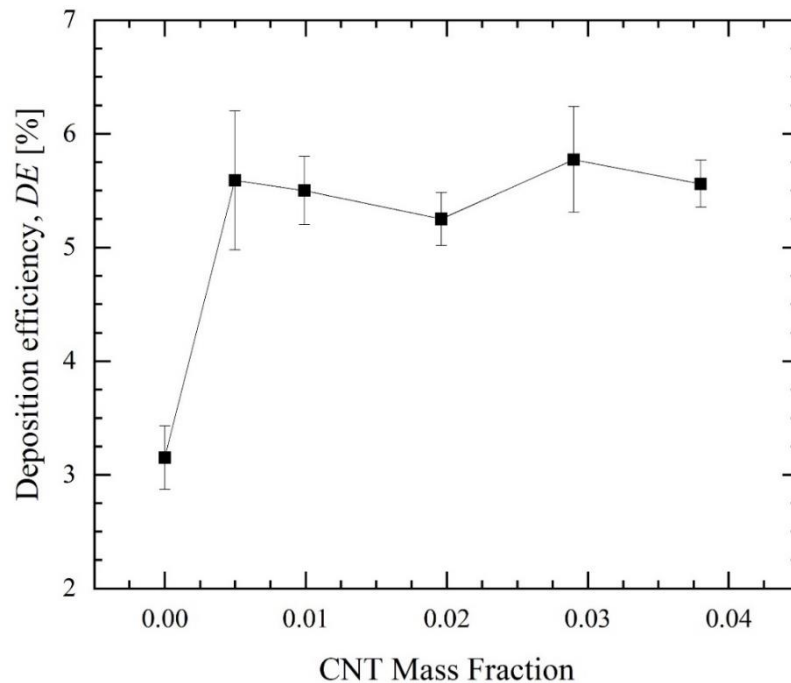


Figure 35: Deposition efficiency of the cold spray process plotted as a function of the mass fraction of CNT filler in the HDPE matrix

The data shown in figure 35 has an evident trend. Even the smallest amount of CNT added to HDPE dramatically boosts the deposition efficiency almost twofold, with the DE for the no CNT loading case around 3.1%, and the lowest CNT loading case ($m_f = 0.498\%$) having an increased DE to about 5.6%. Subsequent increases in the CNT loading do not significantly affect the DE , which stays constant at about 5.5%. The highest CNT loading case ($m_f = 3.8\%$) has a DE of 5.56% as well. Higher mass fraction loadings of CNTs were not evaluated due of the difficulty in synthesizing the CNT-HDPE composite powder with our technique and mass fractions above 4%.

The trends in the results in Figure 35 are different than the data obtained by cold spraying SiO₂-HDPE and Cu-HDPE composite powders [165]. In that study, it was seen that optimum loading concentrations of SiO₂ existed, up to which the deposition efficiency increased and beyond which the deposition efficiency dropped. The Cu-HDPE composites did not fare any better, with even the smallest addition of Cu powders significantly weakening the deposition. A few reasons can be hypothesized for the different trends seen between the different composite powders. In the case of adding CNT to HDPE, despite the best efforts in removing the toluene from the system during the composite powder making process, it could be entirely possible that trace amounts of toluene still exist in the powder after making the sample, and during impact with the substrate, these trace toluene solution acts as a plasticizer for the HDPE powder and the substrate, thereby allowing for conformal contact and good adhesion and deposition. Additionally, using the toluene and the synthesis technique described in Chapter 2, it is expected that the CNTs will be loaded throughout the entirety of the composite particles and not loaded preferentially on the surface of the HDPE powders as is the case for the silicon dioxide and copper nanoparticles. The result is that the downturn observed in the deposition efficiency for the micro and nanoparticle composite powders which we argued was due to surface coverage of the nanoparticles is not expected or observed for the CNT composites.

SEM images of the underside of the deposition at a loading concentration of $m_f = 3.85\%$ is shown in figure 36. The presence of the CNTs can be seen as fibers dispersed within the polymer matrix. Note that the figures are all stretched and aligned in the plane of the sample surface which is also the plane of the substrate on which they were deposited.

The alignment and orientation suggest that during the particle impact and deformation, the CNTs move affinely with the bulk polymer, spreading radially outward from the center of impact as the particle is deformed and spread in the deposition and resulting in a largely 2D network of CNT fibers. This alignment of CNTs might help explain the increased deposition efficiency as alignment of the CNTs will increase energy dissipation during impact.

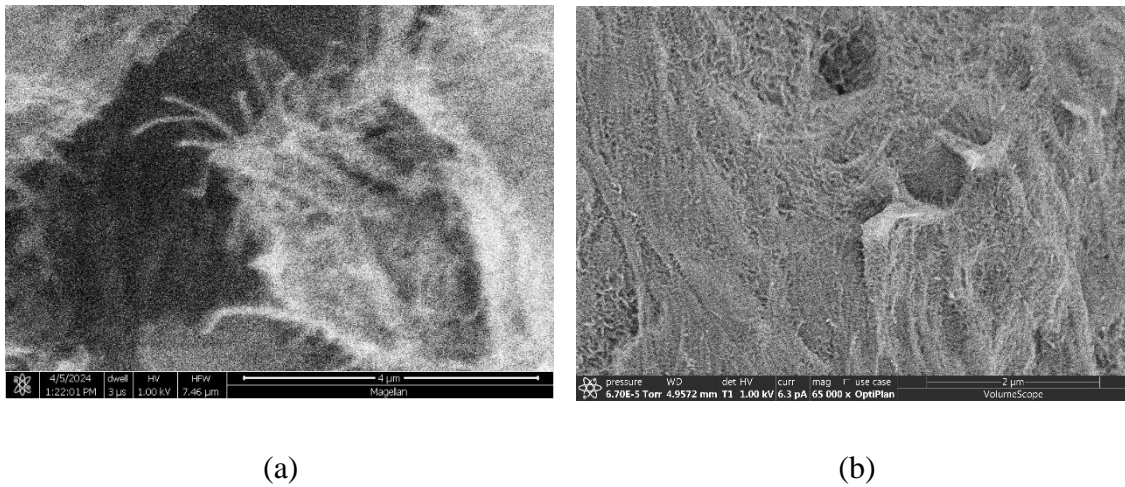


Figure 36: (a)-(b) SEM images at different magnifications of the underside of the CNT-PE composite deposition at a mass fraction $m_f = 3.86\%$

5.2 Conductivity Measurements

Since CNT is known for its conductive abilities, we theorized that adding CNTs to HDPE could make an HDPE deposit conductive. Particularly in the case of cold spraying CNT-HDPE composites, the deformation experienced by the impacting HDPE particle (and by extension the CNTs in the powder) would be biaxial, in a plane that is parallel to the surface of the substrate. If enough CNTs were present in the powder, the repeated impacts would stretch the CNTs out in a plane, and they could potentially form an

interconnecting network. If an electrical current is passed through the sample, this interconnecting network can transmit the current effectively, making the entire sample conductive. To test this hypothesis, conductivity experiments were performed as described previously in Chapter 2. Melt cast PE-CNT powders and cold sprayed PE-CNT deposits were evaluated for their ability to conduct electricity. The melt cast samples were made by melting the PE-CNT powders in a specially designed mold. For both the melt cast and cold sprayed samples, wires were attached at a spacing of 5 mm on the surface of the sample using a conductive epoxy. The wires were attached to a Keithley sourcemeter two point probe, which provided voltages in the range of 10-30V at an increasing step of 0.25V. The probe also measured the resulting current corresponding to each applied voltage. The input current and output voltage were used to measure the conductivity of the sample.

As a control case, pure HDPE was melt-cast into rods to give a baseline for conductivity. The Cu-HDPE cold-sprayed composites from our previous study [165] were first tested for conductivity because copper is known for its conductive abilities. The results are expressed in figure 37. Interestingly, even at the highest concentrations of copper, the Cu-HDPE cold-sprayed composites showed only a slight increase in conductivity above the pure HDPE base case, but remained at or just above the resolution limit of our measurements system at $\sigma_c = 10^{-8}$ S/m. This is attributed to the fact that copper doesn't form an interconnecting network in the deposition. Instead, the copper forms a distribution of sparse agglomerates in the deposit, which is not conducive to good electrical conductivity. The particle distribution can be seen in SEM images of the deposition shown in the previous chapter [165].

CNT-HDPE samples were also melt cast into rods to investigate the effect of the cold spray process on the orientation of CNTs and the effect of the concentration of CNTs in the HDPE powder. The melt cast CNT composites showed an initial increase in conductivity at low concentration from $\sigma_c = 10^{-8}$ to 10^{-7} S/m, but the trend was not entirely clear owing to the noise in the current signal at such low conductivity. An upturn in the conductivity was observed at a mass fraction of 4% to $\sigma_c = 10^{-6}$ S/m which is a full order of magnitude increase in conductivity, but the conductivity is still extremely small. When the conductivity of the melt-cast CNT-HDPE samples is put in context with the conductivity of the cold-sprayed samples, the effect of processing becomes quite clear. The data is shown in Figure 39. Note that the conductivity axis is logarithmic. The cold sprayed samples show extremely low conductivity similar to the pure HDPE at concentrations up to $m_f = 1.96\%$. Increasing the concentration to $m_f = 2.91\%$ was found to result in a dramatic 100,000x increase in conductivity to $\sigma_c = 0.001$ S/m. For reference, the conductivity of the pure CNTs is quoted as 10000S/m by the manufacturers. This threshold concentration is clear evidence that the CNTS have reached the percolation threshold above which they form an interconnected network that allows for easy electrical current flow. The percolation threshold is the boundary, below which the sample is electrically insulating and above which the sample is electrically conductive. This threshold has been well documented in the literature, where for randomly distributed CNTs like in our melt cast samples, a sudden increase in electrical conductivity has been observed at a mass fraction of roughly 4% [156,158,159]. The decrease in the percolation threshold and the dramatic increase in conductivity observed for the cold-sprayed samples demonstrate that processing and in

particular the 2D network of CNTs observed in the SEM in the plane of the substrate that results from the deformation of the powder on impact can have a significant impact on the electrical and possibly the mechanical properties of the composite.

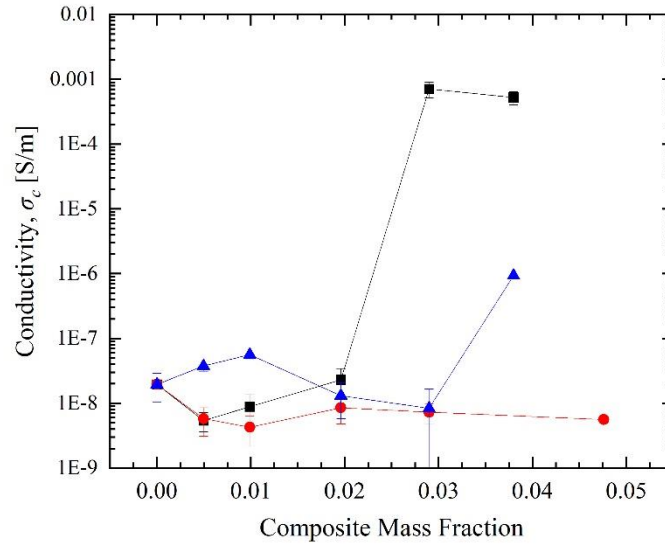


Figure 37: Conductivity tests performed on the cold sprayed CNT-HDPE (-■-), cold sprayed Cu-HDPE (-●-) and melt-cast CNT-HDPE (-▲-) samples

5.3 Young's Modulus

Since carbon nanotubes were well known for their mechanical properties, tensile tests were performed to evaluate the Young's modulus of the cold sprayed CNT composites, and as a reference, the same CNT-HDPE powders were also melt cast and tested. The testing consists of a sample that has the cross section of a square (4mm x 4 mm) and a thickness that is dependent on whether it is melt cast (1.5 mm) or cold sprayed (0.75 mm). The samples were placed between two metal plates and tested in compression in an Instron machine, in accordance with the experimental parameters described in chapter 2.

The linear region of the force – displacement curve was used to estimate the Young’s modulus of the material. The results are presented in figure 38 . Each data point represents a minimum of 3 successful experiments and the error bars show the 95% confidence interval.

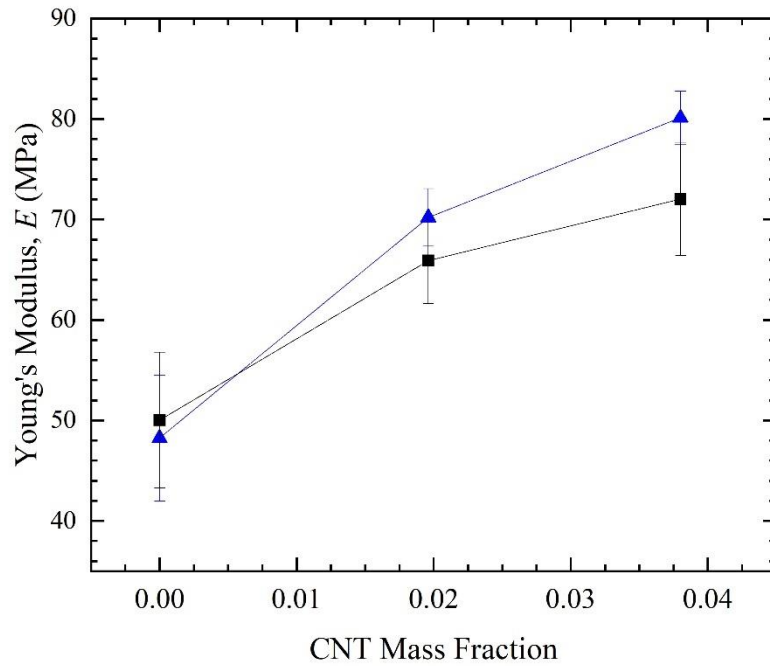


Figure 38: Young’s modulus of the melt cast (-▲-) and cold sprayed (-■-) PE-CNT composites

It can be seen that the presence of CNTs positively benefits the material, with both the mass fractions tested ($m_f = 0.0196$ and $m_f = 0.038$) positively benefiting the Young’s modulus (E) of the material. The pure HDPE had a Youngs modulus of 48.2MPa (melt cast) and 50MPa (cold spray), which goes up to 80.13MPa and 72MPa respectively at the highest mass fraction of added CNTs. This represents approximately a 66 and 44% increase in Youngs modulus of the CNT-HDPE composites, respectively, over their pure HDPE

counterparts. There is also overlap in the values of the Young's modulus measured due to error bars but the trend is clear and consistent. Unlike the conductivity experiments, there is no significant distinction between the melt cast and the cold sprayed samples. It can be safely concluded that CNTs can be used to positively impact the strength of a polymer matrix and the very presence of CNTs boosts the properties of the base material. However, when creating coatings of composite materials, cold spray can be used to preferentially add properties to the coating, and the strength of the cold sprayed samples are comparable to their melt cast counterparts, a trend that was observed for other polymer cold sprayed samples [77]. This further underscores the efficacy of cold spray as an additive manufacturing and coating technique and opens multiple avenues of investigation into its use as a viable method for various applications.

5.4 Conclusions

This chapter focuses on cold spray depositions of CNT-HDPE composites on HDPE substrate. In order to make the composites, CNT was first put into toluene to make a slurry. The CNT-toluene slurry was then mixed with HDPE powder. This mixture was then pressed into a sheet in a vacuum hot press at 90°C. The sheet was cut into 4 pieces that were stacked on top of each other, and this stack was pressed again in the hot press under the same conditions. This cut and stack process was repeated 2 more times. The final sheet was milled down into powder in a ball mill.

The first set of experiments focuses on deposition efficiency of the cold spray process. The pure HDPE powder, with no addition of CNT particles, had a $DE = 3.1\%$ on HDPE substrates.

However, even the slightest addition of CNT to HDPE powders, at a mass fraction $m_f = 0.498\%$ boosted the deposition efficiency to 5.5%. Further addition of CNT to HDPE did not increase the deposition efficiency any further, which remains around 5.5%. This is a huge benefit for cold spray as a deposition technique as it allows for good deposition of CNT based nanocomposites using the cold spray process. The high deposition efficiency was theorized to be because of the toluene, which is a part of the process used to make the CNT-HDPE composites. Despite best efforts to remove it through vacuum, traces of toluene may still be present in the CNT-HDPE powders, and act as a plasticizer to aid deposition onto HDPE substrates.

The next set of experiments focused on understanding the electrical conductivity of the deposition. This was done by attaching wires using conductive epoxy to the depositions. The wires were attached to a sourcemeter and an input voltage was imposed to measure the output current. For reference, the CNT-HDPE powders were also melt-cast into a block of similar dimensions to the deposition, to understand the effect of cold spraying on the electrical conductivity and orientation of CNTs in the deposit. It was observed that at a mass fraction of $m_f = 2.98\%$, the cold sprayed CNT composites showed a dramatic increase in electrical conductivity. This critical concentration is known as the percolation threshold. However, the corresponding melt cast samples did not show any electrical conductivity. The cold sprayed Cu-HDPE composites from chapter 4 were also tested in a similar fashion but did not show any electrical conductivity.

Finally, because CNTs offer increased strength, the composites were also tested to evaluate their Young's modulus. As a reference case, the composite powders at the same concentrations were also melt cast into test blocks. The experiment was performed in compression and the linear region of the stress strain curve was used to calculate the Young's modulus. It was seen that the

addition of the CNTs increased the Young's modulus of the composite material. What was also interesting to note was that the Young's modulus of the melt cast samples was nearly identical to the Young's modulus of the cold sprayed sample. This result has been observed for other polymeric materials in literature and this result is a nice validation of that observation.

CHAPTER 6

CONCLUSIONS

The overall aim of this dissertation has been to interrogate cold spray as a viable technique to coat polymers and polymer composites on a variety of substrates. Cold spray is an additive manufacturing technique that utilizes compressed gas to propel powders at high velocities towards the target substrate to create a coating. Well studied in the context of metal powders and metal substrates, cold spray for polymer powders is gaining traction because of the numerous advantages offered by the technique itself. Research in the recent years has focused on understanding and characterizing different polymeric materials for use in a cold spray system, but there is much left to explore. To that extent, three major research studies were conducted. The first focused on depositing polymer particles on metal substrates, the second on polymer-silica and polymer-metal nanocomposites coating polymer substrates, and the third focused on CNT based composite materials for cold spray.

The first study is on polymer particles coating metal substrates using cold spray. High Density Polyethylene (HDPE) polymer particles were sprayed on aluminium substrates. Parameters that were varied include the particle and substrate temperature, roughness of the substrate, and the presence of an intermediate primer polymer layer. Deposition efficiency was used as the first metric to quantify deposition and is defined as the ratio of the mass of the deposition on the substrate to the total amount of powder used in the experiment. On untreated room-temperature aluminum substrates, it was seen that increasing the particle temperature from 40°C to 80°C more than doubled the deposition efficiency from 0.38% to 0.81%. The reason for this improved deposition is that the

increase in temperature softens the polymer, thereby allowing it to deform and flow better upon impact on the substrate, which causes it to conformally map to the surface of the substrate.

Surface roughness was also an important factor that decided the deposition efficiency. Substrates were treated with sandpapers of various grit designations in order to increase the surface roughness. Two types of treatment were done to the substrates: random and unilateral scratching. Random scratching means that the sandpaper was moved in a random fashion over the substrate surface, and unilateral means that sandpaper was moved in a back and forth fashion in the same direction over the substrate surface. Randomly scratching the substrate with 50-grit sandpaper and holding it at room temperature yielded a deposition efficiency of 1.6%, which was the highest. Using sandpapers of higher grit designations, and varying the scratching patterns between random and unidirectional yielded varying levels of deposition efficiency all of which were greater than that for an untreated, smooth substrate (with an efficiency of 0.81%). Comparatively, the adhesion strength, defined as the stress required to separate the substrate and the deposit showed a much higher increase as a function of roughening the substrate. Deposits required a stress of 25kPa to be separated from room temperature smooth substrates versus 293 kPa to be separated from room temperature substrates randomly scratched with 50-grit sandpaper, which is an improvement of an order of magnitude. In general, scratching the surface improved both deposition efficiency and adhesion strength with randomly scratched surfaces performing better than their corresponding unidirectionally scratched counterparts.

Roughening the substrate increases the area that the polymer has to interact with the substrate. Roughening the substrates also introduces random peaks and valleys in the topology of the substrate, which act as points of localized stress concentrations for the impacting polymer particles. This makes the polymer deform better plastically at the point of contact between itself and the substrate, which makes it flow better. This also makes it difficult for the polymer to be affected by aerodynamic or secondary particle impact stresses that seek to dislodge an existing deposited particle. Also, roughening the substrate makes it difficult for a crack to propagate through the interface of the polymer and the substrate, which is beneficial as it is also a factor for good adhesion between the polymer and the substrate.

Finally, the presence of an intermediate primer polymer layer on the substrate was studied. Previous research has shown that like-on-like deposition is very favourable, that is a polymer particle can interact with a polymer substrate very favourably, as compared to a polymer particle impacting a metal substrate. Hence, 1,2,3 and 4 layers of 12 μm thick LDPE were melt cast onto the aluminum substrates. A linear correlation was observed between the number of LDPE layers and deposition efficiency, with 4 layers of LDPE yielding an efficiency of 3.35%.

Polymer composite cold spray was also studied. In particular, SiO_2 micro and nano particles and Cu nanoparticles were added as filler materials to the HDPE matrix. In order

to form the composite powders, micro and nanoparticles of SiO₂ were milled together with HDPE powder. The resulting composite powder was cold sprayed onto HDPE substrates, and the amount of powder that forms the deposit was measured against the total amount of powder used in the experiment to calculate the efficiency of the process. The effect of the mass fraction of the added SiO₂ on the efficiency and quality of the cold spray deposition was investigated. In both the micro and nano SiO₂ composites, the addition of SiO₂ to HDPE initially increased the deposition efficiency at low mass fraction, however, an optimal mass fraction of a few percent was found that maximized the deposition efficiency above the efficiency of pure HDPE powder. For the micro-SiO₂ composites, in the highest deposition efficiency was 3.8 %, compared to the 2.4 % efficiency for the pure HDPE powders. A similar number for maximum efficiency, 3.9 %, was observed for the nano-SiO₂ composites. Beyond the optimal mass fraction, the further addition of SiO₂ to the HDPE was found to be detrimental to the deposition efficiency. As a result, at the highest particle loadings tested, a decrease in the deposition efficiency well below the efficiency of the pure HDPE powder was observed.

Several physical mechanisms were proposed to explain the observed trends in deposition efficiency. Increasing the mass fraction of SiO₂ increased the density of the composite particle resulting in an increase in the kinetic energy of the powders upon impact of the substrate. It has been shown in the literature that increasing impact kinetic energy positively affects the cold spray deposition efficiency. However, the presence of the SiO₂ particles on the interface of the HDPE powder can also have a negative effect on deposition efficiency. Surface coverage of SiO₂ hinders the interaction and mixing between the HDPE

of the particle and the substrate. This interaction is vital for the particle adhesion, as has been documented in the literature. This is especially true for the nano-SiO₂ powders, which, due to the small size of the SiO₂ particles, quickly saturate the surface of the HDPE particle and thereby driving the optimal mass fraction to lower values compared to the micron sized SiO₂ particles. Furthermore, SiO₂ is a hard material, which coupled with the kinetic energy of composite particle can also lead to substrate erosion. More research is still needed to fully understand the complex dynamics of composite particle impact and adhesion necessary for high efficiency, good quality cold spray deposition. Additionally, further work to develop composite polymer powders with bulk loading of micro and nanoparticles rather than surface loading might help extend the deposition window to higher mass fractions of added particles. In addition to SiO₂ particles, copper nanoparticles were also added in order to study the effect of particle density. Deposition efficiencies of copper-HDPE composites were in general no better than pure HDPE. In fact, unlike SiO₂-HDPE composites, at low mass fractions of copper <0.99 %, the deposition efficiency was found to decrease compared to pure HDPE before recovering at higher mass fractions. These observations led to the discovery of a narrow window of good deposition between mass fractions between 1.5 % and 4 % for Cu-HDPE composite powders where deposition efficiencies at least as good as pure HDPE were achievable. SEM imaging of the Cu-HDPE composite powders revealed high particle loadings on the surface of the HDPE powder even at the lowest mass fractions tested. Due to the conductivity of the copper in the Cu-HDPE composite powders, the presence of copper was definitively shown through EDS while the location of the copper nanoparticles is easily identified in SEM images of the coatings after cold spray deposition through backscatter SEM. These measurements

suggest a path for future studies to focus on the changes to the solid state properties like electrical and thermal conductivity of the cold sprayed composite deposits with changing SiO₂ and Cu concentration and processing conditions.

Finally, HDPE-CNT composite powders were also studied for cold spraying. The composite powders were made by making a suspension of CNTs in toluene and then mixing the appropriate amount of the CNT-toluene solution to the corresponding amount of HDPE. The mixture was then hot pressed under vacuum to form a sheet that was cut, stacked and hot pressed 3 times before being milled into a fine powder. It was observed that even the mere presence of CNTs in the HDPE matrix caused a dramatic increase in the efficiency of the cold spray process. However, there was no further increase in deposition efficiency with the increase in concentration of the CNTs in the HDPE matrix. The deposition efficiency stayed constant around 5.5% for any concentration of CNT in the HDPE matrix. Since CNTs are known for their electrical conductivity, the cold sprayed composite deposits were evaluated for their ability to transmit electricity. It was seen that beyond the critical loading concentration of 1.98% CNTs, the composites were able to conduct electricity. The critical concentration, above which CNT composites show electrical conductivity is known as the percolation threshold. However, the same HDPE - CNT powders do not show any conductivity at the same concentrations if they are melt-cast into a rod with dimensions comparable to the cold spray deposits. This further shows the effect of cold spray as a coating/processing technique, and is evidence for the biaxial stretching experienced by the CNTs in the HDPE matrix as the composite powder is cold sprayed. As a further comparison, the Cu composite powder was also tested in the same

conductivity setup for its ability to conduct electricity. However, at all the loading concentrations studied, the copper composites showed no electrical conductivity. SEM images of the deposits of the copper composite powder revealed that the copper tends to agglomerate in the deposit instead of being uniformly dispersed. This provides a hindrance to the current to be freely transported across the copper particles in the deposit, and hence the copper composites are not good conductors of electricity. Young's modulus was also estimated for cold sprayed and melt cast CNT-HDPE composites. It was seen that the CNTs increased the Young's modulus for both the melt cast and the cold sprayed samples and there was no significant difference between the two types of samples. These results open the door to studying cold spray as a promising technique for creating coatings of various polymer and polymer composite powders on a variety of substrates.

CHAPTER 7

A NOTE TO THE NEXT STUDENT

There are plenty of directions to go in, from this dissertation work, which will be described in this chapter. But before that, it is imperative that a few warnings be added to the next researcher in order to ensure successful results. First, the hopper should always be filled to more than half its capacity. Any less, and the flow rate from the hopper will be too high regardless of the mesh that is glued to the hopper. This will cause clogging at the nozzle. To clean the nozzle, remove the stainless steel fixture from the rest of the setup. Do not remove the nozzle from the stainless steel fixture, because the nozzle has a tapered thread and the steel fixture has a straight thread. It is very difficult to attach them once they are separated. Poke through the end of the nozzle with a stick and then blow air to clean the nozzle. If there is only enough powder to fill less than half the hopper, then add anywhere between 2 and 6 steel ball bearings. This will increase the mass of the hopper and dampen the vibrations. Periodically, apply WD-40 to the pneumatic actuator setup to lubricate it as it can get stuck quite easily. Make sure the compressed air flow is turned on before running the hopper. Check the pressure gauge to ensure that the pressure is between 55 and 70 psi. Any higher, and there is mostly a clogged nozzle. Any lower, and there is poor deposition. Make sure that all the plugs are connected and the power outlets are active. If not, please fix them before turning the machine on. Almost all the problems with the setup arise because there is no power supply to one component of the machine. If the compressor has any issues, check the black reset button on the back. Make sure that the fume hood is fully operational before running any experiments. Follow all the safety

protocols established by EHS when working with nanomaterials. Do not turn on the compressed air setup when the heater of the cold spray bed is on, because this causes the Repetier host program to crash and ruin your experiment. Use the slic3R program to generate G code. Edit both the slic3R program and the Repetier host program together to ensure that they have the same printer, bed and nozzle settings. Failure to ensure this will result in poor coatings. When the containment box is on the setup, make sure that the homing function is turned off. Use JB metal weld only to fix the setup. Usually, the washers have issues staying on the pipe fittings and JB weld will fix the issue. Make sure JB weld is applied to both sides of the washer. Make sure that the 220V supply for the heaters is connected (the power outlet is next to the AC, and the plug is black and white with three prongs and a cylindrical shape). If the plug is disconnected, turn off all components of the cold spray machine before attaching the 220V plug.

Now let us look at a few directions in which the research can progress. The technique described for the CNT composite synthesis is quite robust and can be used for a variety of scenarios. For example, the silica and copper nanomaterials can be substituted in place of the CNTs, and this will be a very nice complementary study to the work done in chapter 4. This will also tell us how the processing technique affects the deposition efficiency and the distribution of the nanomaterials in the bulk of the deposit. It is also worthwhile looking at modifying the VRC systems cold spray machine in the polymer science department. The system has a rotary powder feeder, for which the powder feeder drum can be replaced by a 3D printed custom designed model, which takes inspiration from the meshes that are attached to the hopper of the current cold spray machine, in order to

make the VRC system spray polymer powders. Finally, the question of synthesis plays an important role in cold spray. A very difficult and worthwhile problem to solve would be to look at synthesizing thermoplastic powders, preferably HDPE, but with more control over the molecular weight, the polydispersity and the branching of the polymer chain, and how these characteristics affect the spray process. A further reinforcement of the process would involve redesigning the hopper and the feed system. For this, the system should be designed in such a way that the hopper is cold (at room temperature), but the powders are dropped into a stream of air that is at a high temperature (but still below the melt temperature of HDPE). This will allow for a higher efficiency of the process. This exercise is left as a study for the next student. Another promising direction to go in, is to look at the formation or creation of smooth coatings on the surface of the substrate. The typical deposition is a line, that has the cross section of a triangle. If you draw lines next to one another, the cross section of this deposition will look like a series of mountains right next to one another. The valley regions in between these mountains need to be filled to exact height of the peak of the mountain in order to ensure a smooth coating. Calculating the amount of powder required to fill in this gap and then the deposition efficiency of this back fill process is also a worthy study.

BIBLIOGRAPHY

- [1] L. Treloar, Introduction to polymer science, Springer-Verlag, New York, 1970.
- [2] S.L. Aggarwal, O.J. Sweeting, Polyethylene: Preparation, Structure, and Properties, *Chem Rev* 57 (1957) 665–742.
- [3] R.G. Larson, Instabilities in viscoelastic flows, *Rheol Acta* 31 (1992) 213–263..
- [4] A.J.. Peacock, Handbook of polyethylene : structures, properties, and applications, Marcel Dekker, 2000.
- [5] C.W. Bunn, Chemical Crystallography, Oxford University Press, London, 1946.
- [6] S. Chowdhury, S. Nepal, A. Bhattarai, B. Saha, Coatings made from chemicals: A review, *Vietnam Journal of Chemistry* 61 (2023) 673–692.
- [7] B. Bhushan, B.K. Gupta, Handbook of Tribology: Materials, coatings, and surface treatments, (1991).
- [8] J.T. DeMasi-Marcin, D.K. Gupta, Protective coatings in the gas turbine engine, *Surf Coat Technol* 68–69 (1994) 1–9.
- [9] H. Hornberger, S. Virtanen, A.R. Boccaccini, Biomedical coatings on magnesium alloys - a review, *Acta Biomater* 8 (2012) 2442–2455.
- [10] B. Fotovvati, N. Namdari, A. Dehghanhadikolaei, On coating techniques for surface protection: A review, *Journal of Manufacturing and Materials Processing* 3 (2019).
- [11] H.G. Prengel, W.R. Pfouts, A.T. Santhanam, State of the art in hard coatings for carbide cutting tools, *Surf Coat Technol* 102 (1998) 183–190.
- [12] J. de Damborenea, C. Navas, J.A. García, M.A. Arenas, A. Conde, Corrosion-erosion of TiN-PVD coatings in collagen and cellulose meat casing, *Surf Coat Technol* 201 (2007) 5751–5757.
- [13] P.P. Luff, M. White, The structure and properties of evaporated polyethylene thin films, *Thin Solid Films* 6 (1970) 175–195.

- [14] A. Takeno, N. Okui, T. Kitoh, M. Muraoka, S. Umemoto, T. Sakai, Preparation and piezoelectricity of β form poly(vinylidene fluoride) thin film by vapour deposition, *Thin Solid Films* 202 (1991) 205–211.
- [15] T. Maruyama, S. Arai, Electrochromic properties of niobium oxide thin films prepared by radio-frequency magnetron sputtering method, *Appl Phys Lett* 63 (1993) 869–870
- [16] B.S. Meyerson, UHV/CVD Growth of Si and Si:Ge Alloys: Chemistry, Physics, and Device Applications, *Proceedings of the IEEE* 80 (1992) 1592–1608.
- [17] D. Vernardou, M.E. Pemble, D.W. Sheel, Vanadium oxides prepared by liquid injection MOCVD using vanadyl acetylacetonate, *Surf Coat Technol* 188–189 (2004) 250–254
- [18] Y. Li, D. Mann, M. Rolandi, W. Kim, A. Ural, S. Hung, A. Javey, J. Cao, D. Wang, E. Yenilmez, Q. Wang, J.F. Gibbons, Y. Nishi, H. Dai, Preferential Growth of Semiconducting Single-Walled Carbon Nanotubes by a Plasma Enhanced CVD Method, *Nano Lett* 4 (2004) 317–321.
- [19] A. Dehghanhadikolaei, J. Ansary, R. Ghoreishi, Sol-gel process applications: A mini-review, *Proceedings of the Nature Research Society* 2 (2018) 02008.
- [20] A.A. Tracton, *Coatings Materials and Surface Coatings*, CRC Press, Boca Raton, 2006
- [21] A. Dehghan Ghadikolaei, M. Vahdati, Experimental study on the effect of finishing parameters on surface roughness in magneto-rheological abrasive flow finishing process, *Proc Inst Mech Eng B J Eng Manuf* 229 (2015) 1517–1524.
- [22] D. Wang, G.P. Bierwagen, Sol-gel coatings on metals for corrosion protection, *Prog Org Coat* 64 (2009) 327–338
- [23] M.L. Zheludkevich, I.M. Salvado, M.G.S. Ferreira, Sol-gel coatings for corrosion protection of metals, *J Mater Chem* 15 (2005) 5099–5111.

- [24] G.L. Wilkes, A.B. Brennan, H.-H. Huang, D. Rodrigues, B. Wang, The Synthesis, Structure and Property Behavior of Inorganic-Organic Hybrid Network Materials Prepared by The Sol Gel Process, *MRS Proceedings* 171 (1989) 15–29.
- [25] J.L.W. Noell, G.L. Wilkes, D.K. Mohanty, J.E. McGrath, The preparation and characterization of new polyether ketone-tetraethylorthosilicate hybrid glasses by the sol-gel method, *J Appl Polym Sci* 40 (1990) 1177–1194.
- [26] N. Namdari, P. Mosaddegh, Experimental and simulation studies on the mold replicability in the thermoforming process, *Journal of Polymer Engineering* 39 (2019) 397–405.
- [27] R. Rizvi, N. Namdari, Damage induced surface texturing of short fiber-PDMS composite materials in *Proceedings of the ANTEC 2018*.
- [28] C.J. Lawrence, The mechanics of spin coating of polymer films, *Phys Fluids* 31 (1988) 2786–2795
- [29] Z. Du, S. Wen, J. Wang, C. Yin, D. Yu, J. Luo, Z. Du, S. Wen, J. Wang, C. Yin, D. Yu, J. Luo, The Review of Powder Coatings, *Journal of Materials Science and Chemical Engineering* 4 (2016) 54–59
- [30] X. Wu, I. Wyman, Z.-Q. Liu, Y. Wang, G. Zhang, J. Lin, Z. Liu, H. Hu, Preparation of superamphiphobic polymer-based coatings via spray- and dip-coating strategies, *Prog Org Coat* 90 (2016) 463–471
- [31] C.R.C. Lima, N.F.C. de Souza, F. Camargo, Study of wear and corrosion performance of thermal sprayed engineering polymers, *Surf Coat Technol* 220 (2013) 140–143
- [32] R. Lupoi, W. O' Neill, Deposition of Metallic Coatings on Polymer Surfaces using Cold Spray, *Surf Coat Technol* 205 (2010) 2167–2173.
- [33] B. Yildirim, S. Muftu, A. Gouldstone, Modeling of high velocity impact of spherical particles, *Wear* 270 (2011) 703–713

- [34] L. Pawlowski, *The Science and Engineering of Thermal Spray Coatings: Second Edition*, John Wiley and Sons, 2008
- [35] E. Petrovicova, L.S. Schadler, Thermal spraying of polymers, *International Materials Reviews* 47 (2002) 169–190.
- [36] H. Koivuluoto, A Review of Thermally Sprayed Polymer Coatings, *Journal of Thermal Spray Technology* 31 (2022) 1750–1764
- [37] J.R. Davis, *Handbook of Thermal Spray Technology*, ASM international, Almere, 2004.
- [38] M.S. Kramer, L.E. Byrnes, G.L. Holmes, *Method and apparatus for application of thermal spray coatings to engine blocks*, 1992.
- [39] M.L. Thorpe, H.J. Richter, A pragmatic analysis and comparison of HVOF processes, *Journal of Thermal Spray Technology* 1 (1992) 161–170.
- [40] J. Fernández, M. Gaona, J.M. Guilemany, Effect of heat treatments on HVOF hydroxyapatite coatings, *Journal of Thermal Spray Technology* 16 (2007) 220–228.
- [41] A. Scrivani, U. Bardi, L. Carrafiello, A. Lavacchi, F. Niccolai, G. Rizzi, A comparative study of high velocity oxygen fuel, vacuum plasma spray, and axial plasma spray for the deposition of CoNiCrAlY bond coat alloy, *Journal of Thermal Spray Technology* 12 (2003) 504–507.
- [42] G. Bolelli, L. Lusvarghi, T. Varis, E. Turunen, M. Leoni, P. Scardi, C.L. Azanza-Ricardo, M. Barletta, Residual stresses in HVOF-sprayed ceramic coatings, *Surf Coat Technol* 202 (2008) 4810–4819.
- [43] A. Scrivani, S. Ianelli, A. Rossi, R. Groppetti, F. Casadei, G. Rizzi, A contribution to the surface analysis and characterisation of HVOF coatings for petrochemical application, *Wear* 250 (2001) 107–113.
- [44] A. Lekatou, E. Regoutas, A.E. Karantzalis, Corrosion behaviour of cermet-based coatings with a bond coat in 0.5 M H₂SO₄, *Corros Sci* 50 (2008) 3389–3400.

- [45] Z. Zhou, L. Wang, F.C. Wang, H.F. Zhang, Y.B. Liu, S.H. Xu, Formation and corrosion behavior of Fe-based amorphous metallic coatings by HVOF thermal spraying, *Surf Coat Technol* 204 (2009) 563–570.
- [46] D. Toma, W. Brandl, G. Marginean, Wear and corrosion behaviour of thermally sprayed cermet coatings, *Surf Coat Technol* 138 (2001) 149–158.
- [47] J.H. Bulloch, A.G. Callagy, An in situ wear-corrosion study on a series of protective coatings in large induced draft fans, *Wear* 233–235 (1999) 284–292.
- [48] J. Knuuttila, S. Ahmaniemi, T. Mäntylä, Wet abrasion and slurry erosion resistance of thermally sprayed oxide coatings, *Wear* 232 (1999) 207–212.
- [49] S. Kartik Nemani, R. Kishore Annavarapu, B. Mohammadian, A. Raiyan, J. Heil, M. Ashraful Haque, A. Abdelaal, H. Sojoudi, S.K. Nemani, R.K. Annavarapu, B. Mohammadian, A. Raiyan, J. Heil, M.A. Haque, A. Abdelaal, H. Sojoudi, Surface Modification of Polymers: Methods and Applications, *Adv Mater Interfaces* 5 (2018) 1801247.
- [50] L.C. Betancourt-Dougherty, R.W. Smith, Effects of load and sliding speed on the wear behaviour of plasma sprayed TiC□NiCrBSi coatings, *Wear* 217 (1998) 147–154.
- [51] N.P. Padture, M. Gell, E.H. Jordan, Thermal barrier coatings for gas-turbine engine applications, *Science* (1979) 296 (2002) 280–284.
- [52] H. Assadi, T. Schmidt, H. Richter, J.-O. Kliemann, K. Binder, F. Gärtner, T. Klassen, H. Kreye, On Parameter Selection in Cold Spraying, *Journal of Thermal Spray Technology* 2011 20:6 20 (2011) 1161–1176.
- [53] M. Gardon, A. Latorre, M. Torrell, S. Dosta, J. Fernández, J.M. Guilemany, Cold gas spray titanium coatings onto a biocompatible polymer, *Mater Lett* 106 (2013) 97–99
- [54] A. Moridi, S.M. Hassani-Gangaraj, M. Guagliano, M. Dao, Cold spray coating: review of material systems and future perspectives, *Surface Engineering* 36 (2014) 369–395.

- [55] V.K. Champagne, The Repair of Magnesium Rotorcraft Components by Cold Spray, *Journal of Failure Analysis and Prevention* 8 (2008) 164–175.
- [56] A.M. Vilardell, N. Cinca, A. Concustell, S. Dosta, I.G. Cano, J.M. Guilemany, Cold spray as an emerging technology for biocompatible and antibacterial coatings: state of art, *J Mater Sci* 50 (2015) 4441–4462
- [57] Y. Xu, I.M. Hutchings, Cold spray deposition of thermoplastic powder, *Surf Coat Technol* 201 (2006) 3044–3050
- [58] Z. Khalkhali, W. Xie, V.K. Champagne, J.-H. Lee, J.P. Rothstein, A comparison of cold spray technique to single particle micro-ballistic impacts for the deposition of polymer particles on polymer substrates, *Surf Coat Technol* (2018) 99–107.
- [59] C. Chen, X. Xie, Y. Xie, X. Yan, C. Huang, S. Deng, Z. Ren, H. Liao, Metallization of polyether ether ketone (PEEK) by copper coating via cold spray, *Surf Coat Technol* 342 (2018) 209–219
- [60] M. Grujicic, C.L. Zhao, W.S. Derosset, D. Helfritch, Adiabatic shear instability based mechanism for particles/substrate bonding in the cold-gas dynamic-spray process, *Mater Des* 24 (2004) 681–688.
- [61] M. Grujicic, J.R. Saylor, D.E. Beasley, W.S. DeRosset, D. Helfritch, Computational analysis of the interfacial bonding between feed-powder particles and the substrate in the cold-gas dynamic-spray process, *Appl Surf Sci* 219 (2003) 211–227.
- [62] C.J. Li, H.T. Wang, Q. Zhang, G.J. Yang, W.Y. Li, H.L. Liao, Influence of spray materials and their surface oxidation on the critical velocity in cold spraying, *Journal of Thermal Spray Technology* 19 (2010) 95–101.
- [63] W.Y. Li, H. Liao, C.J. Li, H.S. Bang, C. Coddet, Numerical simulation of deformation behavior of Al particles impacting on Al substrate and effect of surface oxide films on interfacial bonding in cold spraying, *Appl Surf Sci* 253 (2007) 5084–5091
- [64] H. Che, P. Vo, S. Yue, Metallization of carbon fibre reinforced polymers by cold spray, *Surf Coat Technol* 313 (2017) 236–247.

- [65] F. Meng, D. Hu, Y. Gao, S. Yue, J. Song, Cold-spray bonding mechanisms and deposition efficiency prediction for particle/substrate with distinct deformability, *Mater Des* 109 (2016) 503–510
- [66] Z. Khalkhali, K.S. Rajan, J.P. Rothstein, Peening Effect of Glass Beads in the Cold Spray Deposition of Polymeric Powders, *Journal of Thermal Spray Technology* 29 (2020) 657–669.
- [67] C. Chen, X. Xie, Y. Xie, X. Yan, C. Huang, S. Deng, Z. Ren, H. Liao, Metallization of polyether ether ketone (PEEK) by copper coating via cold spray, *Surf Coat Technol* 342 (2018) 209–219.
- [68] N.K. Singh, K.Z. Uddin, J. Muthulingam, R. Jha, B. Koohbor, A Modeling Study of Bonding Mechanisms Between Similar and Dissimilar Materials in Cold Spraying on Polymeric Substrates, *Journal of Thermal Spray Technology* 31 (2022) 508–524.
- [69] N.K. Singh, K.Z. Uddin, J. Muthulingam, R. Jha, B. Koohbor, Analyzing the Effects of Particle Diameter in Cold Spraying of Thermoplastic Polymers, *Journal of Thermal Spray Technology* 30 (2021) 1226–1238.
- [70] G. Yang, W. Xie, M. Huang, V.K. Champagne, J.-H. Lee, J. Klier, J.D. Schiffman, Polymer Particles with a Low Glass Transition Temperature Containing Thermoset Resin Enable Powder Coatings at Room Temperature, *Ind Eng Chem Res* 58 (2019) 908–916.
- [71] A.M. Vilardeell, N. Cinca, A. Concustell, S. Dosta, I.G. Cano, J.M. Guilemany, Cold spray as an emerging technology for biocompatible and antibacterial coatings: state of art, *J Mater Sci* 50 (2015) 4441–4462
- [72] T.B. Bush, Z. Khalkhali, V. Champagne, D.P. Schmidt, J.P. Rothstein, Optimization of Cold Spray Deposition of High-Density Polyethylene Powders, *Journal of Thermal Spray Technology* 26 (2017) 1548–1564.
- [73] R. Nikbakht, S.H. Seyedein, S. Kheirandish, H. Assadi, B. Jodoin, Asymmetrical bonding in cold spraying of dissimilar materials, *Appl Surf Sci* 444 (2018) 621–632.

- [74] H. Assadi, F. Gärtner, T. Stoltenhoff, H. Kreye, Bonding mechanism in cold gas spraying, *Acta Mater* 51 (2003) 4379–4394.
- [75] T. Hussain, Cold Spraying of Titanium: A Review of Bonding Mechanisms, Microstructure and Properties, *Key Engineering Materials* 533 (2013) 53–90.
- [76] K. Sundara Rajan, J.P. Rothstein, Cold Spray Deposition of High-Density Polyethylene Polymer Particles on Metal Substrates, *Journal of Thermal Spray Technology* 31 (2022) 1765–1775.
- [77] Z. Khalkhali, J.P. Rothstein, Characterization of the cold spray deposition of a wide variety of polymeric powders, *Surf Coat Technol* 383 (2019).
- [78] T. Schmidt, F. Gärtner, H. Assadi, H. Kreye, Development of a generalized parameter window for cold spray deposition, *Acta Mater* 54 (2006) 729–742.
- [79] V.K. Champagne, D.J. Helfrich, S.P.G. Dinavahi, P.F. Leyman, Theoretical and Experimental Particle Velocity in Cold Spray, *Journal of Thermal Spray Technology* 2010 20:3 20 (2010) 425–431.
- [80] V.K. Champagne, *The cold spray materials deposition process: fundamentals and applications*, Woodhead, 2007.
- [81] Z. Khalkhali, *Cold Spray Deposition of Polymers-Characterization and Cold Spray Deposition of Polymers-Characterization and Optimization*, UMass Amherst, 2019.
- [82] S. Shah, J. Lee, J.P. Rothstein, Numerical Simulations of the High-Velocity Impact of a Single Polymer Particle During Cold-Spray Deposition, *Journal of Thermal Spray Technology* 2017 26:5 26 (2017) 970–984.
- [83] M.S. Kaminskyj, M.S. Schwenger, D.A. Brennan, F.M. Haas, J.F. Stanzione, Effects of Polymer Crystallinity on Deposition Efficiency and Porosity in Cold Spray of PEKK, *Thermal Spray 2022: Proceedings from the International Thermal Spray Conference* 84369 (2022) 82–88.
- [84] T.W. Bacha, N.K. Singh, I.M. Nault, B. Koohbor, F.M. Haas, J.F. Stanzione, Thermal Gradients Govern Impact Dynamics in Thermoplastic Polymer Cold Spray,

- [85] C.A. Bernard, H. Takana, G. Diguët, K. Ravi, O. Lame, K. Ogawa, J.Y. Cavallé, Thermal gradient of in-flight polymer particles during cold spraying, *J Mater Process Technol* 286 (2020) 116805.
- [86] T.W. Bacha, D.A. Brennan, Ü. Tiitma, F.M. Haas, J.F. Stanzione, Effects of Powder Feedstock Pre-Heating on Polymer Cold Spray Deposition, *Thermal Spray 2022: Proceedings from the International Thermal Spray Conference* 84369 (2022) 44–55.
- [87] D.A. Brennan, T.W. Bacha, Ü. Tiitma, F.M. Haas, J.F. Stanzione, Systematic Study of the Effects of Powder Preconditioning on Flowability and Deposition in Polymer Cold Spray, *Thermal Spray 2022: Proceedings from the International Thermal Spray Conference* 84369 (2022) 683–694.
- [88] J. Muthulingam, A.G. Padmanaban, N.K. Singh, T.W. Bacha, J.F. Stanzione, F.M. Haas, R. Jha, J.-H. Lee, B. Koohbor, Molecular Weight Controls Interactions between Plastic Deformation and Fracture in Cold Spray of Glassy Polymers, *ACS Omega* (2023).
- [89] A. Gangineri Padmanaban, T.W. Bacha, J. Muthulingam, F.M. Haas, J.F. Stanzione, B. Koohbor, J.H. Lee, Molecular-Weight-Dependent Interplay of Brittle-to-Ductile Transition in High-Strain-Rate Cold Spray Deposition of Glassy Polymers, *ACS Omega* 7 (2022) 26465–26472
- [90] A. Papyrin, V. Kosarev, S. Klinkov, A. Alkhimov, V. Fomin, *Cold Spray Technology*, Elsevier, Amsterdam, 2007.
- [91] L. He, M. Hassani, A Review of the Mechanical and Tribological Behavior of Cold Spray Metal Matrix Composites, *Journal of Thermal Spray Technology* 2020 29:7 29 (2020) 1565–1608
- [92] H. Parmar, F. Tucci, P. Carlone, T.S. Sudarshan, Metallisation of polymers and polymer matrix composites by cold spray: state of the art and research perspectives, (2021).
- [93] H. Wang, P. Li, W. Guo, G. Ma, H. Wang, Copper-Based Composite Coatings by Solid-State Cold Spray Deposition: A Review, *Coatings* 13 (2023) 479.

- [94] F. Rubino, F. Tucci, V. Esperto, A.S. Perna, A. Astarita, P. Carlone, A. Squillace, Metallization of fiber reinforced composite by surface functionalization and cold spray deposition, *Procedia Manuf* 47 (2020) 1084–1088.
- [95] D.W. Lee, B.R. Yoo, Advanced silica/polymer composites: Materials and applications, *Journal of Industrial and Engineering Chemistry* 38 (2016) 1–12.
- [96] H. Zou, S. Wu, J. Shen, Polymer/Silica Nanocomposites: Preparation, characterization, properties, and applications, *Chem Rev* 108 (2008) 3893–3957.
- [97] S. Mallakpour, M. Naghdi, Polymer/SiO₂ nanocomposites: Production and applications, *Prog Mater Sci* 97 (2018) 409–447.
- [98] P.G. Jeelani, P. Mulay, R. Venkat, C. Ramalingam, Multifaceted Application of Silica Nanoparticles. A Review, *Silicon* 12 (2020) 1337–1354.
- [99] F. Akhter, A.A. Rao, M.N. Abbasi, S.A. Wahocho, M.A. Mallah, H. Anees-ur-Rehman, Z.A. Chandio, A Comprehensive Review of Synthesis, Applications and Future Prospects for Silica Nanoparticles (SNPs), *Silicon* 14 (2022) 8295–8310.
- [100] S.R. Zhai, C.S. He, D. Wu, Y.H. Sun, Hydrothermal synthesis of mesostructured aluminosilicate nanoparticles assisted by binary surfactants and finely controlled assembly process, *J Non Cryst Solids* 353 (2007) 1606–1611.
- [101] W. Zhao, J. Gu, L. Zhang, H. Chen, J. Shi, Fabrication of uniform magnetic nanocomposite spheres with a magnetic core/mesoporous silica shell structure, *J Am Chem Soc* 127 (2005) 8916–8917.
- [102] J. Kim, J.E. Lee, J. Lee, J.H. Yu, B.C. Kim, K. An, Y. Hwang, C.H. Shin, J.G. Park, J. Kim, T. Hyeon, Magnetic fluorescent delivery vehicle using uniform mesoporous silica spheres embedded with monodisperse magnetic and semiconductor nanocrystals, *J Am Chem Soc* 128 (2006) 688–689.
- [103] D.R. Radu, C.Y. Lai, J.W. Wiench, M. Pruski, V.S.Y. Lin, Gatekeeping Layer Effect: A Poly(lactic acid)-coated Mesoporous Silica Nanosphere-Based Fluorescence Probe for Detection of Amino-Containing Neurotransmitters, *J Am Chem Soc* 126 (2004) 1640–1641.

- [104] S.M. Abdelghany, D.J. Quinn, R.J. Ingram, B.F. Gilmore, R.F. Donnelly, C.C. Taggart, C.J. Scott, Gentamicin-loaded nanoparticles show improved antimicrobial effects towards *Pseudomonas aeruginosa* infection, *Int J Nanomedicine* 7 (2012) 4053–4063
- [105] S. Agnihotri, R. Pathak, D. Jha, I. Roy, H.K. Gautam, A.K. Sharma, P. Kumar, Synthesis and antimicrobial activity of aminoglycoside-conjugated silica nanoparticles against clinical and resistant bacteria, *New Journal of Chemistry* 39 (2015) 6746–6755.
- [106] W.H. De Jong, P.J.A. Borm, Drug delivery and nanoparticles: Applications and hazards, *Int J Nanomedicine* 3 (2008) 133.
- [107] Y. Wang, Q. Zhao, N. Han, L. Bai, J. Li, J. Liu, E. Che, L. Hu, Q. Zhang, T. Jiang, S. Wang, Mesoporous silica nanoparticles in drug delivery and biomedical applications, *Nanomedicine* 11 (2015) 313–327.
- [108] F. Torney, B.G. Trewyn, V.S.Y. Lin, K. Wang, Mesoporous silica nanoparticles deliver DNA and chemicals into plants, *Nature Nanotechnology* 2007 2:5 2 (2007) 295–300.
- [109] R. Suriyaprabha, G. Karunakaran, R. Yuvakkumar, P. Prabu, V. Rajendran, N. Kannan, Growth and physiological responses of maize (*Zea mays* L.) to porous silica nanoparticles in soil, *Journal of Nanoparticle Research* 14 (2012) 1–14.
- [110] M.H. Siddiqui, M.H. Al-Whaibi, Role of nano-SiO₂ in germination of tomato (*Lycopersicon esculentum* seeds Mill.), *Saudi J Biol Sci* 21 (2014) 13–17.
- [111] M. Kalteh, Z. Taj Alipour, S. Ashraf, M.M. Aliabadi, A.F. Nosratabadi, Effect of silica Nanoparticles on Basil (*Ocimum basilicum*) Under Salinity Stress, *Journal of Chemical Health Risks* 4 (2014) 49–55.
- [112] A.J. Kinloch, R.D. Mohammed, A.C. Taylor, C. Eger, S. Sprenger, D. Egan, The effect of silica nano particles and rubber particles on the toughness of multiphase thermosetting epoxy polymers, *J Mater Sci* 40 (2005) 5083–5086.

- [113] D. Jiao, S. Zheng, Y. Wang, R. Guan, B. Cao, The tribology properties of alumina/silica composite nanoparticles as lubricant additives, *Appl Surf Sci* 257 (2011) 5720–5725.
- [114] A. Behzadi, A. Mohammadi, Environmentally responsive surface-modified silica nanoparticles for enhanced oil recovery, *Journal of Nanoparticle Research* 18 (2016) 1–19.
- [115] I. Kim, A.J. Worthen, K.P. Johnston, D.A. DiCarlo, C. Huh, Size-dependent properties of silica nanoparticles for Pickering stabilization of emulsions and foams, *Journal of Nanoparticle Research* 18 (2016) 1–12
- [116] M.I. Din, R. Rehan, Synthesis, Characterization, and Applications of Copper Nanoparticles, *Anal Lett* 50 (2017) 50–62.
- [117] I.A. Ivanova, D.S. Daskalova, L.P. Yordanova, E.L. Pavlova, Copper and Copper Nanoparticles Applications and Their Role against Infections: A Minireview, *Processes* 2024, Vol. 12, Page 352 12 (2024) 352.
- [118] M.C. Crisan, M. Teodora, M. Lucian, Copper Nanoparticles: Synthesis and Characterization, Physiology, Toxicity and Antimicrobial Applications, *Applied Sciences* 2022, Vol. 12, Page 141 12 (2021) 141.
- [119] P. Harikumar, A. Aravind, Antibacterial Activity of Copper Nanoparticles and Copper Nanocomposites against Escherichia Coli Bacteria P S Harikumar Centre for Water Resources Development and Management Antibacterial Activity of Copper Nanoparticles and Copper Nanocomposites against Escherichia Coli Bacteria, *Article in International Journal of Sciences* (2016).
- [120] M.F. Al-Hakkani, Biogenic copper nanoparticles and their applications: A review, *SN Appl Sci* 2 (2020) 1–20.
- [121] J. Salvo, C. Sandoval, Role of copper nanoparticles in wound healing for chronic wounds: literature review, *Burns Trauma* 10 (2022).
- [122] N. Cioffi, L. Torsi, N. Ditaranto, G. Tantillo, L. Ghibelli, L. Sabbatini, T. Blevè-Zacheo, M. D'Alessio, P.G. Zambonin, E. Traversa, Copper nanoparticle/polymer

composites with antifungal and bacteriostatic properties, *Chemistry of Materials* 17 (2005) 5255–5262.

- [123] D. Longano, N. Ditaranto, L. Sabbatini, L. Torsi, N. Cioffi, Synthesis and antimicrobial activity of copper nanomaterials, in: *Nano-Antimicrobials: Progress and Prospects*, Springer-Verlag Berlin Heidelberg, 2014: pp. 85–117.
- [124] L. Tamayo, M. Azócar, M. Kogan, A. Riveros, M. Páez, Copper-polymer nanocomposites: An excellent and cost-effective biocide for use on antibacterial surfaces, *Materials Science & Engineering C* 69 (2016) 1391–1409.
- [125] U. Bogdanović, V. Vodnik, M. Mitrić, S. Dimitrijević, S.D. Škapin, V. Žunič, M. Budimir, M. Stoiljković, Nanomaterial with high antimicrobial efficacy copper/polyaniline nanocomposite, *ACS Appl Mater Interfaces* 7 (2015) 1955–1966.
- [126] D.N. Bikiaris, K.S. Triantafyllidis, HDPE/Cu-nanofiber nanocomposites with enhanced antibacterial and oxygen barrier properties appropriate for food packaging applications, *Mater Lett* 93 (2013) 1–4.
- [127] K. Singh, V. Khanna, V. Chaudhary, Effect of Hybrid Reinforcements on the Mechanical Properties of Copper Nanocomposites, *ECS Journal of Solid State Science and Technology* 11 (2022) 097001
- [128] G. Chai, Y. Sun, J. Sun, Q. Chen, Mechanical properties of carbon nanotube–copper nanocomposites, *Journal of Micromechanics and Microengineering* 18 (2008) 035013.
- [129] E.T. Thostenson, Z. Ren, T.W. Chou, Advances in the science and technology of carbon nanotubes and their composites: a review, *Compos Sci Technol* 61 (2001) 1899–1912.
- [130] P.F.J. Harris, *Carbon Nanotube Science Synthesis, Properties and Applications*, Cambridge University Press, Cambridge, 2009.

- [131] A. Jorio, M.S. Dresselhaus, G. Dresselhaus, Carbon Nanotubes: Advanced Topics in the Synthesis, Structure, Properties and Applications, Springer-Verlag, Heidelberg, 2008.
- [132] H. Dai, Carbon nanotubes: opportunities and challenges, Surf Sci 500 (2002) 218–241.
- [133] T.W. Ebbesen, P.M. Ajayan, Large-scale synthesis of carbon nanotubes, Nature 1992 358:6383 358 (1992) 220–222.
- [134] P.M. Ajayan, S.C. Tsang, P.J.F. Harris, M.L. &green, N. Hamada, S. Sawada, S. &oshiyama, J.W. Mintmire, B.I. Dunlap, C.T. &white, R. Saito, F. Fujita, G. Dresselhaus, M.S.; D.W. &dresselhaus, J.W. &mintmire, Cobalt-catalysed growth of carbon nanotubes with single-atomic-layer walls, Nature 1993 363:6430 363 (1993) 605–607
- [135] A.M. Cassell, J.A. Raymakers, J. Kong, H. Dai, Large Scale CVD Synthesis of Single-Walled Carbon Nanotubes, Journal of Physical Chemistry B 103 (1999) 6484–6492.
- [136] P. Nikolaev, M.J. Bronikowski, R.K. Bradley, F. Rohmund, D.T. Colbert, K.A. Smith, R.E. Smalley, Gas-phase catalytic growth of single-walled carbon nanotubes from carbon monoxide, Chem Phys Lett 313 (1999) 91–97.
- [137] J. Kong, H.T. Soh, A.M. Cassell, C.F. Quate, H. Dai, J. Kong, H.T. Soh, A.M. Cassell, C.F. Quate, H. Dai, Synthesis of individual single-walled carbon nanotubes on patterned silicon wafers, Nature 395 (1998) 878–881.
- [138] J. Kong, A.M. Cassell, H. Dai, Chemical vapor deposition of methane for single-walled carbon nanotubes, Chem Phys Lett 292 (1998) 567–574.
- [139] J. Doh, J. Lee, Prediction of the mechanical behavior of double walled-CNTs using a molecular mechanics-based finite element method: Effects of chirality, Comput Struct 169 (2016) 91–100

- [140] J. Doh, S.I. Park, Q. Yang, N. Raghavan, The effect of carbon nanotube chirality on the electrical conductivity of polymer nanocomposites considering tunneling resistance, *Nanotechnology* 30 (2019) 465701.
- [141] N. Saifuddin, A.Z. Raziah, A.R. Junizah, Carbon Nanotubes: A Review on Structure and Their Interaction with Proteins, *J Chem* 2013 (2013) 676815.
- [142] S. Ogata, Y. Shibutani, Ideal tensile strength and band gap of single-walled carbon nanotubes, *Phys Rev B* 68 (2003) 165409.
- [143] T. McNally, P. Potschke, *Polymer-Carbon Nanotube Composites: Preparation, Properties and Applications*, Woodhead Publishing, Cambridge, 2011.
- [144] C. Stéphan, T.P. Nguyen, B. Lahr, W. Blau, S. Lefrant, O. Chauvet, Raman spectroscopy and conductivity measurements on polymer-multiwalled carbon nanotubes composites, 2015.
- [145] Q. Zhao, H.D. Wagner, Raman spectroscopy of carbon-nanotube-based composites, *Philosophical Transactions of the Royal Society A: Mathematical, Physical and Engineering Sciences* 362 (2004) 2407–2424.
- [146] M.S.P. Shaffer, A.H. Windle, Fabrication and Characterization of Carbon Nanotube/Poly(vinyl alcohol) Composites, *Advanced Materials* 11 (1999).
- [147] K.P. Ryan, M. Cadek, V. Nicolosi, S. Walker, M. Ruether, A. Fonseca, J.B. Nagy, W.J. Blau, J.N. Coleman, Multiwalled carbon nanotube nucleated crystallization and reinforcement in poly (vinyl alcohol) composites, *Synth Met* 156 (2006) 332–335
- [148] M. Cadek, J.N. Coleman, V. Barron, K. Hedicke, W.J. Blau, Morphological and mechanical properties of carbon-nanotube-reinforced semicrystalline and amorphous polymer composites, *Appl Phys Lett* 81 (2002) 5123–5125.
- [149] D. Qian, E.C. Dickey, R. Andrews, T. Rantell, Load transfer and deformation mechanisms in carbon nanotube-polystyrene composites, *Appl Phys Lett* 76 (2000) 2868–2870.

- [150] R. Andrews, D. Jacques, D. Qian, T. Rantell, Multiwall carbon nanotubes: Synthesis and application, *Acc Chem Res* 35 (2002) 1008–1017.
- [151] K.Q. Xiao, L.C. Zhang, I. Zarudi, Mechanical and rheological properties of carbon nanotube-reinforced polyethylene composites, *Compos Sci Technol* 67 (2007) 177–182.
- [152] M. Moniruzzaman, J. Chattopadhyay, W.E. Billups, K.I. Winey, Tuning the mechanical properties of SWNT/nylon 6,10 composites with flexible spacers at the interface, *Nano Lett* 7 (2007) 1178–1185.
- [153] R. Haggemueller, W. Zhou, J.E. Fischer, K.I. Winey, Production and characterization of polymer nanocomposites with highly aligned single-walled carbon nanotubes, *J Nanosci Nanotechnol* 3 (2003) 105–110.
- [154] P. Miaudet, A. Derré, M. Maugey, C. Zakri, P.M. Piccione, R. Inoubli, P. Poulin, Shape and temperature memory of nanocomposites with broadened glass transition, *Science* (1979) 318 (2007) 1294–1296.
- [155] A.B. Dalton, S. Collins, E. Muñoz, J.M. Razal, V.H. Ebron, J.P. Ferraris, J.N. Coleman, B.G. Kim, R.H. Baughman, Super-tough carbon-nanotube fibres, *Nature* 2003 423:6941 423 (2003) 703–703.
- [156] W. Bauhofer, J.Z. Kovacs, A review and analysis of electrical percolation in carbon nanotube polymer composites, *Compos Sci Technol* 69 (2009) 1486–1498.
- [157] J.Z. Kovacs, K. Andresen, J.R. Pauls, C.P. Garcia, M. Schossig, K. Schulte, W. Bauhofer, Analyzing the quality of carbon nanotube dispersions in polymers using scanning electron microscopy, *Carbon N Y* 45 (2007) 1279–1288.
- [158] T. McNally, P. Pötschke, P. Halley, M. Murphy, D. Martin, S.E.J. Bell, G.P. Brennan, D. Bein, P. Lemoine, J.P. Quinn, Polyethylene multiwalled carbon nanotube composites, *Polymer (Guildf)* 46 (2005) 8222–8232.
- [159] I. Alig, P. Pötschke, D. Lellinger, T. Skipa, S. Pegel, G.R. Kasaliwal, T. Villmow, Establishment, morphology and properties of carbon nanotube networks in polymer melts, *Polymer (Guildf)* 53 (2012) 4–28.

- [160] B.C. Jaime Grunlan, A.R. Mehrabi, M. V Bannon, J.L. Bahr, J.C. Grunlan, A.R. Mehrabi, M. V Bannon, J.L. Bahr, Water-Based Single-Walled-Nanotube-Filled Polymer Composite with an Exceptionally Low Percolation Threshold, *Advanced Materials* 16 (2004) 150–153
- [161] M.B. Bryning, M.F. Islam, J.M. Kikkawa, A.G. Yodh, Very Low Conductivity Threshold in Bulk Isotropic Single-Walled Carbon Nanotube–Epoxy Composites, *Advanced Materials* 17 (2004) 1186–1191.
- [162] A.S. Alhulaifi, G.A. Buck, W.J. Arbegast, Numerical and experimental investigation of cold spray gas dynamic effects for polymer coating, *Journal of Thermal Spray Technology* 21 (2012) 852–862.
- [163] W. Lock Sulen, K. Ravi, C. Bernard, Y. Ichikawa, K. Ogawa, Deposition Mechanism Analysis of Cold-Sprayed Fluoropolymer Coatings and Its Wettability Evaluation, *Journal of Thermal Spray Technology* 29 (2020) 1643–1659.
- [164] P. Albers, M. Maier, M. Reisinger, B. Hannebauer, R. Weinand, Physical boundaries within aggregates - Differences between amorphous, para-crystalline, and crystalline Structures, *Crystal Research and Technology* 50 (2015) 846–865.
- [165] K. Sundara Rajan, J.P. Rothstein, Cold spray deposition of high density polyethylene composite powders, *Surf Coat Technol* 484 (2024).